1 Report No	2 Government Accession No	3 Recipient's Catalog No
NASA CR-167879		

4 Title and Subtitle	5 Report Date
COMPUTER MODELING OF FAN-EXIT-SPLITTER SPACING EFFECTS ON F100 RESPONSE TO DISTORTION	March 1982
	6 Performing Organization Code
7 Author(s)	8 Performing Organization Report No
M. Shaw, R. W. Murdock	FR-15596
	10 Work Unit No
9 Performing Organization Name and Address	11 Contract or Grant No
UNITED TECHNOLOGIES CORPORATION Pratt & Whitney Aircraft Group Government Products Division West Palm Beach, Florida 33402	NAS3-22739
	13 Type of Report and Period Covered
12 Sponsoring Agency Name and Address	Final Report
National Aeronautics and Space Administration Washington, D.C.	14 Sponsoring Agency Code

15 Supplementary Notes

16 Abstract

The distortion response of the F100(3) engine has been analytically determined to be effected by the fan exit splitter configuration. The sensitivity for a proximate splitter fan is calculated to be slightly greater than a remote splitter configuration with identical airfoils. Predicted response was based upon a Multiple Segment Parallel Compressor Model modified to include a bypass ratio representation that effects the performance characteristics of the last rotor and intermediate case struts. The study points out the predicted distortion response requires an accurate definition of row pre- and post-stall undistorted operation. Recommendation for planned NASA Lewis Research Center distortion testing of an F100(3) are included.

17 Key Words (Suggested by Author(s))	18 Distribution Statement
Turbofan Inlet flow distortion Compressor stall Parallel compressor model Fan-Exit-Splitter	Unclassified - Limited - All requests outside the Department of Defense should be referred to: USAF Tactical Engines Program Office (ASD/YZE) Wright Patterson AFB, OH 45433

19 Security Classif (of this report)	20 Security Classif (of this page)	21 No of Pages	22 Price
Unclassified	Unclassified	104	$5.00

FOREWORD

This report was prepared for the National Aeronautics and Space Administration, Lewis Research Center, under Contract NAS3-22739. The report documents the modifications to the Pratt & Whitney Aircraft Multiple Segment Parallel Compressor Model to analyze the distortion response of a F100(3) proximate splitter fan. Predicted response to inlet pressure and temperature circumferential distortion is made with the modified model and comparisons of response is made between remote and proximate splitter fans. Mr. H. G. Hurrell was the NASA Project Manager for this contract. The P&WA Program Manager was Mr. M. Shaw with technical support by Mr. R. W. Murdoch.

CONTENTS

Section	*Page*
INTRODUCTION	1
DISTORTION MODEL DESCRIPTION	2
General Theory	2
Modification of Analytical Model	2
Undistorted Arc Stall Characteristics	2
Undistorted Post Stall Characteristics	15
ANALYSIS PROCEDURE	25
General	25
Stall Criteria	25
Distortion Response Parameters	26
Individual Distortion Response	27
RESULTS AND DISCUSSION	29
Pressure Distortion	29
Temperature Distortion	33
Detailed Flow Field Analysis	41
Comparison of Distortion Response for Engines With Proximate and Remote Splitters	50
CONCLUSIONS	76
RECOMMENDATIONS	77
APPENDIX I	78
Blade Row Performance Characteristics	78
APPENDIX II	99
Definition of Model Input Performance Parameters	99
APPENDIX III	101
F100(3) $k\theta$ Distortion Descriptor System	101
REFERENCES	103
LIST OF SYMBOLS	104

LIST OF ILLUSTRATIONS

Figure		*Page*
1	F100(3) Engine Compression System With Proximate Splitter	3
2	Parallel Compressor Segment Match Comparison for 2 and 18 Segments	4
3	Bypass Ratio Effect on Fan Characteristics	5
4	Comparison of F100(3) Rig Data and Remote Splitter Model Predictions	6
5	Undistorted Test Data Allows Definition of Limited Flow Range of Necessary Performance Characteristics	7
6	Schematic of Remote Splitter and Proximate Splitter Configurations	9
7	F100(3) Splitter Configuration Affects Location of Radial Turning of Streamlines	10
8	Total Pressure Warpage at Fan Exit, Comparison of F100(3) Remote and Proximate Splitters	11
9	Comparison of FX219-19 and Rig 108 Speed/Flow Relationships	12
10	F100(3) Proximate Splitter Fan Speedlines	13
11	Total Pressure Warpage at Fan Exit, F100(3) Proximate Splitter Fan Model	14
12	F100(3) Remote Splitter Fan Streamline Shapes	16
13	Total Pressure Warpage at Fan Exit, F100(3) Revised Remote Splitter Fan Model	17
14	Effect of Input Bypass Ratio on Revised Remote Splitter Model Predicted Fan Performance	18
15	F100(3) Remote Splitter Fan Data Compared to Revised Remote Splitter Model Predictions	19
16	Engine FX219-19 Run 82 Undistorted Speedlines	21
17	Model Predicted Lapse Rate Compared to FX219-19 Test Results	22
18	Model Predicted Pressure Distortion Attenuation Compared to FX219-19 Test Results	23
19	Model Predicted Temperature Distortion Generation Compared to Remote Splitter Test Results	24
20	Stall Criteria: Max Static Pressure at Exit Station	26
21	Six Inlet Distortion Cases	27

LIST OF ILLUSTRATIONS (Continued)

Figure		*Page*
22	Predicted F100(3) Proximate Splitter Fan Surge Lines With Pressure Distortion	30
23	Predicted F100(3) Proximate Splitter Fan Circumferential Pressure Distortion $K\theta$ Sensitivity	31
24	Predicted F100(3) Proximate Splitter Fan Circumferential Pressure Distortion $\Delta P_T/P_T$ Sensitivity	32
25	Predicted F100(3) Proximate Splitter Fan Pressure Distortion Attenuation	34
26	Predicted F100(3) Proximate Splitter Fan Pressure Distortion Attenuation: $K\theta$	35
27	Predicted F100(3) Proximate Splitter Fan Pressure Distortion Attenuation: $\Delta P_T/P_T$	36
28	Predicted F100(3) Proximate Splitter Fan Temperature Distortion Generation	37
29	Predicted F100(3) Proximate Splitter Fan Temperature Distortion Generation: $K\theta_{TEMP}$	38
30	Predicted F100(3) Proximate Splitter Fan Temperature Distortion Generation: $\Delta T_T/T_T$	39
31	Predicted F100(3) Proximate Splitter Fan Surge Lines With Temperature Distortion	40
32	Predicted F100(3) Proximate Splitter Fan Circumferential Temperature Distortion $K\theta_{TEMP}$	42
33	Predicted F100(3) Proximate Splitter Fan Circumferential Temperature Distortion $\Delta T_T/T_T$ Sensitivity	43
34	Predicted F100(3) Proximate Splitter Fan Temperature Distortion Attenuation	44
35	Predicted F100(3) Proximate Splitter Fan Temperature Distortion Attenuation: $K\theta_{TEMP}$	45
36	Predicted F100(3) Proximate Splitter Fan Temperature Distortion Attenuation: $\Delta T_T/T_T$	46
37	Predicted F100(3) Proximate Splitter Fan Pressure Distortion Generation	47
38	Predicted F100(3) Proximate Splitter Fan Pressure Distortion Generation: $K\theta$	48

LIST OF ILLUSTRATIONS (Continued)

Figure		*Page*
39	Predicted F100(3) Proximate Splitter Fan Surge Lines With Pressure Distortion Generation: $\Delta P_T/P_T$	49
40	Predicted F100(3) Proximate Splitter Fan Core Exit Circumferential Profiles ~ Case 1 (22% $\Delta P_T/P_T$/180 Deg)	51
41	Predicted F100(3) Proximate Splitter Fan Core Exit Circumferential Profiles ~ Case 2 (22% $\Delta P_T/P_T$/90 Deg)	52
42	Predicted F100(3) Proximate Splitter Fan Core Exit Circumferential Profiles ~ Case 4 (18% $\Delta T_T/T_T$/180 Deg)	53
43	Predicted F100(3) Proximate Splitter Fan Total Pressure Profiles ~ Case 1 (22% $\Delta P_T/P_T$/180 Deg)	54
44	Predicted F100(3) Proximate Splitter Fan Total Temperature Profiles ~ Case 1 (22% $\Delta P_T/P_T$/180 Deg)	55
45	Predicted F100(3) Proximate Splitter Fan Static Pressure Profiles ~ Case 1 (22% $\Delta P_T/P_T$/180 Deg)	56
46	Predicted F100(3) Proximate Splitter Fan Total Pressure Profiles ~ Case 2 (22% $\Delta P_T/P_T$/90 Deg)	57
47	Predicted F100(3) Proximate Splitter Fan Total Temperature Profiles ~ Case 2 (22% $\Delta P_T/P_T$/90 Deg)	58
48	Predicted F100(3) Proximate Splitter Fan Static Pressure Profiles ~ Case 2 (22% $\Delta P_T/P_T$/90 Deg)	59
49	Predicted F100(3) Proximate Splitter Fan Total Pressure Profiles ~ Case 4 (18% $\Delta T_T/T_T$/180 Deg)	60
50	Predicted F100(3) Proximate Splitter Fan Total Temperature Profiles ~ Case 4 (18% $\Delta T_T/T_T$/180 Deg)	61
51	Predicted F100(3) Proximate Splitter Fan Static Pressure Profiles ~ Case 4 (18% $\Delta T_T/T_T$/180 Deg)	62
52	Predicted F100(3) Proximate Splitter Fan Circumferential Pressure Distortion $K\theta$ Sensitivity, Compared to Remote Splitter Predictions (CR-159754)	64
53	Predicted F100(3) Proximate Splitter Circumferential Temperature Distortion $K\theta_{TEMP}$ Sensitivity, Compared to Remote Splitter Predictions (CR-159754)	65
54	Predicted F100(3) Proximate Splitter Fan Pressure Distortion Attenuation: $K\theta$, Compared to Remote Splitter Predictions (CR-159754)	66

LIST OF ILLUSTRATIONS (Continued)

Figure		*Page*
55	Predicted F100(3) Proximate Splitter Fan Temperature Distortion Generation: $K\theta_{TEMP}$, Compared to Remote Splitter Predictions (CR-159754)	67
56	Predicted F100(3) Proximate Splitter Fan Temperature Distortion Attenuation: $K\theta_{TEMP}$, Compared to Remote Splitter Predictions (CR-159754)	68
57	Predicted F100(3) Proximate Splitter Fan Pressure Distortion Generation: $K\theta$, Compared to Remote Splitter Predictions (CR-159754)	69
58	Comparison of FX219-19 Proximate Splitter Fan Undistorted and 180 Deg Distortion Surge Lines	71
59	FX219-19 Proximate Splitter Fan Surge $K\theta$	72
60	FX219-19 Proximate Splitter Fan Circumferential Lapse Rate	73
61	F100 Remote Splitter Fan Circumferential Lapse Rate	74

LIST OF TABLES

Table		*Page*
1	Circumferential Pressure and Temperature Distortion Study Cases.....	25
2	Comparison of Remote and Proximate Splitter MSPC Model Predictions...	63
3	Comparison of Model Predicted Stall Limiting Fan Stream for Proximate and Remote Splitter Fans.....	75

SUMMARY

This report documents the modifications that were made to the Pratt & Whitney Aircraft Multiple Segment Parallel Compressor Model to include a bypass ratio representation permitting analysis of both proximate and remote splitter versions of the F100(3) fan. The response to individual circumferential pressure and temperature distortion for a proximate splitter fan was calculated using the modified model. To evaluate the effect the fan exit splitter has on F100(3) response to inlet distortion, the model predictions for the proximate splitter fan were compared to remote splitter fan predictions previously documented. The splitter proximity was shown to change the third rotor and intermediate case performance. The sensitivity to inlet distortion was determined to be strongly dependent upon the assumed post-stall characteristics. The proximate splitter fan was calculated to be more sensitive to both pressure and temperature distortion than the remote.

INTRODUCTION

The operational suitability of an aircraft propulsion system depends on engine response to inlet pressure and/or temperature distortions. These distortions may result in reduced system stability or a complete loss of stable system operation. Definition of engine response to distortion and assurance of adequate engine stability margin usually requires that extensive testing be conducted. To improve and reduce the amount of experimental stability testing, Pratt & Whitney Aircraft and the NASA-Lewis Research Center (NASA-LeRC) collaborated in developing an analytical model which predicts engine response to circumferential pressure, temperature, and combined pressure and temperature distortion.

Extensive work was accomplished in predicting the response characteristics of a turbofan engine with nonvariable compressor geometry (TF30-P-3) under NASA Contract NAS3-18535. The distortion model was then expanded to include variable fan and compressor geometry effects under NASA Contract NAS3-20610. The expanded model was used to predict distortion response characteristics of the F100(3) remote splitter engine, and to ascertain the levels of distortion required to stall F100(3) engine XD11-8 as part of a pretest planning effort under NASA Contract NAS3-20835. The F100(3) is now delivered with a fan exit proximate splitter for F-16 aircraft applications. The work reported herein consisted of modifying the model to account for the effect of the proximate splitter, predicting fan response to pressure and temperature distortion with the modified model, and comparing the predictions to those made for a remote splitter fan in the previous contract.

The technical effort for this program consisted of two tasks. Both tasks have been subdivided into two sections consistent with the program objectives. In Task I the Pratt & Whitney Aircraft Multiple Segment Parallel Compressor (MSPC) model was modified to analytically evaluate the distortion response of an F100(3) proximate splitter fan and to improve the bypass ratio representation used in the model. The second part of Task I consisted of verifying the modified model through use of a combination of the F100 stability audit correlations, fan rig data, and engine data. In Task II, the modified model was used to predict F100(3) proximate splitter fan response to individual circumferential pressure and temperature distortions of varying distortion amplitude and extent. Additionally, these predictions were compared to those reported in NASA Report CR-159754 for a remote splitter fan to determine the effect the fan exit splitter has on F100(3) engine response to inlet distortion.

DISTORTION MODEL DESCRIPTION

General Theory

The Multiple Segment Parallel Compressor (MSPC) model has been developed by Pratt & Whitney Aircraft to predict compression system response to circumferential inlet distortion. It is capable of simulating the TF30-P-3 and F100(3) engines. The F100(3) engine compression system is shown in Figure 1 with the fan exit proximate splitter. Under this contract the ability to calculate F100(3) proximate splitter fan response has been added. A detailed description of the model is presented in References 1 and 2.

The MSPC analytical distortion model uses an expanded parallel compressor theory to predict response to circumferential distortion. In basic parallel compressor theory, for example, when considering a classical 180 deg pressure distortion pattern, the circumference is divided into two, 180 deg circumferential sections called segments. One segment contains the mass rate of fluid flowing through the low pressure section and the other the mass rate of fluid flowing through the high pressure section. These two segments do not communicate (i.e., there is no transfer of mass between the two) and the segment performance is individually calculated for each. Individual blade and vane row static pressure rise and total temperature rise characteristics are used to describe the compression system operating performance. These characteristics are defined from test data. The parallel compressor model calculates the average operating point by mass averaging the performance of the high and low pressure ratio segment matches.

The MSPC model is not simply on extension of basic parallel compressor theory to multiple segments. Figure 2 compares the segment match for basic two-segment parallel compressor theory described above to the MSPC model match using 18 segments. The MSPC model allows up to 36 parallel segments to be used. As shown in that figure, the 18 segments match over a range of corrected flows. This is due to the continuous distribution of mass flow around the circumference required by the MSPC model. Additionally individual segment performance in the MSPC model is adjusted to account for two-dimensional and unsteady flow effects which are not considered in basic parallel compressor theory. This includes the effect of engine-induced inlet flow redistribution, circumferential crossflows caused by internal compressor cavities, and unsteady flow due to rotor movement through a distorted flow field. Performance variations due to variable geometry are accounted for and include the effect on the flow distortion pattern and a fluid particle as they progress downstream. In the MSPC model the fan has been divided into an independent ID and OD, with separate performance characteristics for each.

Modification of Analytical Model

1. Undistorted Prestall Characteristics

An objective of the contract was to expand the P&WA Multiple Segment Parallel Compressor model to include an improved bypass ratio representation for the F100(3) fan. By properly modeling bypass ratio effects on the fan's undistorted row characteristics, the model can not be used to evaluate the F100(3) distortion response for both the F-16 aircraft application with the proximate splitter fan configuration, and the F-15 aircraft remote splitter engines. It was desirable to build upon work completed under the previous NASA contracts regarding the MSPC model. Phi, Psi, and Lambda row characteristic definitions were retained, but they have been modified by eliminating the bypass ratio dependent wheel speed adjustment to fan characteristics, which the original MSPC model contained. These modified definitions are given in Appendix I. Input parameters to the model, which include total fan flow and bypass ratio, were not altered. Prior to initiating modifications, a review of operation and formulation of fan characteristics was made and is briefly discussed below.

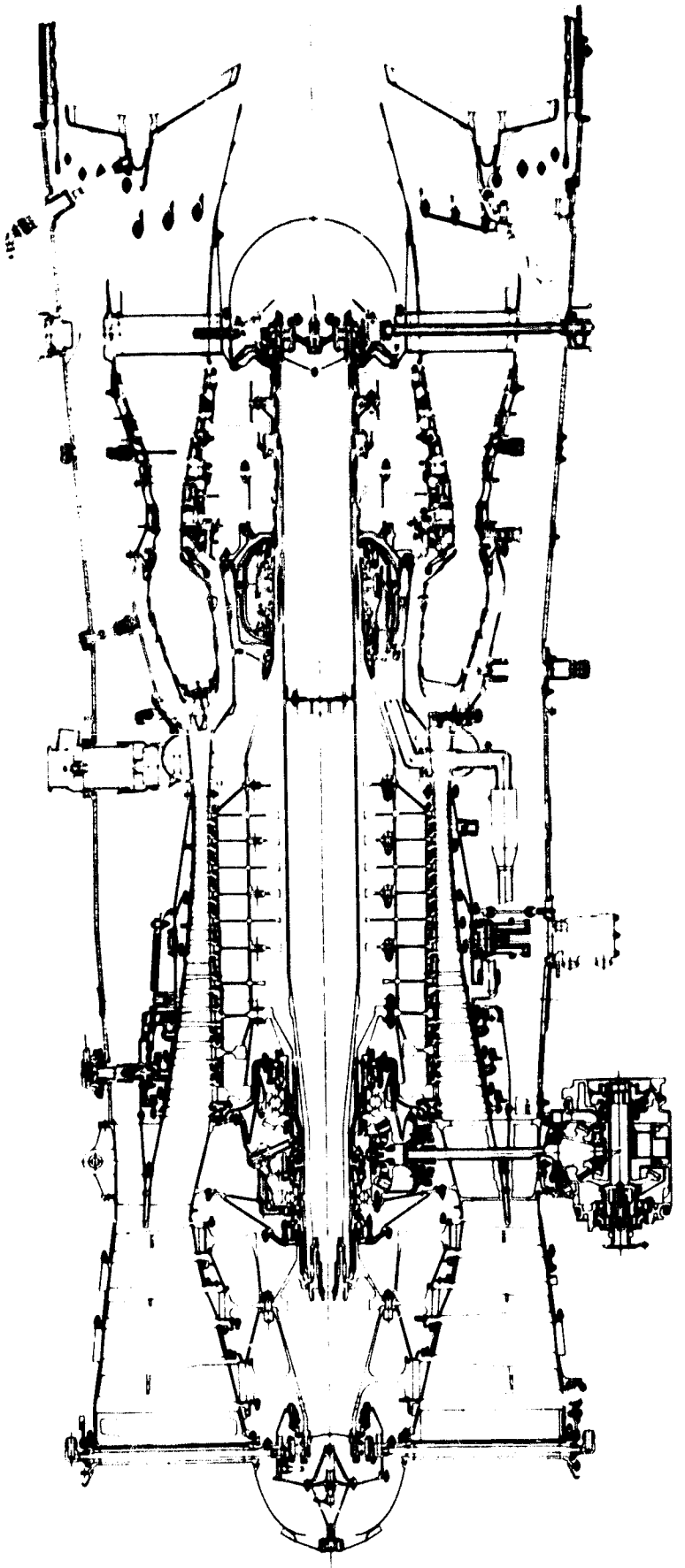

Figure 1. F100(3) Engine Compression System With Proximate Splitter

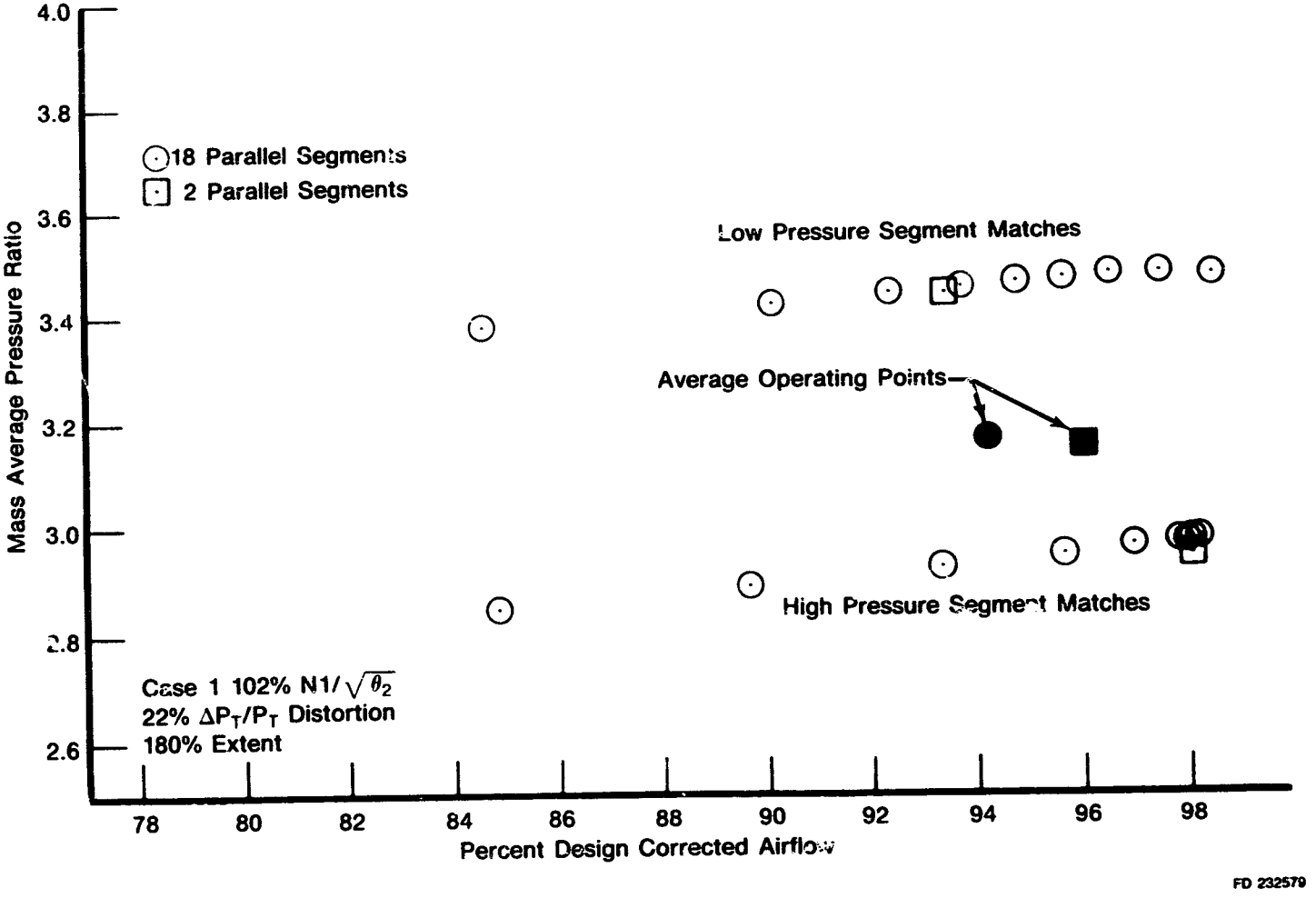

Figure 2. Parallel Compressor Segment Match Comparison for 2 and 18 Segments

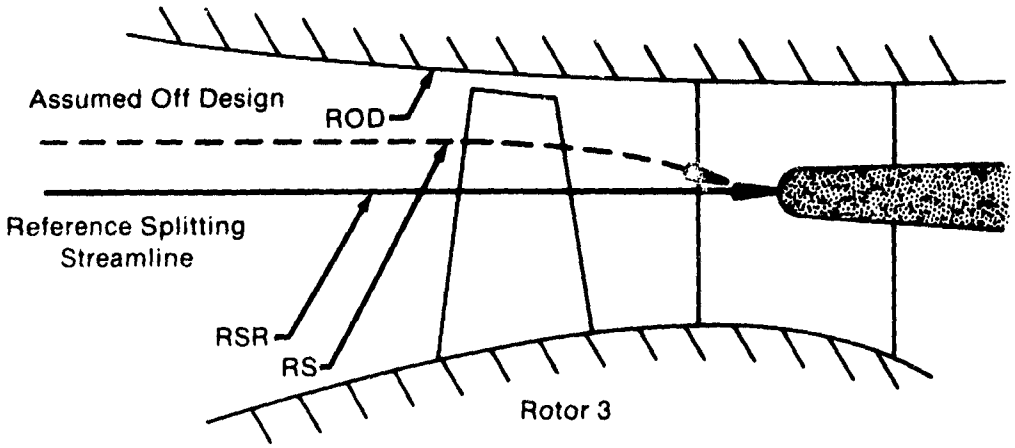

$$\text{Wheel Speed Adjustment} = \frac{\text{Blade Speed at Reference BPR}}{\text{Blade Speed at Off Design BPR}} = \sqrt{\frac{ROD^2 + RSR^2}{ROD^2 + RS^2}}$$

$$PSI = \frac{PS_{out} - PS_{in}}{PS_{in}} \cdot \frac{(N/\sqrt{\theta})^2_{DES}}{(N/\sqrt{\theta})^2} \cdot (\text{Wheel Speed Adjustment})^2$$

$$LAMDA = \frac{TT_{out} - TT_{in}}{TT_{in}} \cdot \frac{(N/\sqrt{\theta})^2_{DES}}{(N/\sqrt{\theta})^2} \cdot (\text{Wheel Speed Adjustment})^2$$

$$PHI/A = \frac{W\sqrt{\theta}}{\delta A} \cdot \frac{(N/\sqrt{\theta})_{DES}}{(N/\sqrt{\theta})} \cdot \text{Wheel Speed Adjustment}$$

FD 169920A
820802
gen 171

Figure 3. Bypass Ratio Effect on Fan Characteristics

The original version of the MSPC model was developed using fan blade row characteristics generated from interstage data acquired on a fan rig containing an aerodynamically remote splitter. Total pressure and total temperature were measured at stator leading edges. To calculate static pressure rise characteristics, the relative stage total pressure loss was split equally between the rotor and stator. In the original MSPC model, the row characteristics for the fan (Phi, Psi, and Lambda) were calculated using a bypass ratio dependent wheel speed adjustment. The wheel speed adjustment, and how it was applied to the row characteristics, is shown in Figure 3. With this definition the model calculated fan undistorted performance matched rig data; however, it did not match engine data generated on an alternate bypass ratio schedule.

Figure 4 shows the 101.5% speedline is significantly affected by the input bypass ratio. This is contrary to test experience and what would be expected for an aerodynamically remote splitter configuration. This limitation of the model does not necessarily invalidate the distortion response predictions previously reported for the F100(3) remote splitter fan in NASA Report CR-159754, Reference 3. Under that contract the undistorted and distorted surge lines were found to have a similar dependence on input bypass ratio. Therefore, the percent loss in surge margin due to an unit amount of inlet distortion, which is called the lapse rate, was considered valid even though the actual stall points were a function of the input bypass ratio. An improved bypass ratio representation is desirable so that in addition to the current effort, the characteristics could be used in other remodels, such as Reference 4, *Extended Frequency Turbofan Model, NAS3-21607.*

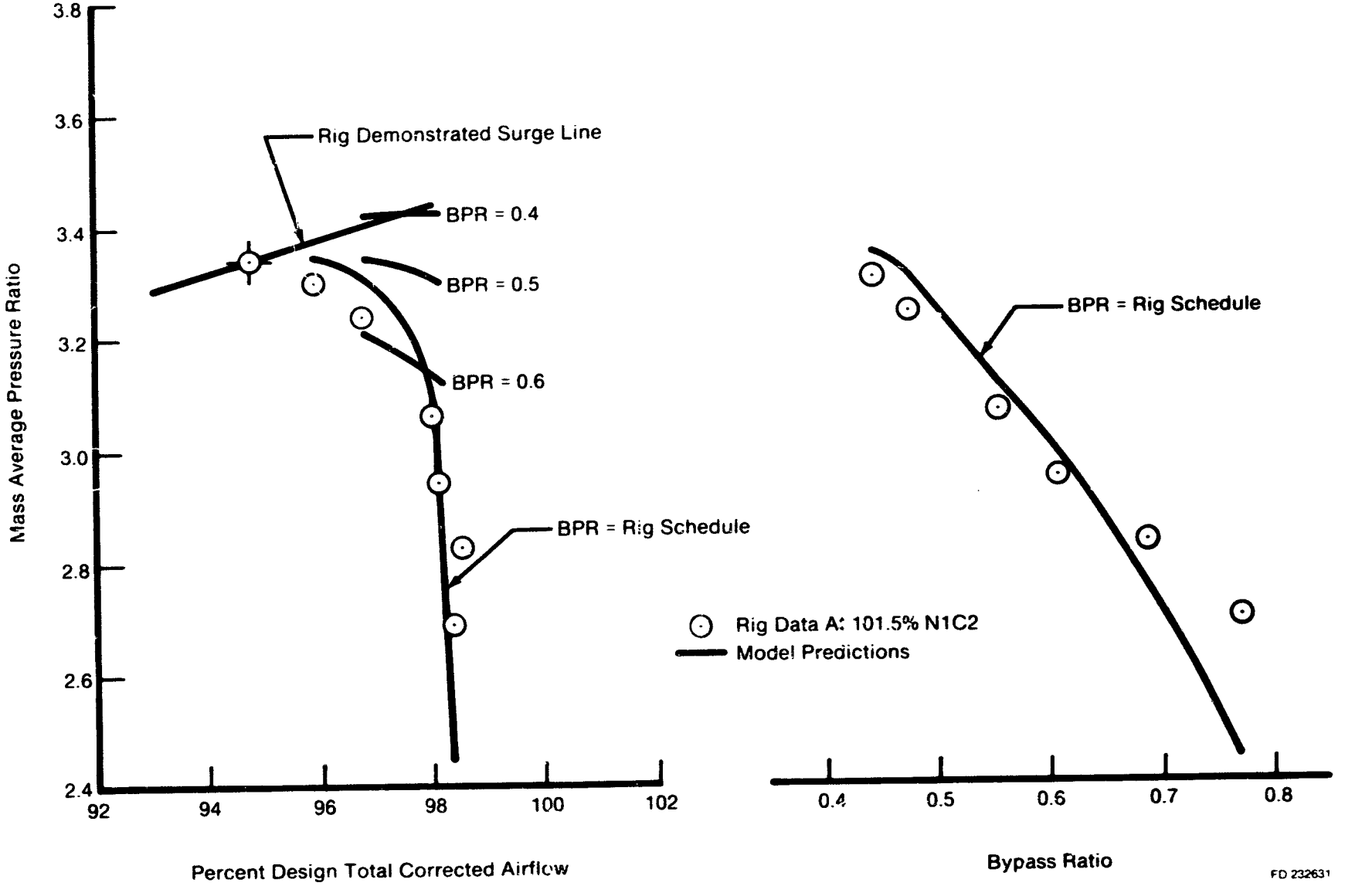

Figure 4. Comparison of F100(3) Rig Data and Remote Splitter Model Predictions

In formulating a more representative bypass ratio dependence, the rig data for both the remote splitter and proximate splitter were reviewed. It was anticipated that a streamline analysis of proximate splitter fan data would properly indicate how the various row characteristics were affected by bypass ratio and splitter spacing. After limited streamline analysis it was evident that in both the remote and proximate splitter fans, the forward stages were relatively unaffected by bypass ratio. Also evident was that only a limited flow range of the characteristic needed by the MSPC model could be defined from the undistorted test data, as is shown in Figure 5. The approach taken was to go back to the original characteristics defined from remote splitter fan data, adopt an algorith similar to that used for the TF30 proximate splitter fan (Reference 5) to model bypass ratio, and to adjust the remote splitter third rotor and intermediate case strut characteristics until overall proximate splitter fan performance was duplicated.

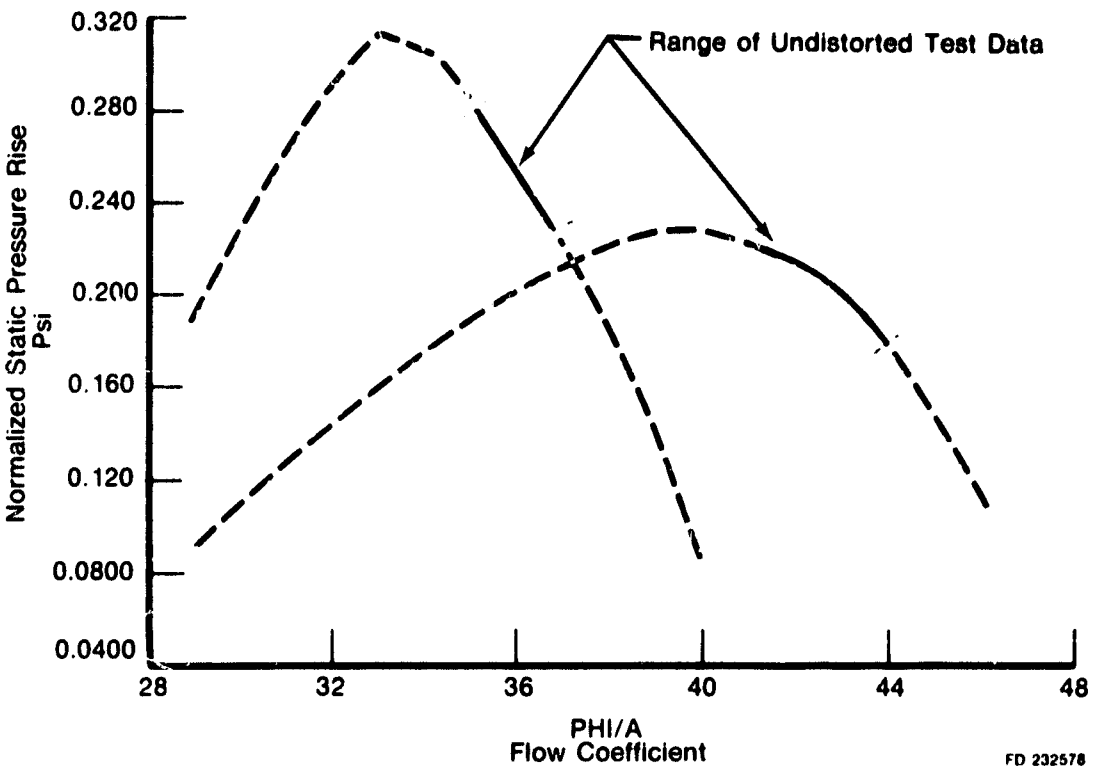

Figure 5. Undistorted Test Data Allows Definition of Limited Flow Range of Necessary Performance Characteristics

In Reference 6, the F100(3) remote splitter fan characteristics are presented. These are not actual data as they include the bypass ratio dependent adjustment to wheel speed, applied as shown in Figure 3. These were modified by removing the adjustment to get back to the original remote splitter fan pressure, rise and temperature rise characteristics. Since the bypass ratio schedule for the remote splitter fan rig was known, the wheel speed adjustment was calculated directly up to the undistorted stalling airflow. For lower mass flows, where the rig bypass ratio schedule is undefined, the wheel speed adjustment at the undistorted stalling airflow was used. Removing the wheel speed adjustment results in the characteristics that are used for the proximate splitter fan from the IGV through stator 2.

Rotor 3 and the intermediate case strut performance characteristics are dependent upon the splitter configuration. The remote and proximate splitter geometry of current F100(3) production engines are compared in Figure 6. The effect of different fan exit splitter spacing is depicted conceptually in Figure 7. As the splitter is moved forward, radial turning of the flow is induced in the fan blading. This turning causes changes in blade work input and both blade and strut row pressure rise. The significance of these changes to overall fan performance is most apparent when comparing fan exit total pressure warpage, $\Delta E'$, as a function of fan exit/duct inlet flow coefficient. Figure 8 shows that a unique pressure warpage curve exists for both F100(3) splitter configurations. Both rig and engine data, which were generated with different bypass ratio schedules, have been shown to fall on these curves. The slope of the curves is greater for the proximate splitter than for the remote, and it is related to the radial turning in the aft blade row.

The effect of radial turning caused by splitter spacing was modeled by modifying the static pressure rise characteristic for the third rotor and including an additional static pressure rise term caused by the radial turning. This is the method employed in the MSPC model to account for the effect of the TF30 proximate splitter. The total fan flow is divided into core side (ID) and duct side (OD) flow by the splitting streamline, with separate pressure rise and temperature rise characteristics for each side. The splitting streamline turns radially across rotor 3 to match the proximate splitter nose. This change in the ID and OD flow area causes an additional static pressure change which is bypass ratio dependent. The following relationship for the static pressure change through a one-dimensional nozzle or diffuser is used.

$$\frac{\Delta P_s}{P_s} = \frac{\gamma \cdot M^2}{1-M^2} \cdot \frac{\Delta A}{A}$$

where: M = Mach number
P_s = Static pressure
A = Flow area

Using the fan characteristics with the adjustement to wheel speed removed, and including the additional rotor 3 static pressure rise term, the MSPC model was executed to calculate undistorted performance for the proximate splitter configuration. The model was run at 5 speeds from 110% to 82.2% of design and compared to a composite map containing test data from fan rig 108E and engine FX219-19. It was necessary to input a speed into the model that was 1.6 to 1.9% greater than that of the test data from the FX219-19 speedlines due to the differences in speed/flow between the rig and the engine shown in Figure 9. Characteristic curves were then adjusted slightly to match documented proximate splitter performance. As seen in Figure 10, the model favorably reproduces the overall mass-averaged performance map. It also identifies the different bypass ratio schedules that were run by the engine and the rig. Figure 11 compares the model calculated pressure warpage to the empirical curve for a proximate splitter fan. Regardless of the bypass ratio schedule used the proximate splitter model matches the empirical curve. The good agreement between the data and the model for both the overall map and pressure warpage curves verifies the modifications made to the characteristics on the unstalled side.

A revised remote splitter version of the MSPC model was executed to verify the treatment of bypass ratio. Fan row performance characteristics are identical to the proximate splitter for the IGV through stator 2. As with the proximate splitter, an additional static pressure change results from diffusion and contraction of the flow streams as the splitting streamline turns radially to match the splitter leading edge. This turning occurs after the third rotor for the remote splitter fan. Thus, proximate and remote splitter fan pressure rise characteristics for rotor 3 and the intermediate case differ.

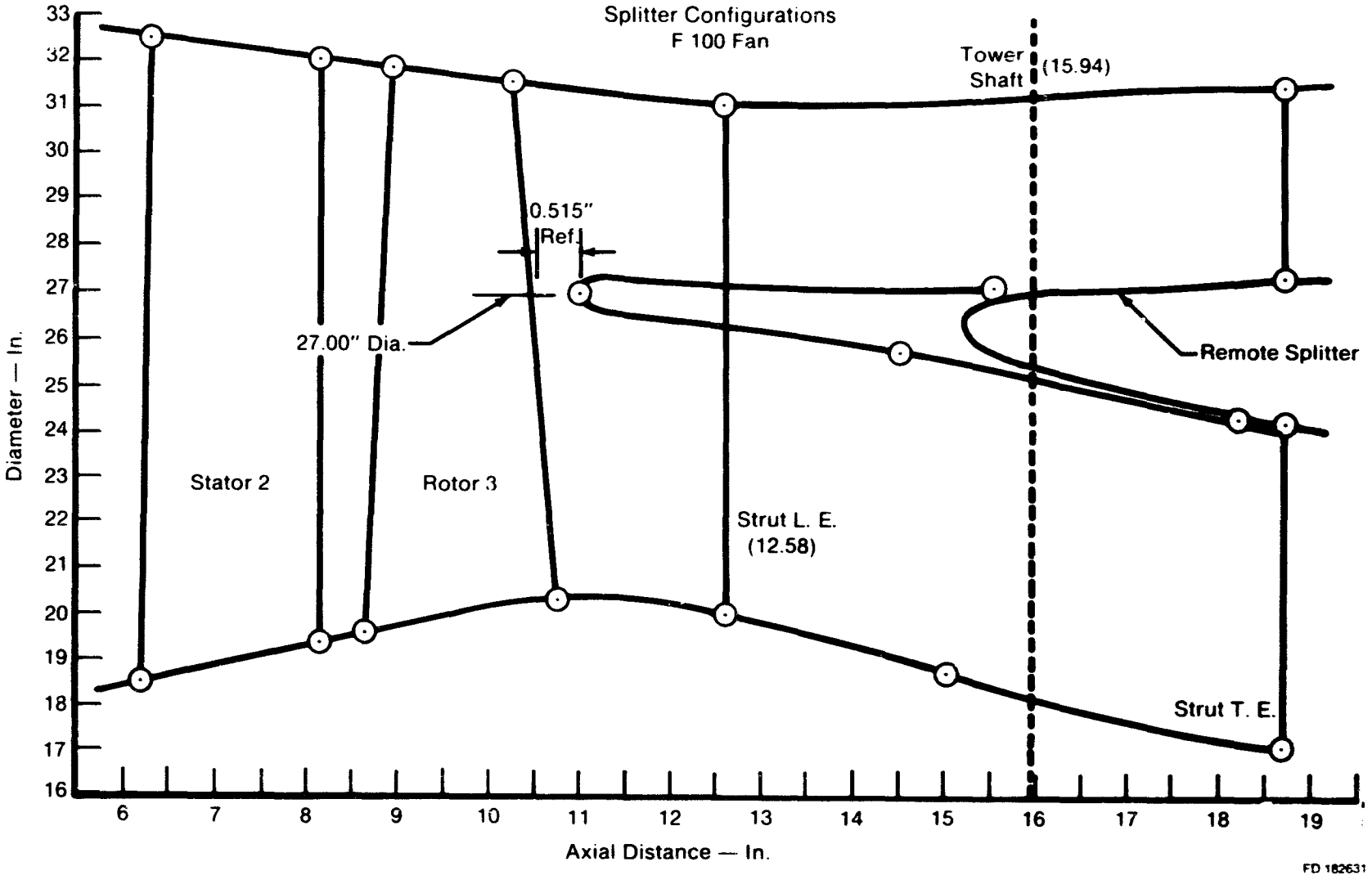

Figure 6. Schematic of Remote Splitter and Proximate Splitter Configurations

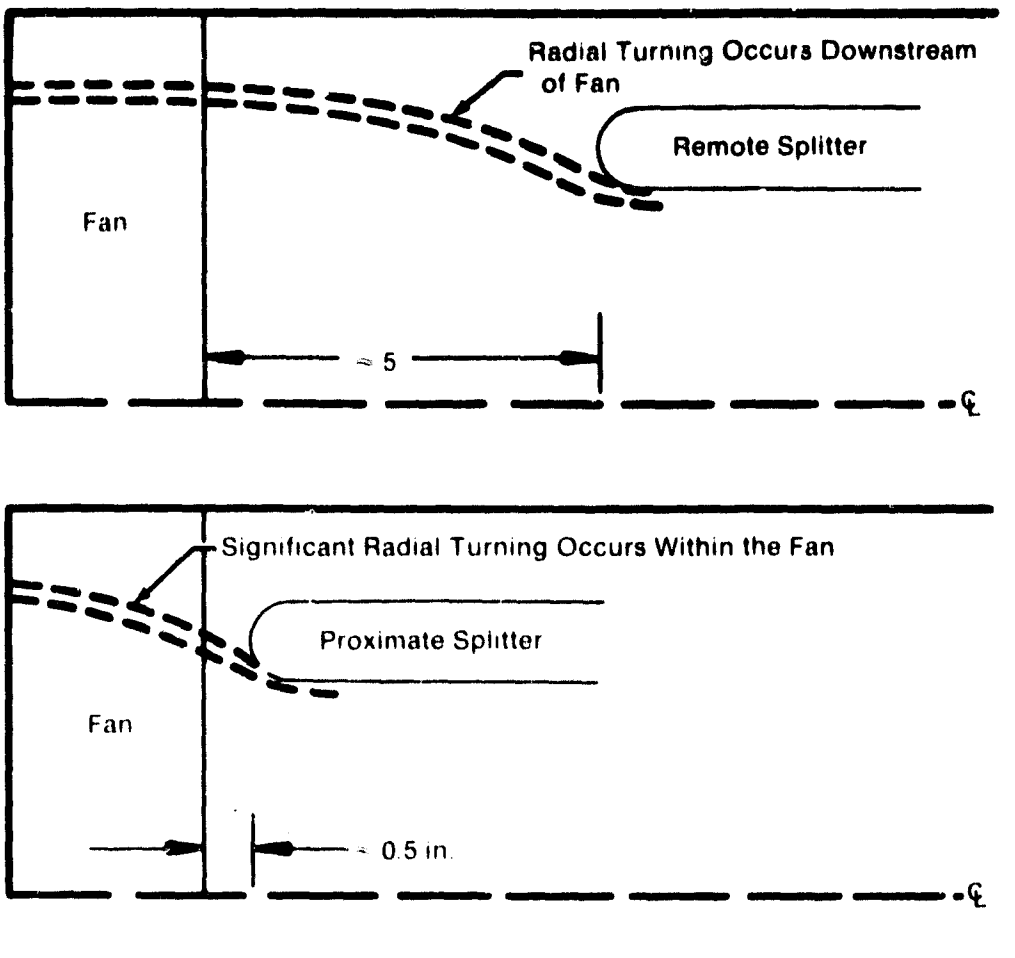

ED 196249

Figure 7. F100(3) Splitter Configuration Affects Location of Radial Turning of Streamlines

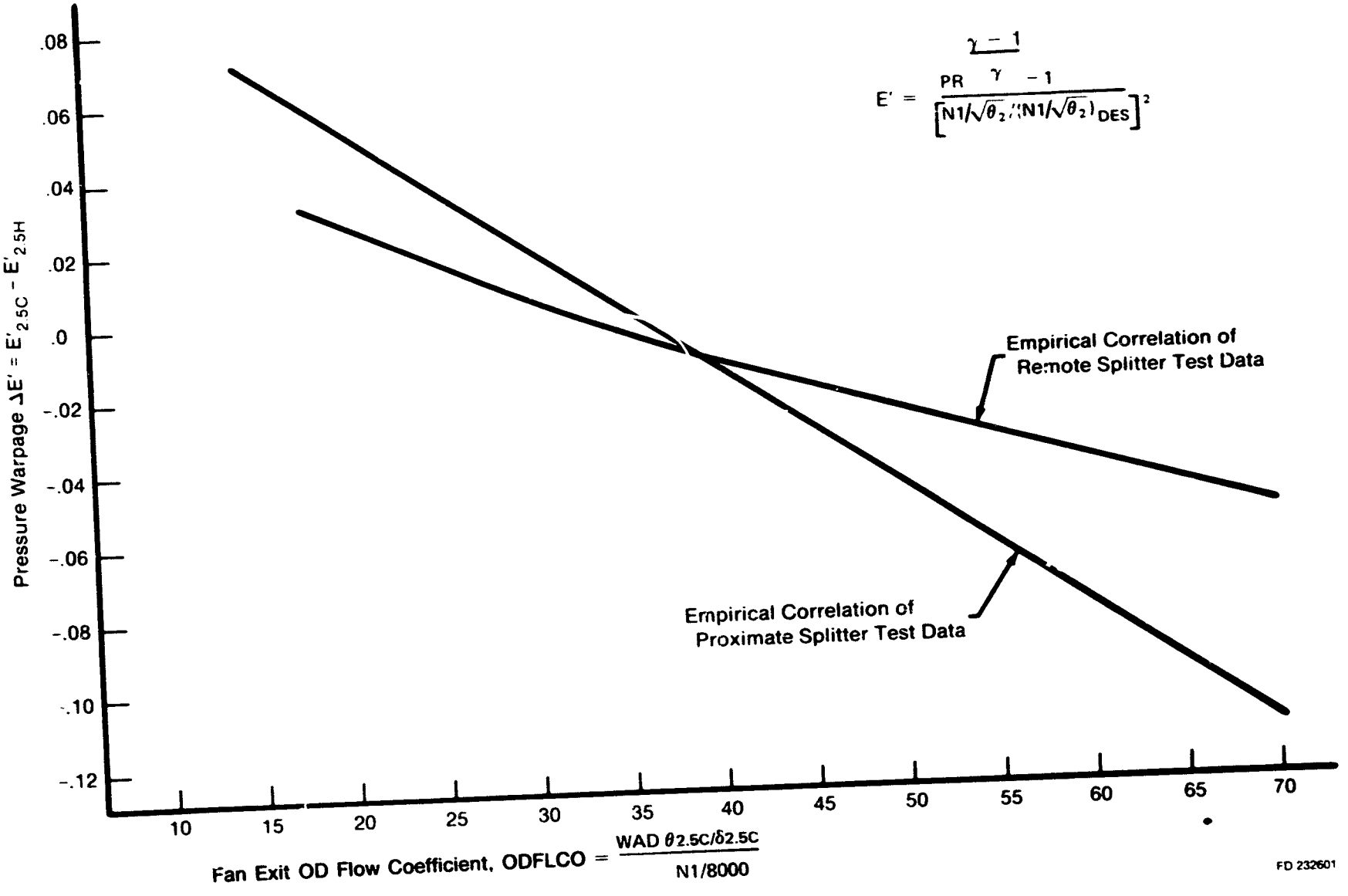

Figure 8. Total Pressure Warpage at Fan Exit, Comparison of F100(3) Remote and Proximate Splitters

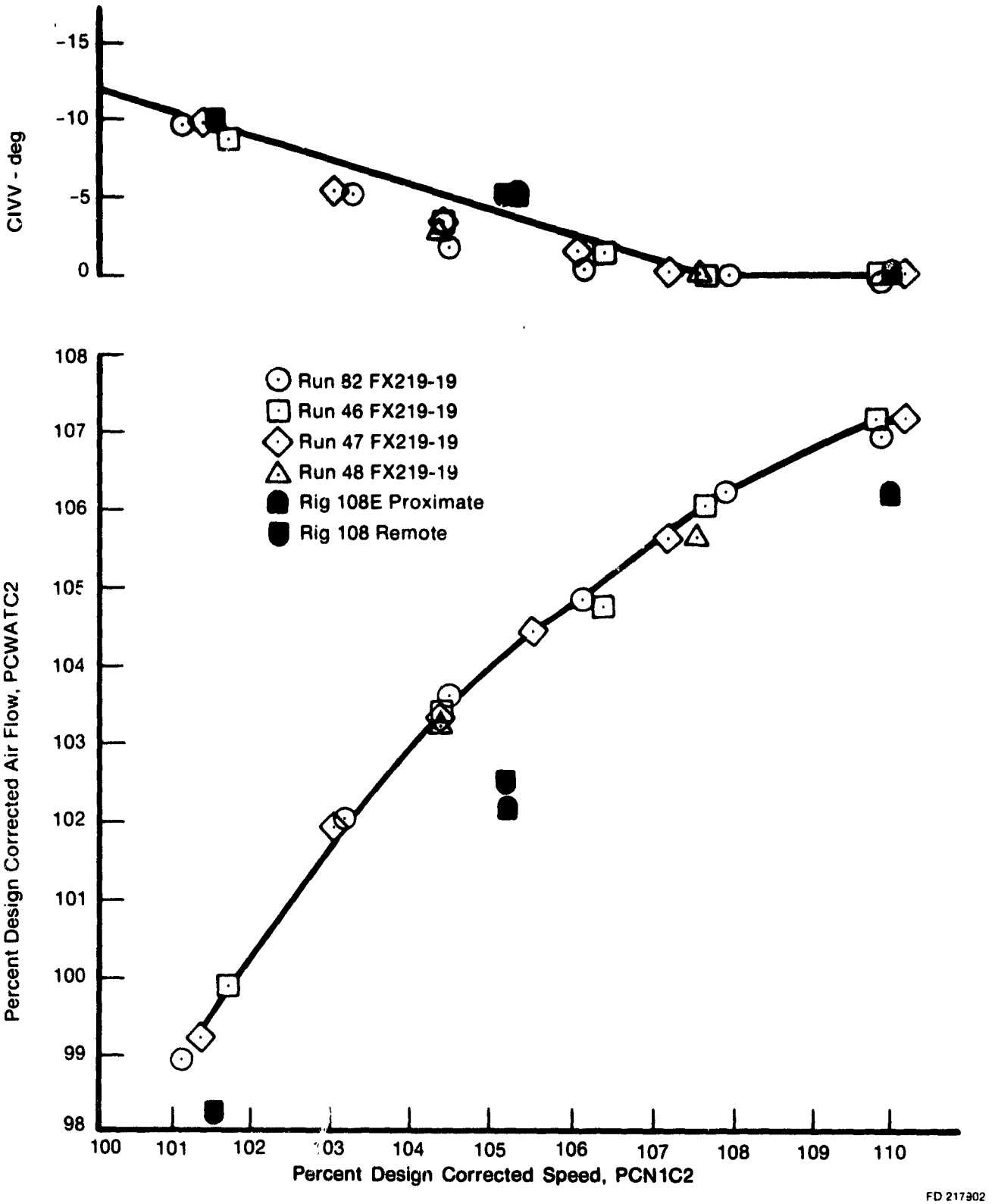

Figure 9. Comparison of FX219-19 and Rig 108 Speed/Flow Relationships

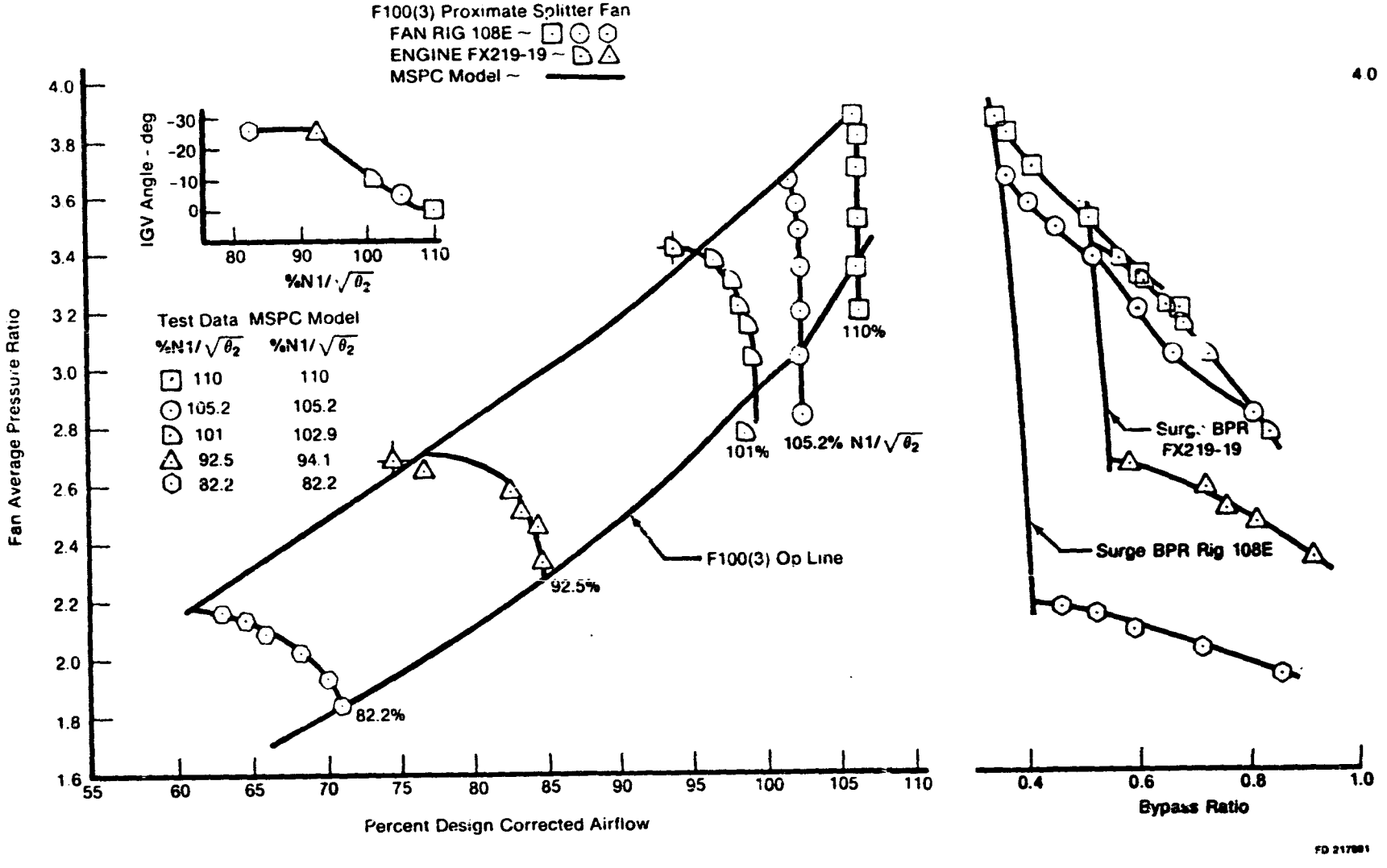

Figure 10. F100(3) Proximate Splitter Fan Speedlines

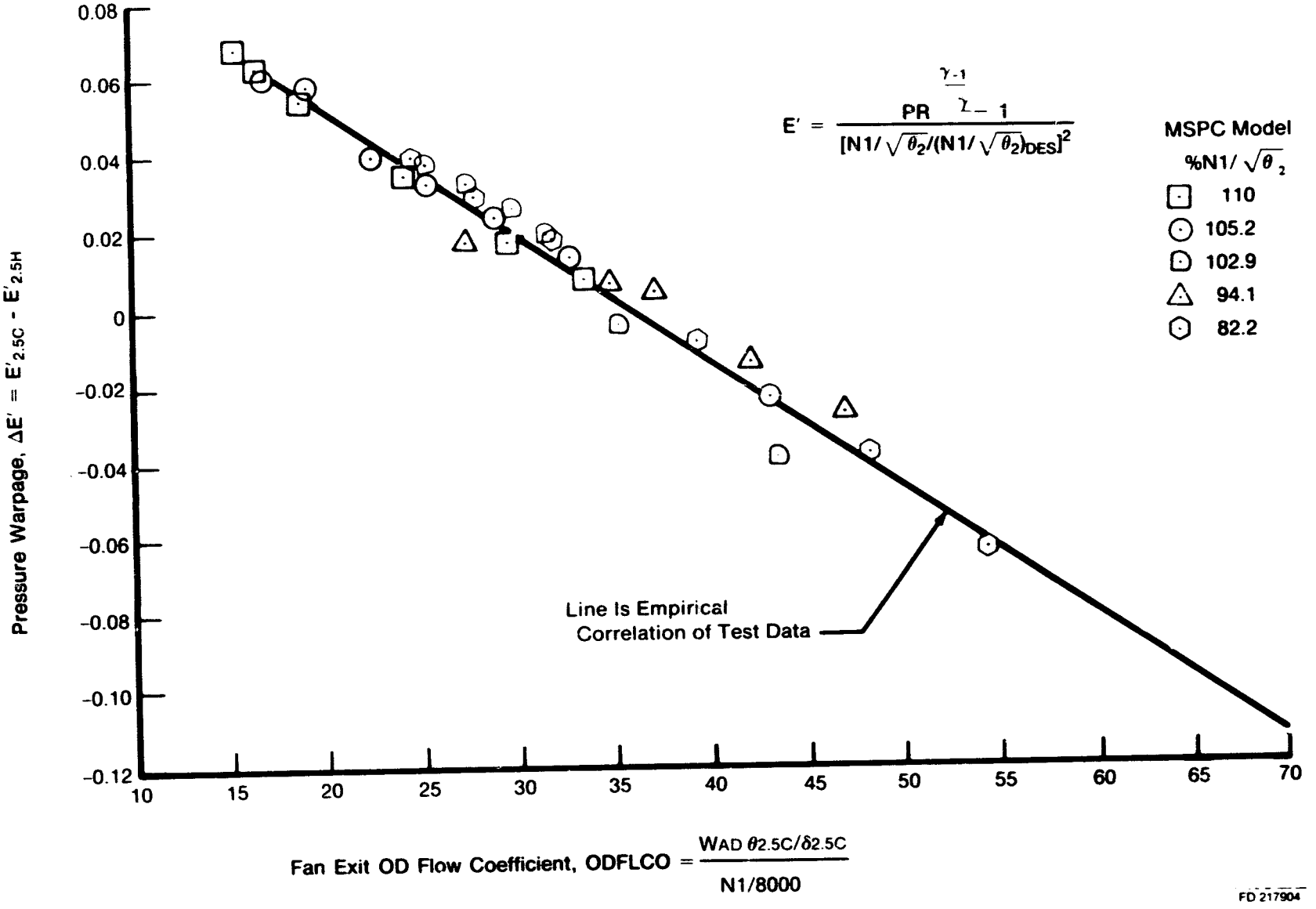

Figure 11. Total Pressure Warpage at Fan Exit, F100(3) Proximate Splitter Fan Model

The determination of the area ratio contribution to pressure warpage for the remote splitter configuration required a trial and error solution. It was unclear at what axial position the upstream duct and core side areas should be calculated. As that location approaches the splitter nose the contribution of area change to static pressure rise is diminished, and in the limit a truly remote splitter could be shown to have no effect on the fan duct and core side pressure rise capabilities. It was assumed at design bypass ratio the splitting streamline is aligned with the splitter nose. For other bypass ratios, the actual splitting streamline shape is represented with a geometric function, Y; where Y is the radial distance between the design and actual splitting streamlines at some axial distance XRS.

$$Y = A \cos \left(\frac{\pi}{2} \frac{XRS}{L} \right)$$

where

A = Radial distance between "design" and actual splitting streamlines at Rotor 3 Leading Edge (R3 LE), which is a function of input BPR

L = Distance from R3 LE to remote splitter nose

XRS = Distance from R3 LE

For example, Figure 12 shows the streamline shape that the model calculates for a bypass ratio of 0.4. Knowing the shape of the splitting streamline, the area change for the ID and OD streams can be calculated and the additional static pressure change found by using the same one-dimensional equation discussed previously.

In determining the proper value of XRS, the axial distance at which the upstream area is calculated, the model was executed for several values and the resultant overall pressure rise and pressure warpage characteristics compared to remote splitter fan data. Three bypass ratio schedules were run: 0.4, 0.8, and the rig data schedule. Upon choosing a value of 5.5 inches for XRS (approximately 1 inch in front of the splitter nose), the model calculations show reasonable agreement to remote splitter fan rig data. In Figures 13 and 14 the model-predicted pressure warpage and overall pressure ratio show that, as would be expected for a remote splitter fan, the bypass ratio has little influence on overall performance. This supports the modeling of bypass ratio used for both the proximate and remote splitter in this contract. The revised remote splitter model was then executed for 5 speeds from 70% to 105% of design with XRS fixed at 5.5. Figures 13 and 15 show that the model-predicted pressure warpage and overall fan performance agree well with remote splitter fan rig test results.

2. Undistorted Post-Stall Characteristics

Fan distortion response is dependent upon post-stall blade and vane row performance characteristics. No post-stall data exists for the F100(3) proximate splitter fan. The verification of the model's stalled characteristics was made through the execution of a pressure distortion test case and comparing the model calculations to proximate splitter fan distortion data. With distortion, the fan operates at local flowrates below the undistorted stall point due to unsteady flow effects in the rotors. A 180-degree, 18% max-min/avg pressure distortion was chosen as the test case. This case approximates distortion testing conducted with a 180-degree, $5\frac{1}{2} \times 5\frac{1}{2} \times 0.063$ mesh screen on FX219-19 at Arnold Engineering and Development Center for the purpose of documenting F100(3) proximate splitter distortion sensitivity. Operating at 100.1% of design air flow on the operating line, FX219-19 was backpressured along a constant 101.7% speedline by reducing engine jet area until stall occurred — a nozzle plug was required to induce stall.

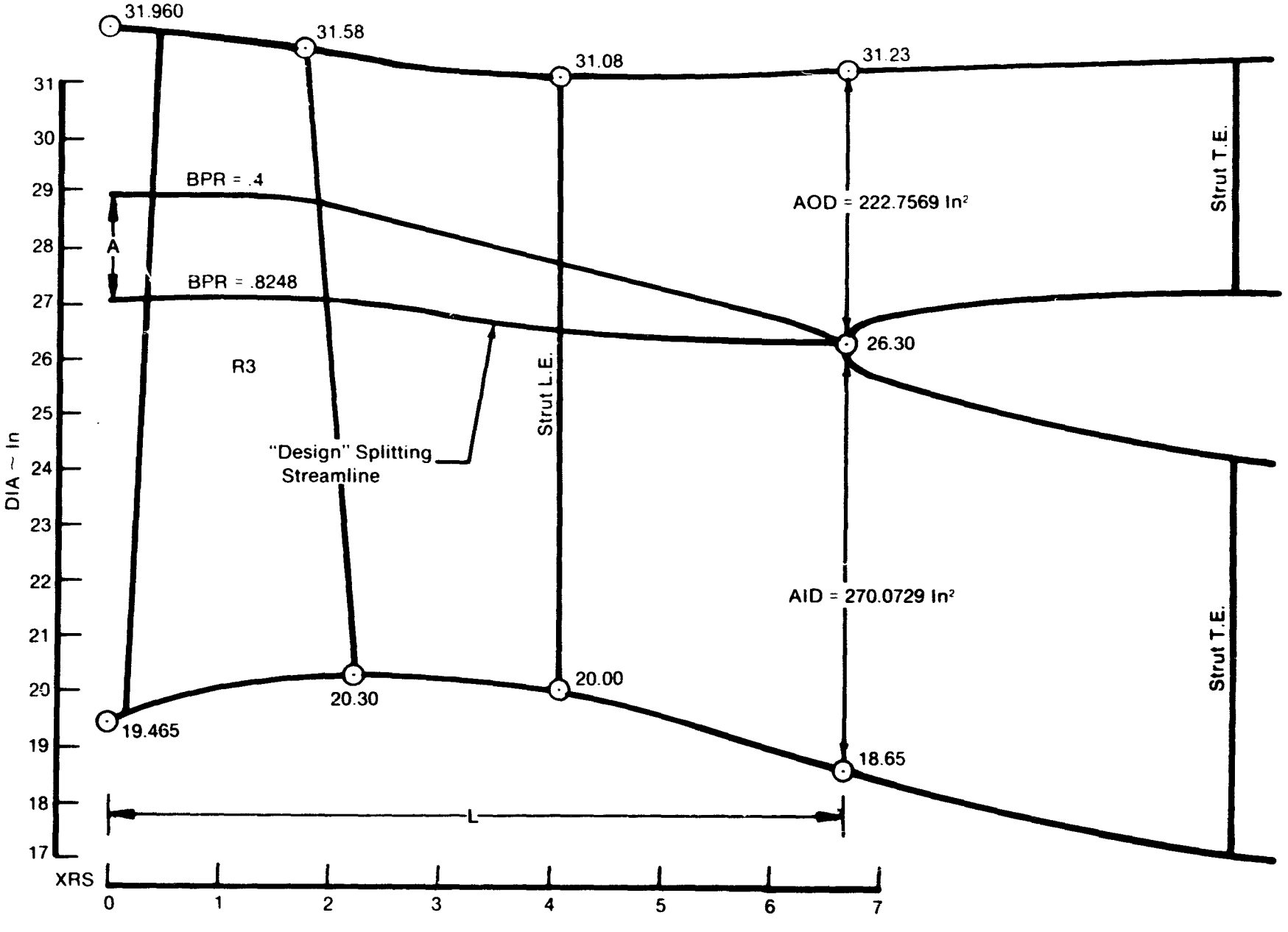

Figure 12. F100(3) Remote Splitter Fan Streamline Shapes

FD 232606

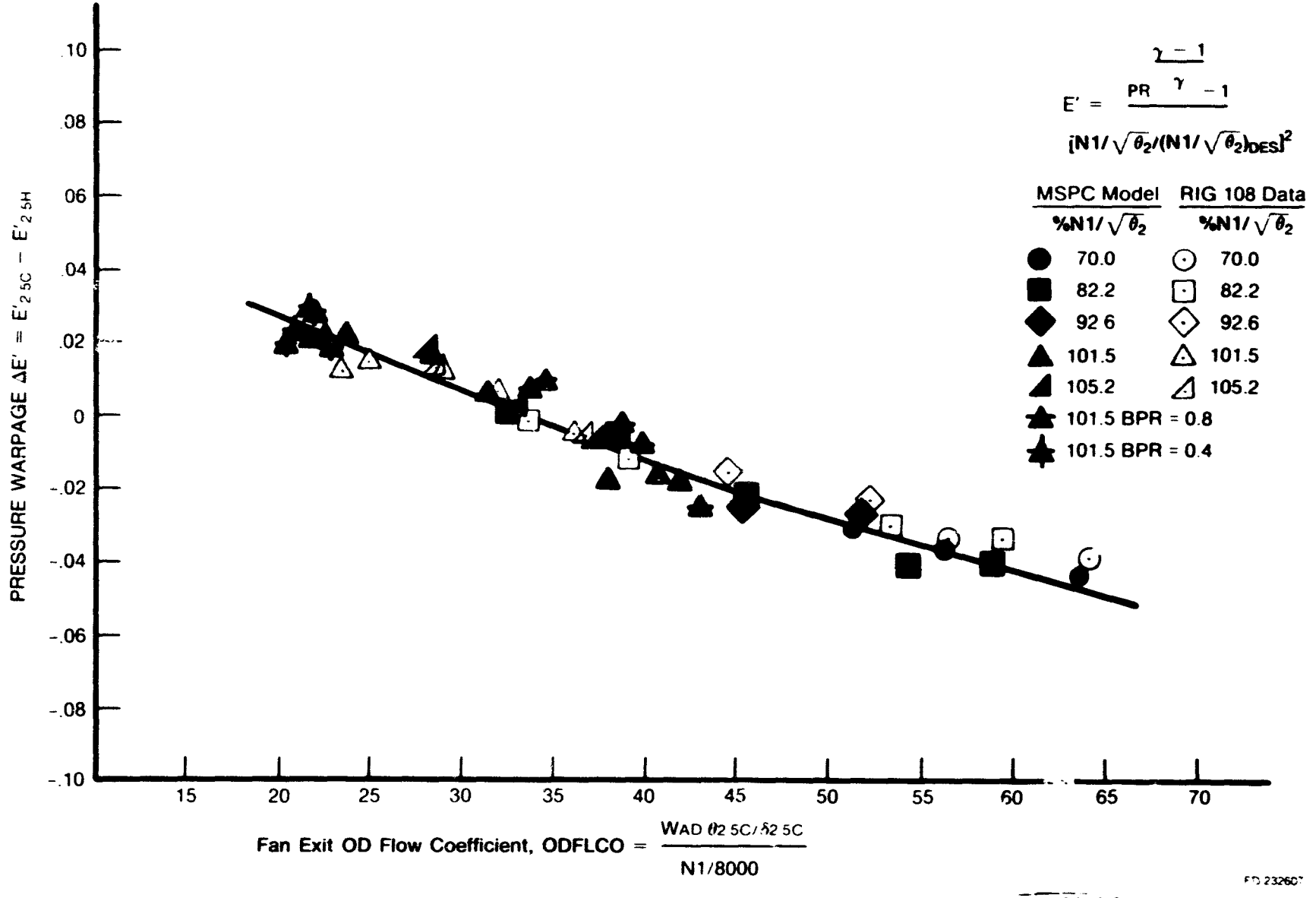

Figure 13. Total Pressure Warpage at Fan Exit, F100(3) Revised Remote Splitter Fan Model

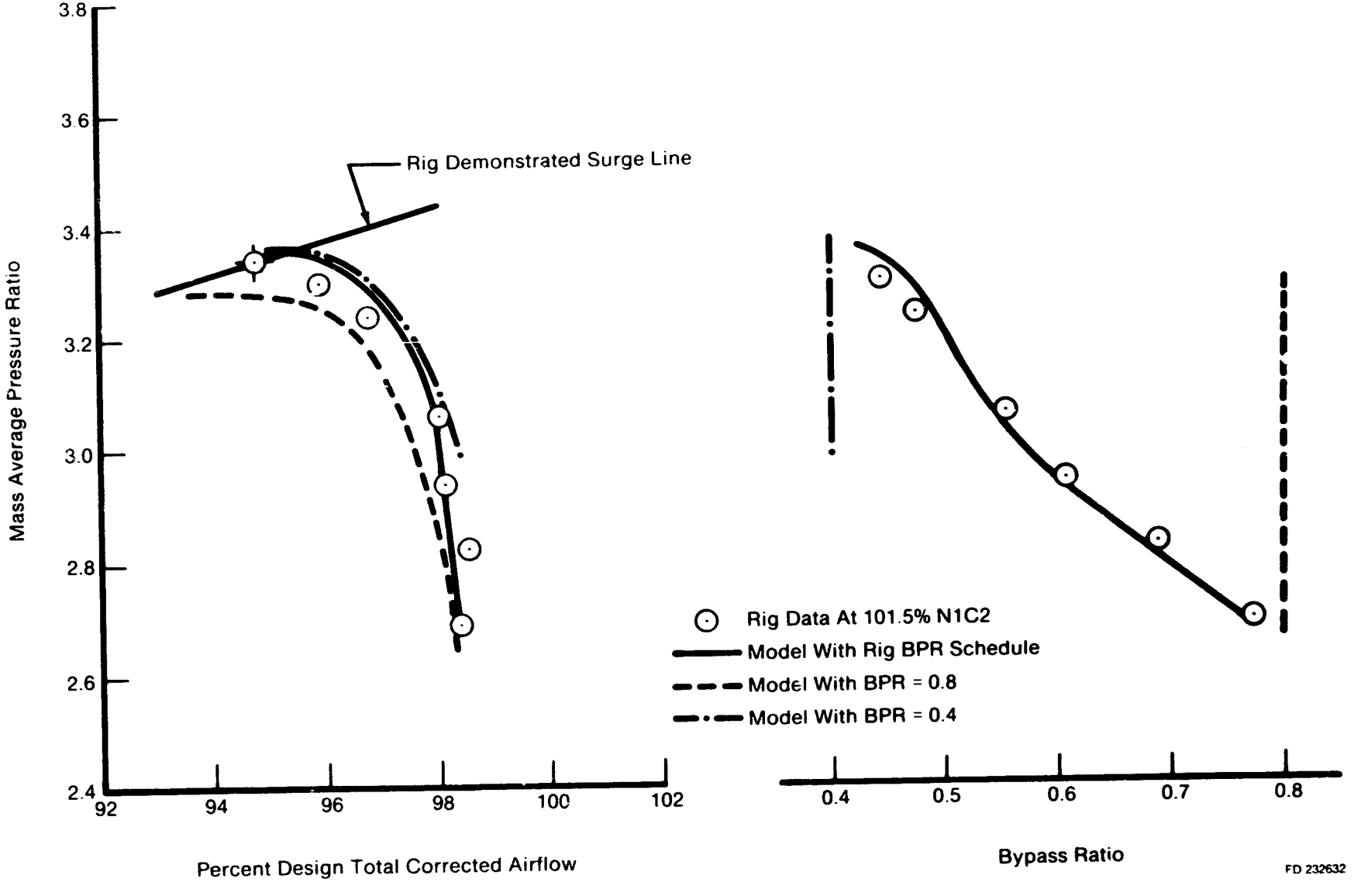

Figure 14. Effect of Input Bypass Ratio on Revised Remote Splitter Model Predicted Fan Performance

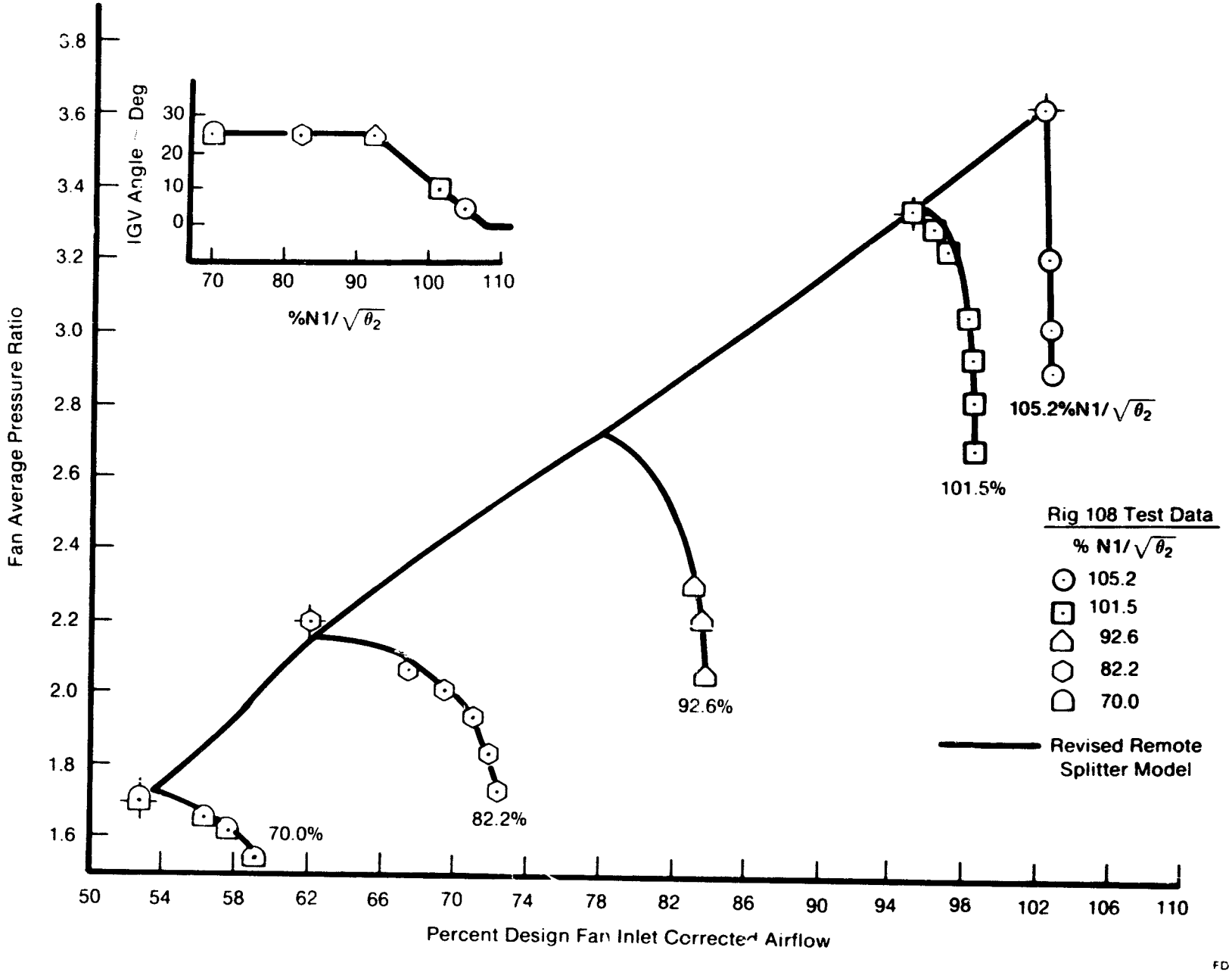

FD 232633

Figure 15. F100(3) Remote Splitter Fan Data Compared to Revised Remote Splitter Model Predictions

The model was run similarly. Input speed was varied until the model matched on the operating line at design flow with the 18% inlet pressure distortion. This required a speed of 103.9% of design and the corresponding on-schedule CIVV of −7 degrees. Holding speed constant, the fan was backpressured in small increments until stall. The bypass ratio at stall was set equal to 0.52. Figure 16 shows the bypass ratio schedule run by engine FX219-19 with an undistorted inlet. The distorted bypass ratio for the test case was chosen to equal the undistorted bypass ratio at stall, 0.52. In order to adequately predict FX219-19 proximate splitter lapse rates, adjustments were required to the model's rotor 3 stalled pressure rise characteristics.

After these adjustments, the proximate splitter fan model was compared to FX219-19 data. The model calculated that the test case stalls at 95.4% of design flow with a pressure ratio of 3.304. Figure 17 compares the calculated lapse rate of 4.37 to the FX219-19 value of 3.4. The attenuation of the inlet pressure distortion is 0.489 (attenuation = $1 - K\theta_{out}/K\theta_{in}$) on the operating line while Figure 18 shows the test value to be 0.417. Figure 19 shows the operating line value of temperature distortion generation for the test case is calculated to be 0.262. It is compared to an empirical relationship generated from remote splitter tests because instrumentation limitations did not allow definition of exit temperature profiles from FX219-19 data. Based on these results, further modifications to the proximate splitter characteristics were considered unnecessary and the proximate splitter version of the MSPC model was verified. The blade row performance characteristics are shown in Appendix I.

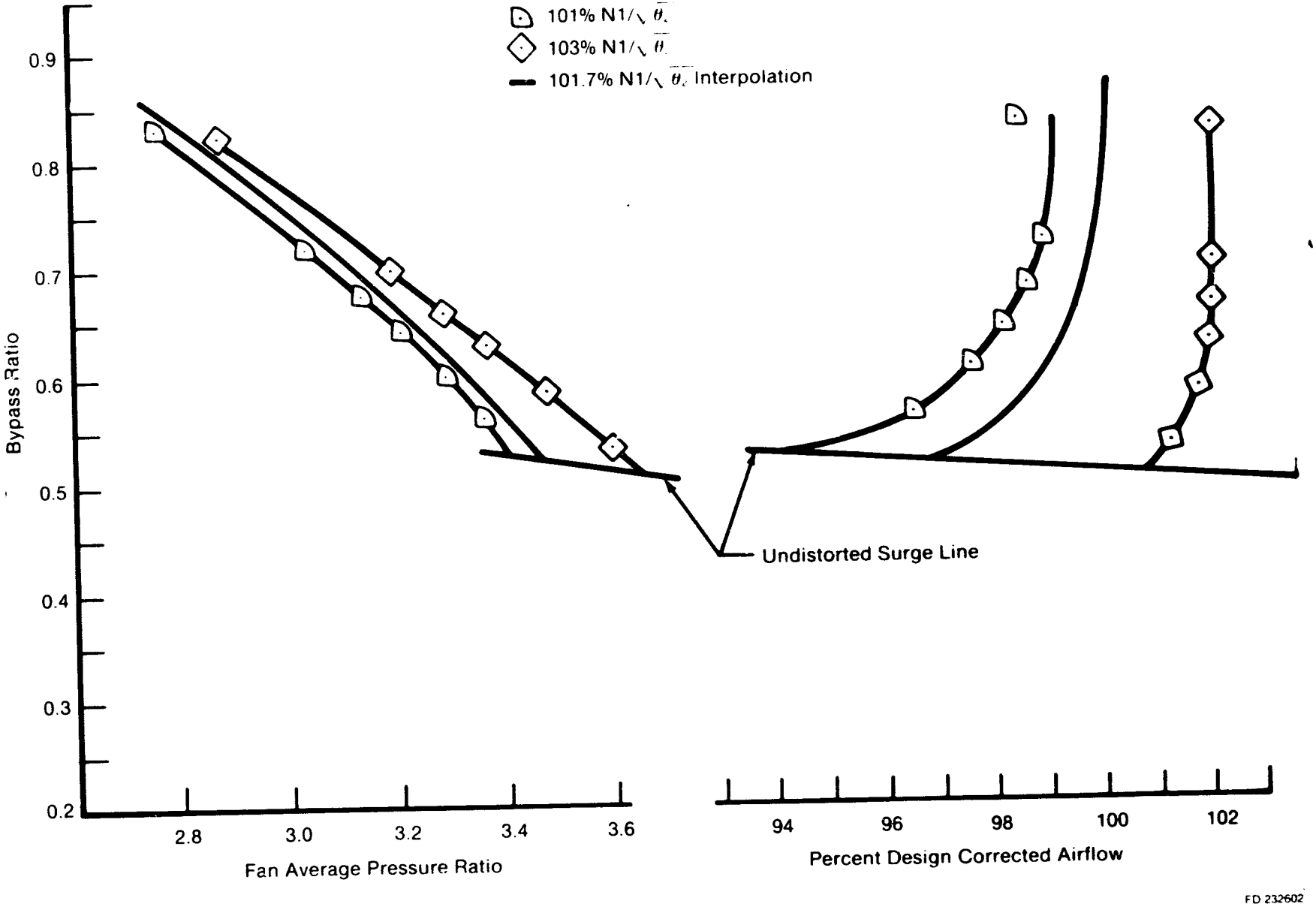

Figure 16. Engine FX219-19 Run 82 Undistorted Speedlines

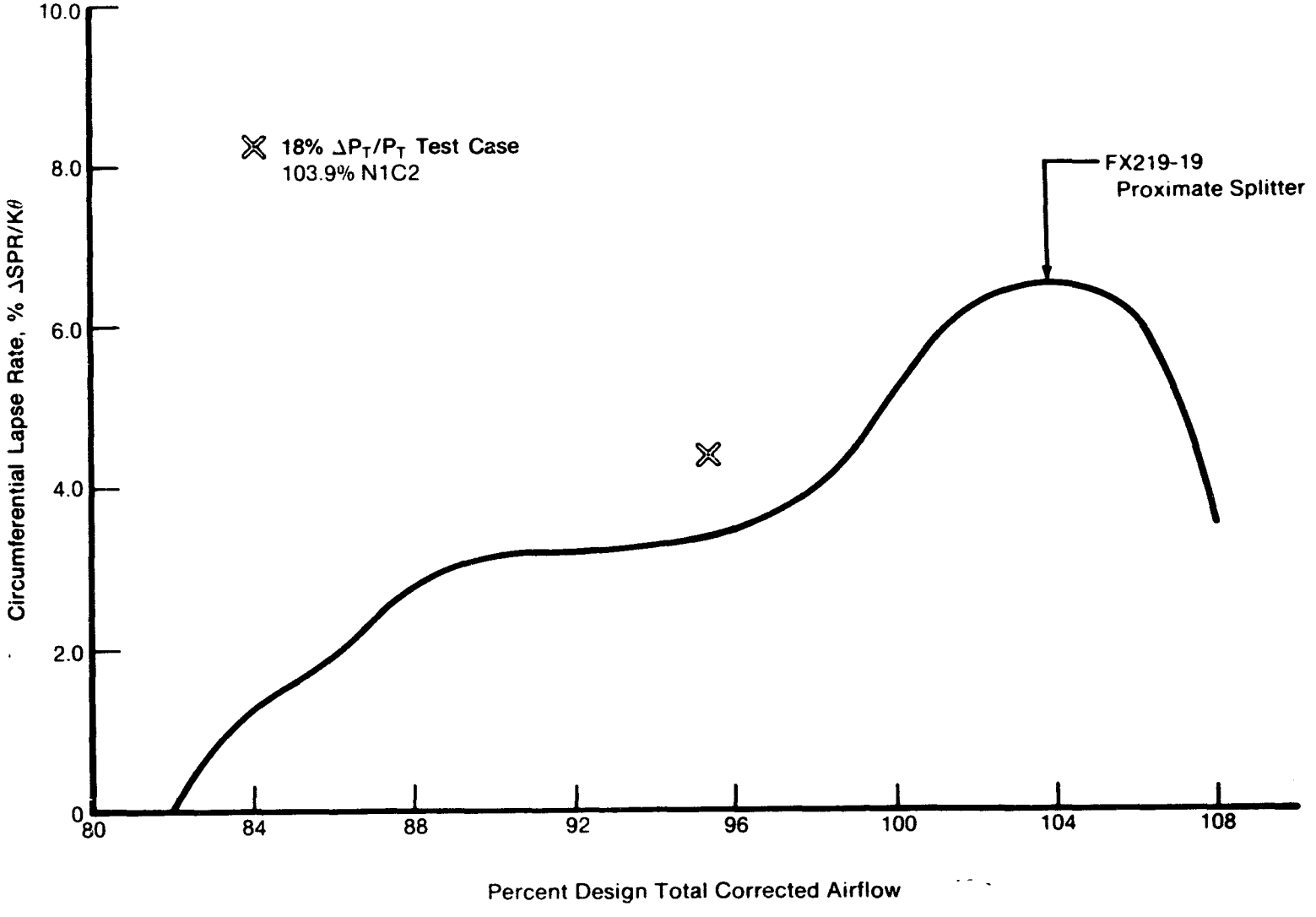

Figure 17. Model Predicted Lapse Rate Compared to FX219-19 Test Results

FD 232603

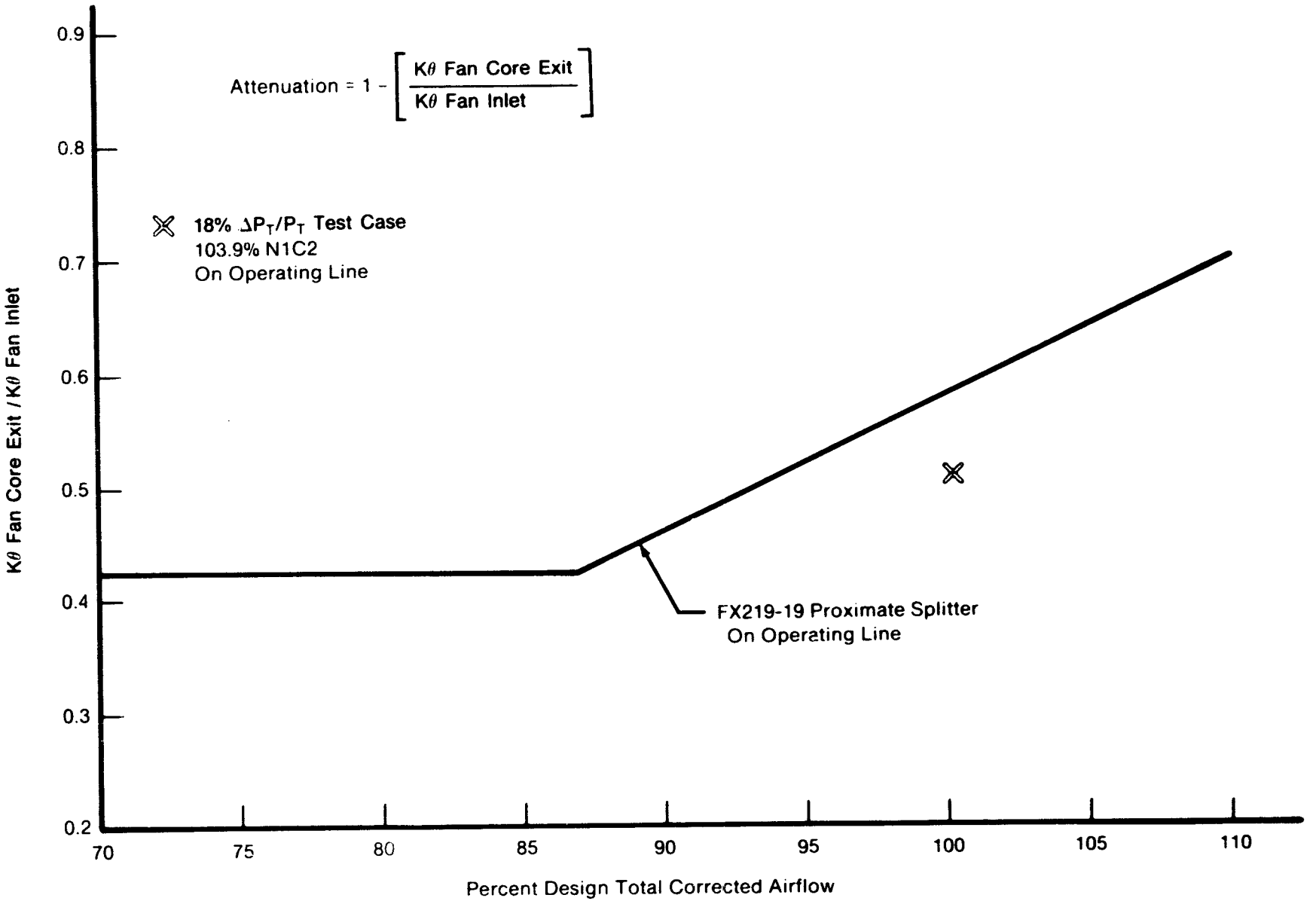

Figure 18. Model Predicted Pressure Distortion Attenuation Compared to FX219-19 Test Results

FD 232804
820802
bt2 968

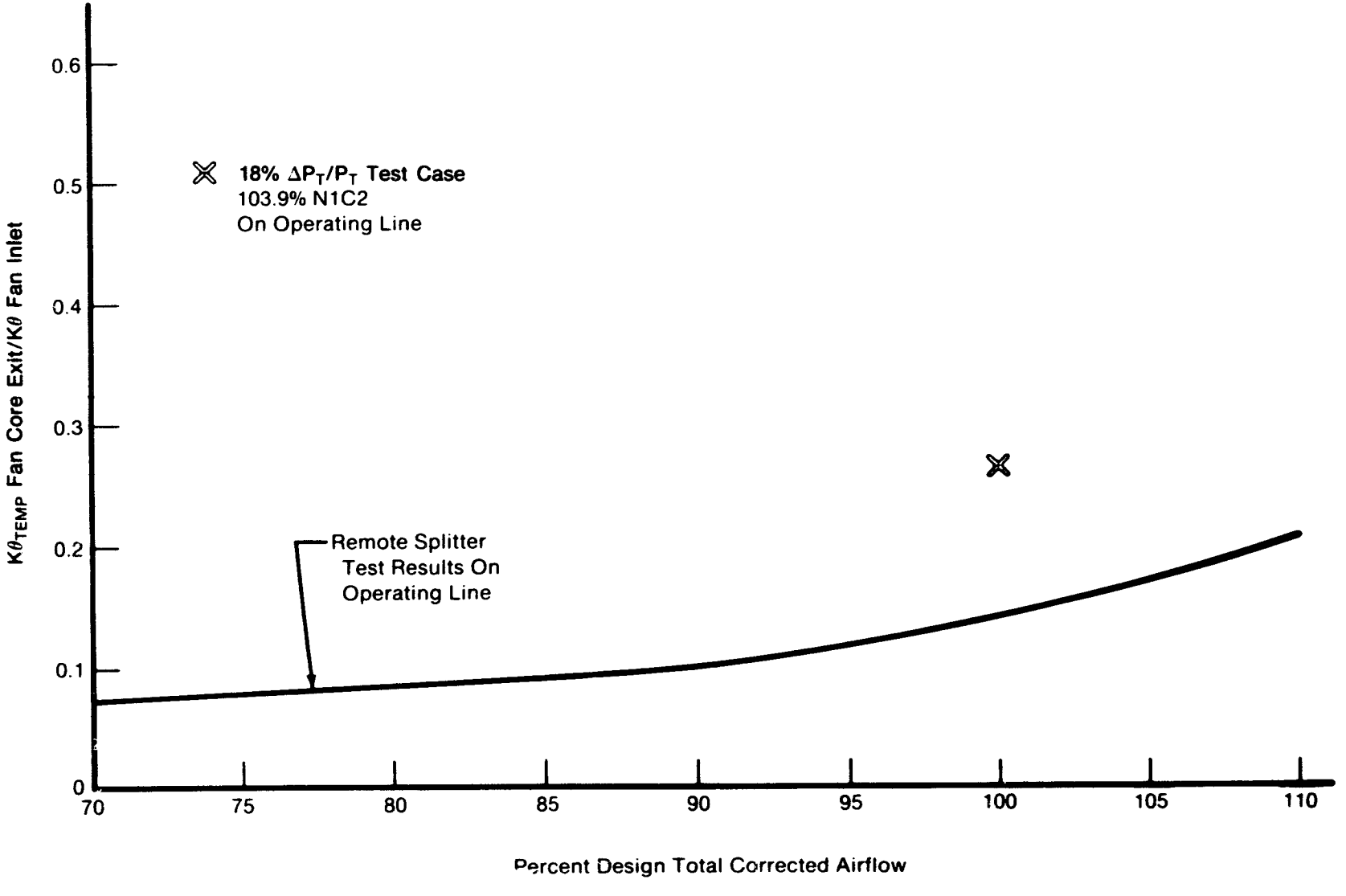

Figure 19. Model Predicted Temperature Distortion Generation Compared to Remote Splitter Test Results

FD 232605

ANALYSIS PROCEDURE

General

F100(3) circumferential distortion response characteristics were predicted for a remote fan exit splitter configuration under a previous NASA contract. These results are reported in CR-159754, Reference 3. Wherever possible, the analysis procedures used were consistent with those established in Reference 3. Considerable effort was saved by taking advantage of this experience gained with the MSPC model. Consistent analysis procedures also allow meaningful comparisons between proximate and remote splitter results.

F100(3) proximate splitter fan distortion response was predicted for six distortion cases, as shown in Table 1.

TABLE 1. CIRCUMFERENTIAL PRESSURE AND TEMPERATURE DISTORTION STUDY CASES

Case	*Distortion Type*	*Distortion Amplitude (Maximum-Minimum)/ Average (%))*	*Extent of Distortion (Deg)*	*Fan Speed (% of Design)*
1	Pressure	22	180	102
2	Pressure	22	90	102
3	Pressure	15	180	102
4	Temperature	18	[1]180	102
5	Temperature	9	[1]180	102
6	Temperature	18	[1]90	102

[1]High temperature distortion sector centered 180°F from T2.5 sensor location

Stall Criteria

Backpressuring both the fan bypass and core section until the maximum exit static pressure was achieved determined the stall limiting air flow for each section. Fan stall occurs when the stall limiting air flow for either the bypass or core section is reached, and the stall point pressure ratio is the mass average of the bypass and core pressure ratios at the fan stalling air flow. The backpressuring process was achieved by incrementally increasing the fan exit static pressure; as the required pressure increases, the average flowrate decreases, as shown in Figure 20. An attempt to increase the pressure beyond the stall point results in a large redistribution of mass flow around the circumference, such that a continuous mass flow distribution cannot be found to satisfy a higher pressure. See Reference 5 for a more detailed explanation.

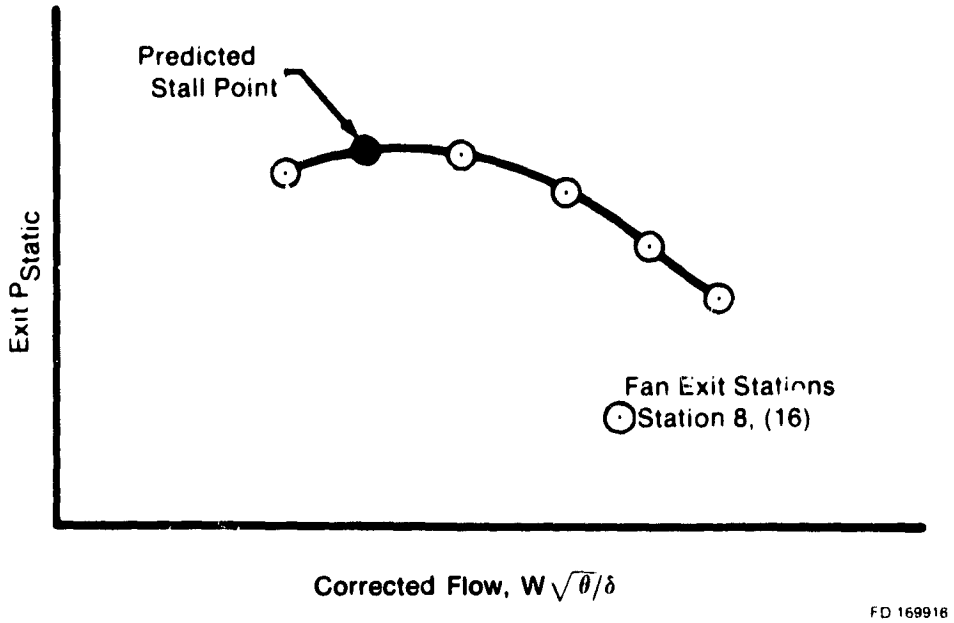

Figure 20. Stall Criteria: Max Static Pressure at Exit Station

Distortion Response Parameters

The determination of compression system response to distortion requires quantifying the magnitude of the inlet distortion and the corresponding loss in surge pressure ratio. As a result, a distortion descriptor system is needed to quantify the distortion. In this study both the F100(3) Kθ distortion descriptor system and the "classical" $\Delta P_T/P_T$ max-min/avg, $\Delta T_T/T_T$ max-min/avg descriptors were used in the response analysis. A brief description of the F100(3) Kθ distortion descriptor system is given in Appendix III. Several parameters were used to define the engine distortion response characteristics:

1. Stall line degradation of the fan — % Δ SPR/Kθ. Surge margin loss was defined as the percentage difference between the mass average undistorted and distorted stall pressure ratio at the distorted stalling air flow rate. Kθ was defined as the inlet distortion level at the distorted stalling airflow.

2. Fan attenuation/generation of pressure and temperature distortion across the fan core stream — defined in terms of the level of component exit distortion for each imposed inlet distortion and predicted both on the operating line and at stall.

3. The distortion path through the stages of the fan — defined in terms of the row by row acoustic and particle flow angles. In addition, the circumferential pressure and temperature profiles were defined at the fan inlet and exit.

Individual Distortion Response

Six distortion cases were examined with the MSPC model to predict F100(3) proximate splitter fan distortion response. Figure 21 shows the three inlet pressure distortion cases and the three inlet temperature distortion cases that were analyzed. These cases vary the distortion amplitude and the circumferential extent. Average inlet total pressure of $5.171\times10^4/m^2$ (7.5 psia) and inlet total temperature 267.9°K (482.3°R) correspond to expected inlet conditions for NASA-LeRC F100(3) distortion tests. Average corrected fan speed is 102% of design or 9842 rpm. A detailed description of model input parameters can be found in Appendix II.

In each distortion case, the fan stall point was defined by increasing the fan exit static pressure (step size = 1.001) while holding the fan corrected speed and bypass ratio constant until stall occurred. Bypass ratio at stall for all cases was chosen to match the bypass ratio at stall of the pressure distortion test case, 0.52. A constant exit static pressure boundary condition was assumed for both the fan bypass stream and fan core stream based on existing F100 test experience. Eighteen parallel compressor segments defined the circumferential flow field through the fan. In calculating fan core exit circumferential distortion, $K\theta$, the model-predicted profile was processed through a Pratt & Whitney Aircraft distortion analysis deck.

Attenuation of inlet pressure distortion across the fan core stream and the corresponding temperature distortion generation have been documented for proximate splitter engine FX219-19 on its operating line. In order to provide a consistent comparison, operating line transfer characteristics were predicted by the model. Each case inlet airflow was varied with speed set at 102% and bypass ratio at 0.775 (as per FX219-19), until the mass-averaged pressure ratio matched the operating line.

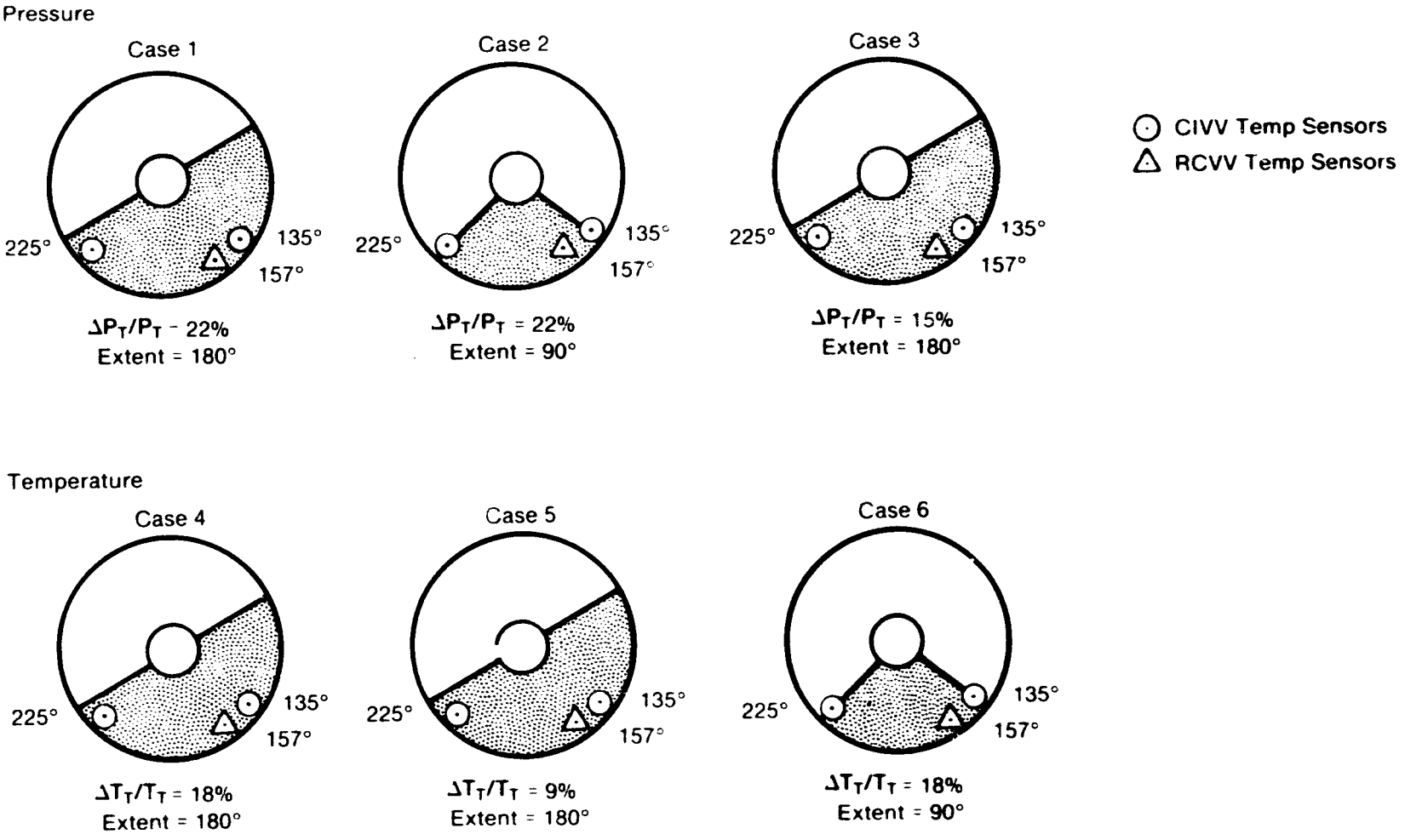

FD 17342-A

Figure 21. Six Inlet Distortion Cases

RESULTS AND DISCUSSION

FAN RESPONSE TO INLET DISTORTION

1. Pressure Distortion

Proximate splitter fan response to inlet pressure distortion was calculated for three different patterns at 102% corrected speed. Additionally, the 18% pressure distortion test case was run at 103.9% corrected speed. Figure 22 shows the predicted fan surge points for these distortions. The 22% $\Delta P_T/P_T$, 180-degree distortion results in a lower surge line than the 15% $\Delta P_T/P_T$, 180-degree distortion, as one would expect. For the same 22% $\Delta P_T/P_T$ distortion amplitude, the 90-degree distortion results in a lower surge line than the 180-degree distortion.

Figures 23 and 24 show a comparison of model-predicted distortion sensitivity to the F100(3) proximate splitter stability correlation which is based on FX219-19 test data. Figure 23 shows this comparison using the F100(3) Kθ distortion factor system, while Figure 24 presents the comparison in terms of the classic $\Delta P_T/P_T$ max-min/avg parameter. The F100(3) proximate splitter stability correlation levels shown in Figure 24 were established by converting the Kθ correlation into an equivalent $\Delta P_T/P_T$. Separate correlation levels result for 90-degree and 180-degree distortion since the $\Delta P_T/P_T$ system only accounts for the distortion level and not its angular extent.

Figure 23 shows that the model predicts the proximate splitter fan is more sensitive to inlet pressure distortion than the F100(3) correlation. The three 180-degree distortions have lapse rates ranging from 4.3 to 5.9, while the correlation lapse rate is 3.4. The 22% $\Delta P_T/P_T$, 90-degree distortion is predicted to have a lapse rate of 10.3 , much higher than the model predictions for 180-degree distortions and the proximate splitter correlation. The lapse rate correlation, shown in Figure 23, was calculated based on engine FX219-19 fan response behind a 180-degree moderate intensity screen. Since the Kθ system accounts for both distortion amplitude and extent, *theoretically* a lapse rate correlation generated from a 90-degree screen would match the one generated with a 180-degree screen; however, this has not been verified as the F100(3) fan has only been tested behind 180-degree distortion screens. The model predicts that for an equal amount of inlet pressure distortion Kθ, a 90-degree distortion will cause a lower surge line than a 180-degree distortion.

When comparing the model-calculated lapse rates to the correlation, it is appropriate to note that the empirical results are estimated to have ± 0.85 uncertainty band width. The model-calculated lapse rates exceeded this band and thus overpredict the lapse rate. It would have been possible to bring cases 1 and 2 within the empirical band, and therefore, show a better match with the correlation, if the post-stall characteristics for the rows ahead of rotor 3 were modified. It could be reasoned that when the model-calculated lapse rates match the proximate splitter correlation, the post-stall characteristics developed for the model must be reasonably representative of actual characteristics. If the only function of the proximate splitter model were to investigate distortion patterns not previously tested, such action might be advisable. But the concern is that further modifications to the proximate splitter model would compromise the comparison to the calculated remote splitter fan distortion response previously reported. By maintaining commonality between proximate and remote splitter fan's post-stall performance characteristics through Stator 2, it is believed the comparison will more accurately show the effect fan exit splitter spacing has on distortion response. In light of the lack of actual definition of post-stall characteristics or a back to back splitter test, this was the course of action taken.

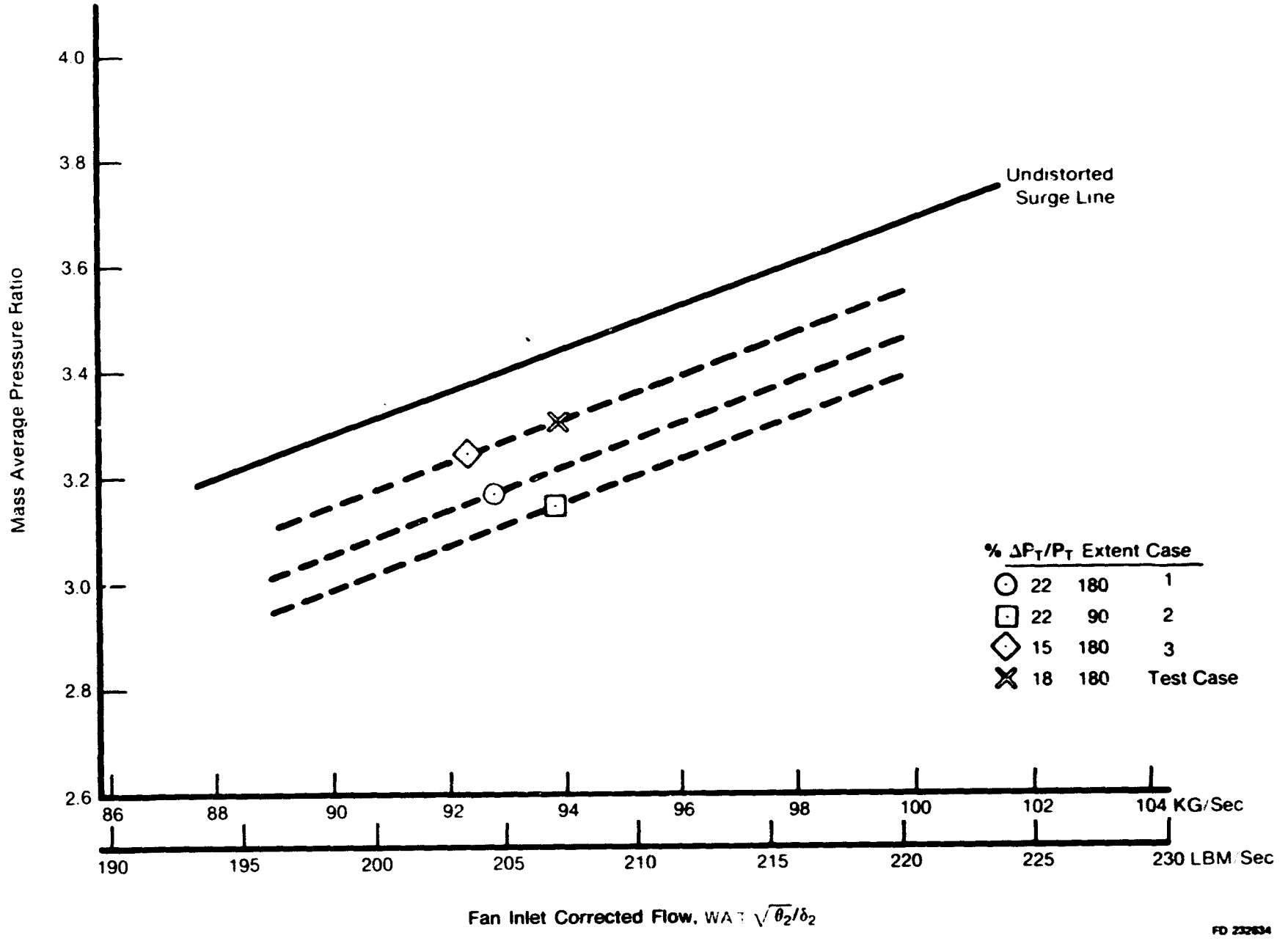

Figure 22. Predicted F100(3) Proximate Splitter Fan Surge Lines With Pressure Distortion

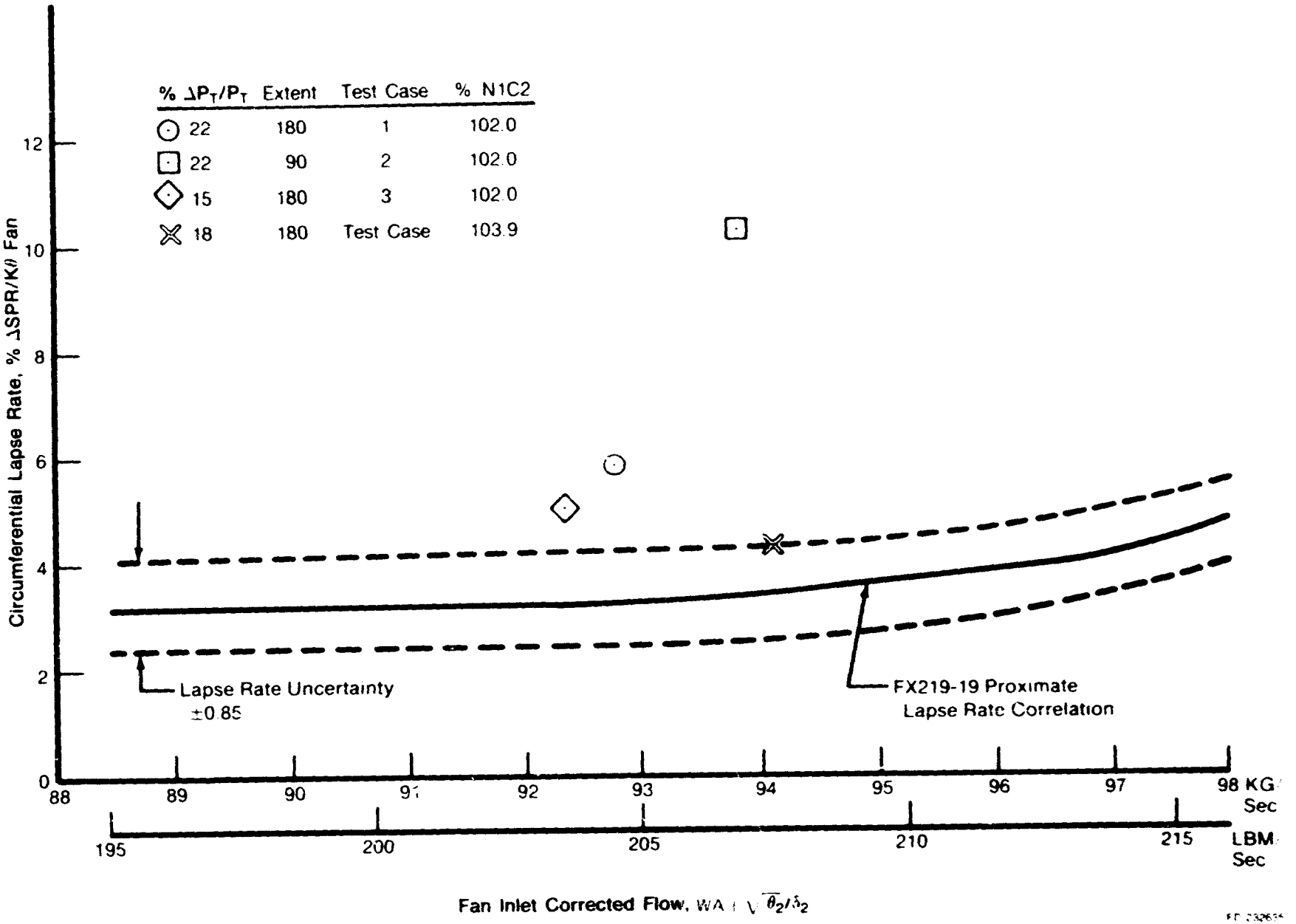

Figure 23. Predicted F100(3) Proximate Splitter Fan Circumferential Pressure Distortion Kθ Sensitivity

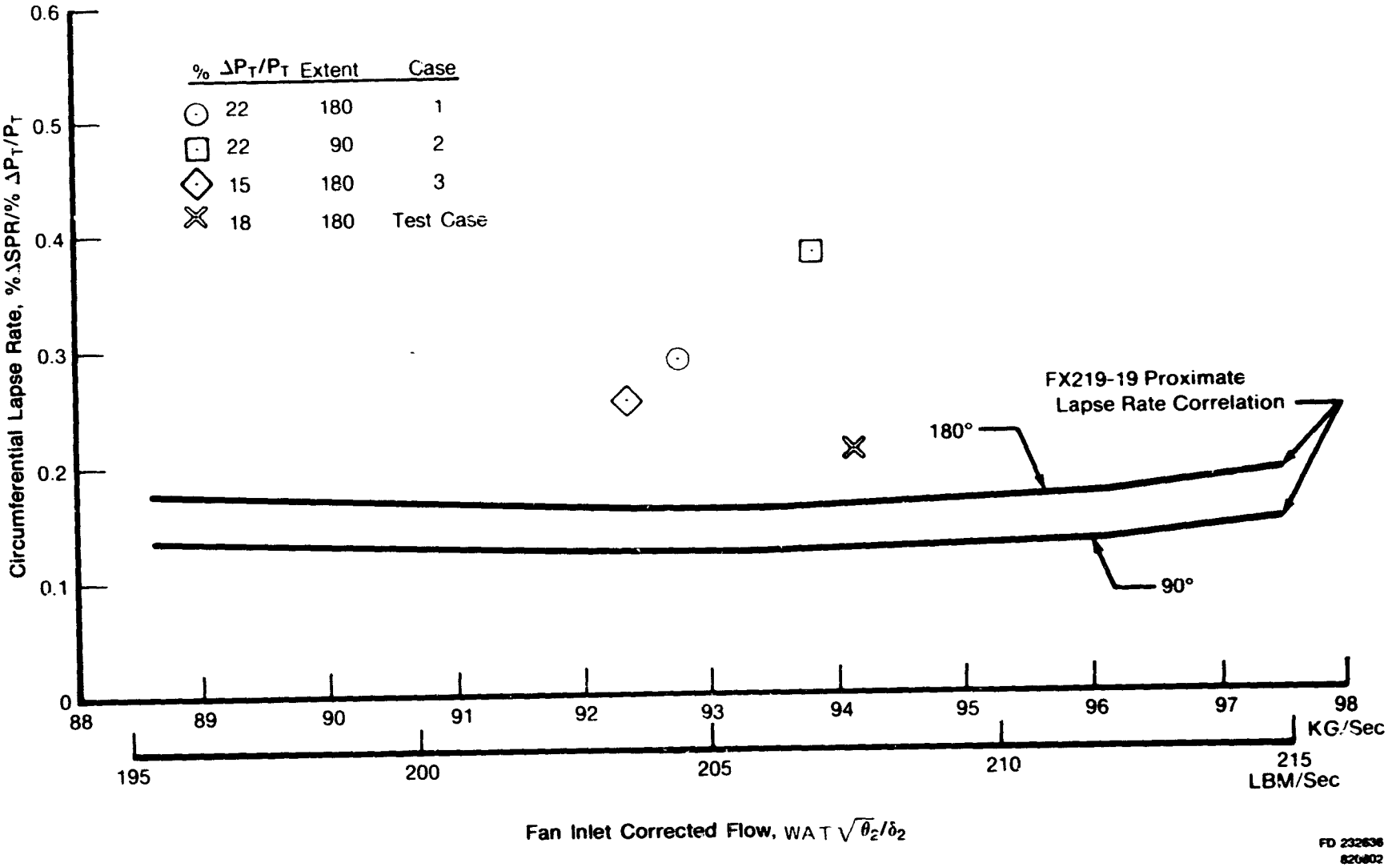

Figure 24. Predicted F100(3) Proximate Splitter Fan Circumferential Pressure Distortion $\Delta P_T/P_T$ Sensitivity

The evaluation of overall compression system operation with inlet distortion requires defining the distortion transfer characteristics of the fan. In the F100(3) engine, attenuation of inlet distortion through the fan results in an inlet temperature distortion at the high-pressure compressor. Therefore, the distortion evaluation includes defining the level of pressure distortion remaining at the fan core stream exit and the level of temperature distortion at the high compressor inlet.

Figures 25, 26, and 27 show the calculated fan core stream pressure distortion attenuation characteristics of the F100(3) proximate splitter fan. The predictions show that the fan significantly attenuates the inlet pressure distortion, thereby reducing the stability threat to the high compressor. Figure 25 shows that the model agrees well with the attenuation calculated from FX219-19 proximate splitter engine tests.

Measured on a $K\theta$ basis, Figure 26 shows that the fan attenuates about half of the inlet circumferential distortion. It is also evident for these high levels of inlet distortion, that as inlet $K\theta$ increases when moving from the operating line to stall, the fan exit $K\theta$ increases proportionally and the ratio of $K\theta_{out}/K\theta_{in}$ remains constant. Figure 27 shows pressure attenuation using the $\Delta P_T/P_T$ max-min/avg descriptor. It shows different attenuation levels result for operating line and stall points when the $\Delta P_T/P_T$ descriptor is used, which means that more distortion amplitude is passed through the fan to the high cmpressor as the fan is backpressured along a constant speedline to stall. Past experience has indicated that the θ system better reflects the engine response to distortion, and therefore, fan exit distortion characteristics based on this system are more representative of the threat to the high-pressure compressor.

The attenuation of the pressure distortion by the fan results in the generation of a fan exit temperature distortion. The temperature distortion results from a difference in the work between the distorted and undistorted region of the fan needed to meet the constant exit static pressure boundary condition. Figures 28, 29, and 30 show the calculated fan core stream temperature distortion generation characteristics of the F100(3) proximate splitter fan.

Figure 28 shows that the model predicts more temperature distortion generation than was calculated from remote splitter fan rig tests. It is compared to a remote splitter empirical relationship because limited instrumentation prevented calculations from FX219-19 proximate splitter data. Figure 29 shows that on a $K\theta$ basis, temperature distortion generation is about 28% of the level of inlet pressure distortion. Figures 26 and 29 infer that for a given speed, the $K\theta$ system collapses the model predictions for pressure attenuation or temperature generation to one characteristic. Figure 30 is the temperature distortion generation based on the max-min/avg system, and it shows a separate characteristic for operating line and stall points. As mentioned earlier, the $K\theta$ system is believed to better quantify the distortion level than the max-min/avg system.

2. Temperature Distortion

F100(3) proximate splitter fan response to inlet temperature distortion was predicted with the MSPC model at 102% corrected speed for three cases, as listed in Table 1. Figure 31 shows the predicted fan surge points for these distortions. The 18% $\Delta T_T/T_T$, 180-degree distortion results in a lower surge line than the 9% $\Delta T_T/T_T$, 180-degree distortion. For the same 18% $\Delta T_T/T_T$ distortion amplitude, the 90-degree distortion gave the same stall line as the 180-degree distortion.

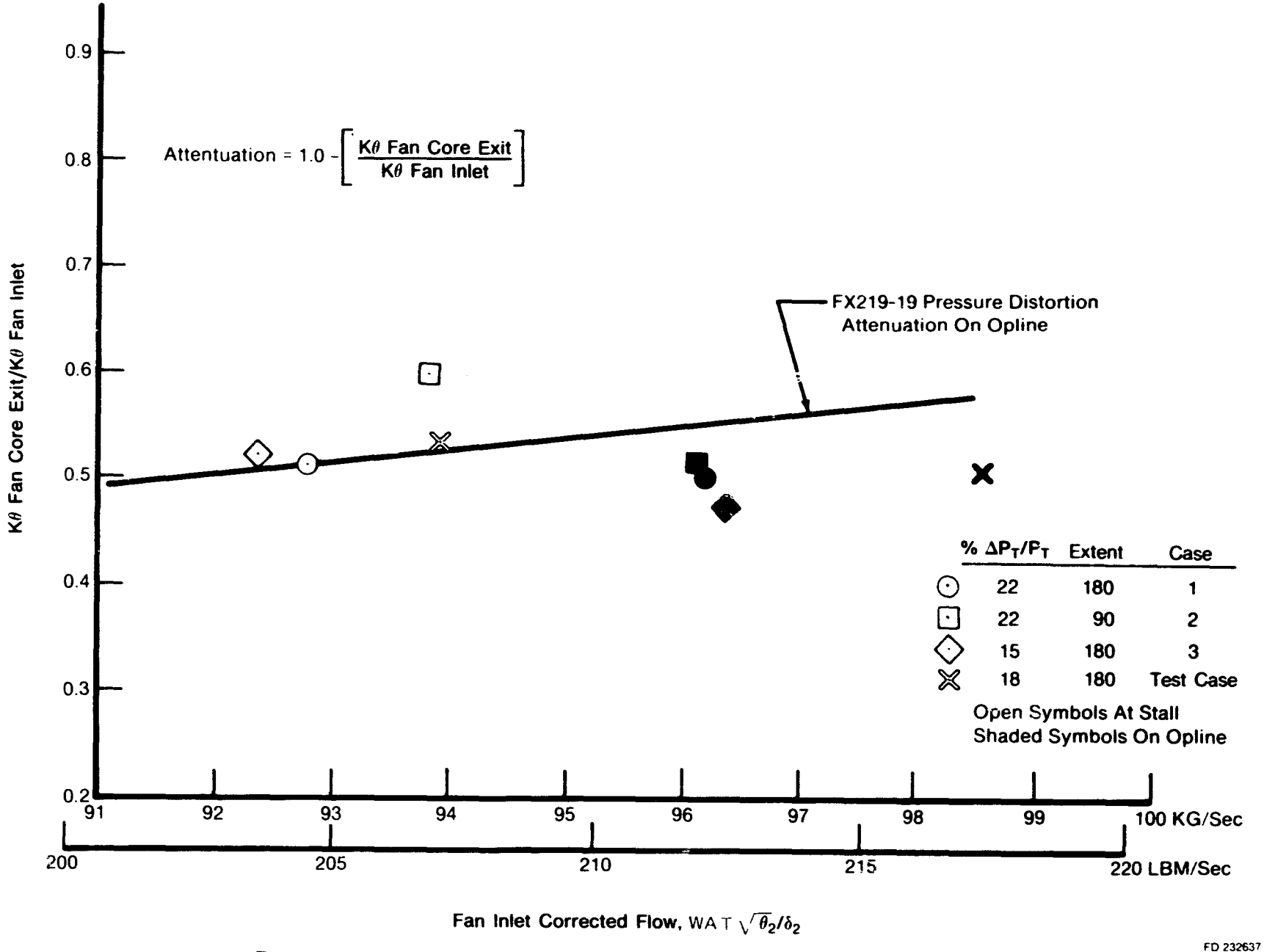

Figure 25. Predicted F100(3) Proximate Splitter Fan Pressure Distortion Attenuation

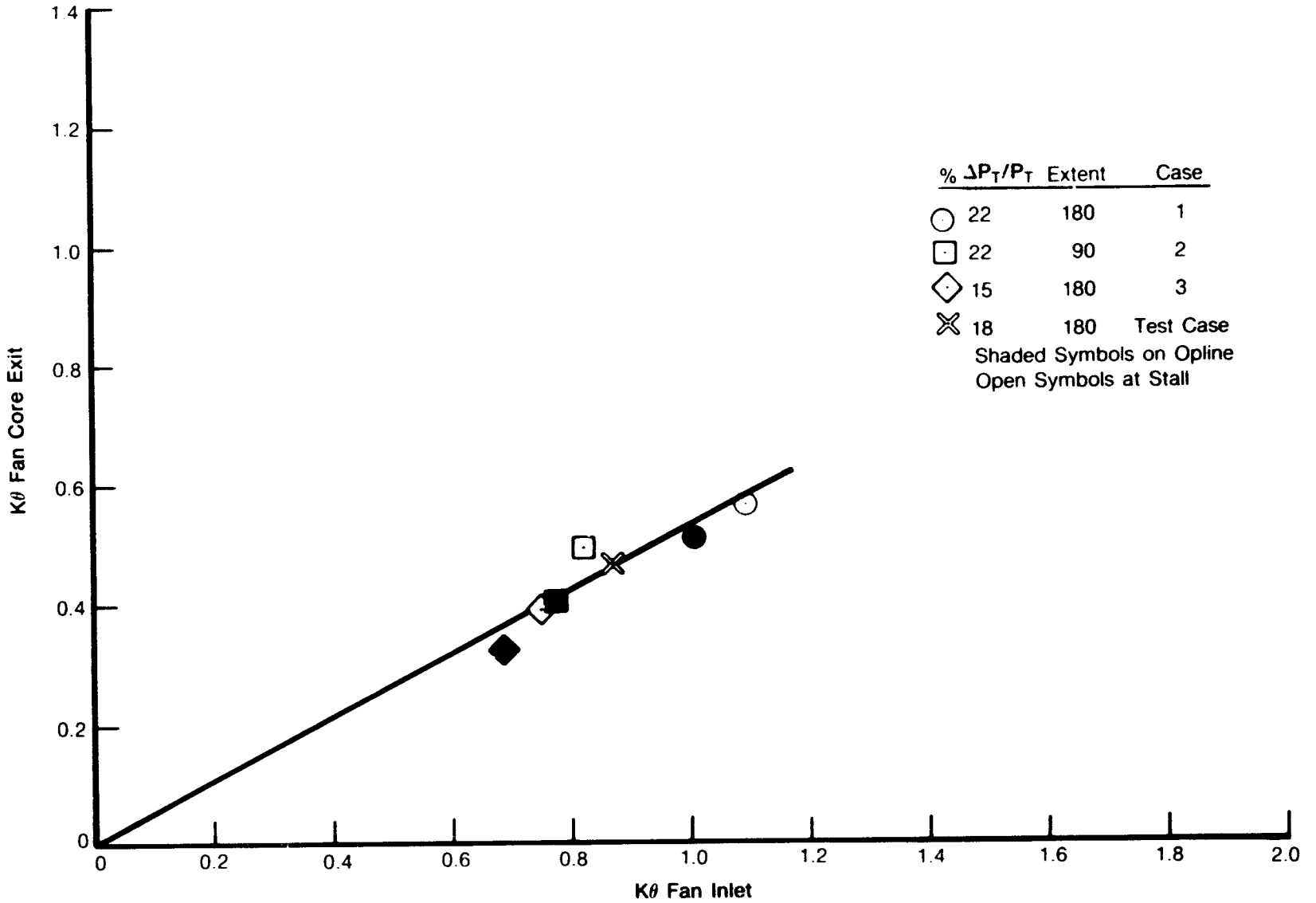

Figure 26. Predicted F100(3) Proximate Splitter Fan Pressure Distortion Attenuation: Kθ

FD 232606
820802
bt2 973

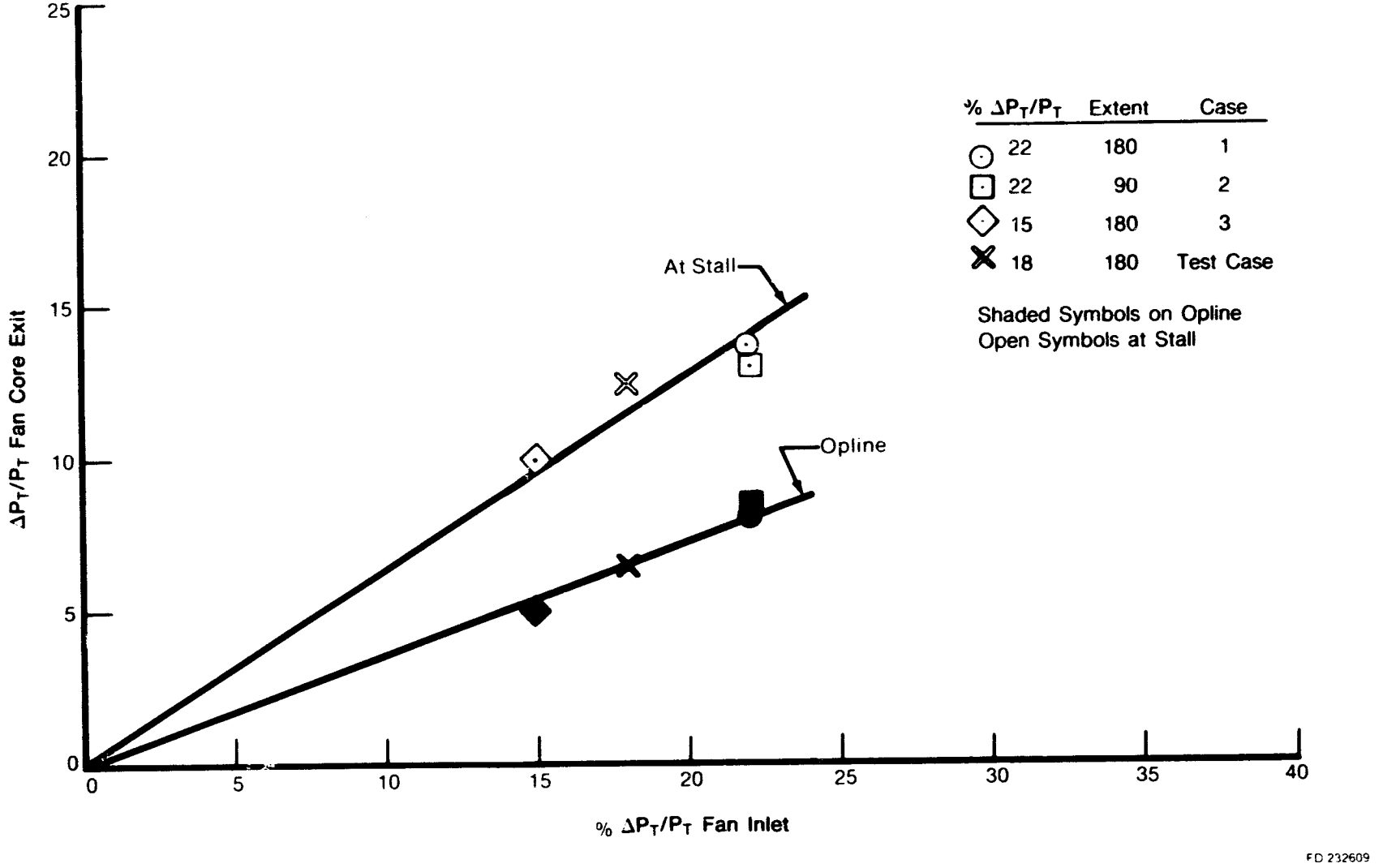

Figure 27. Predicted F100(3) Proximate Splitter Fan Pressure Distortion Attenuation $\Delta P_T/P_T$

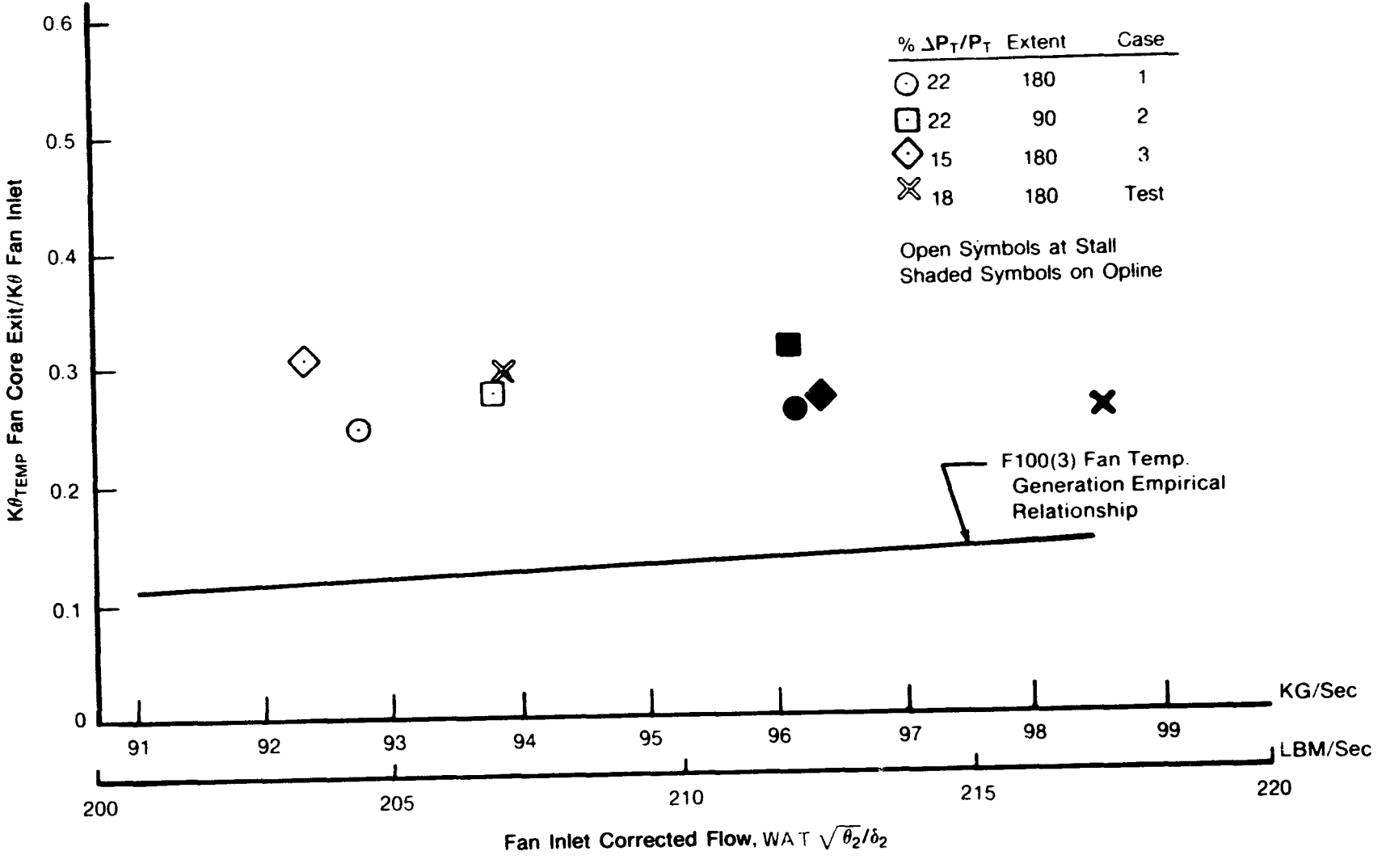

Figure 28. Predicted F100(3) Proximate Splitter Fan Temperature Distortion Generation

FD 232638

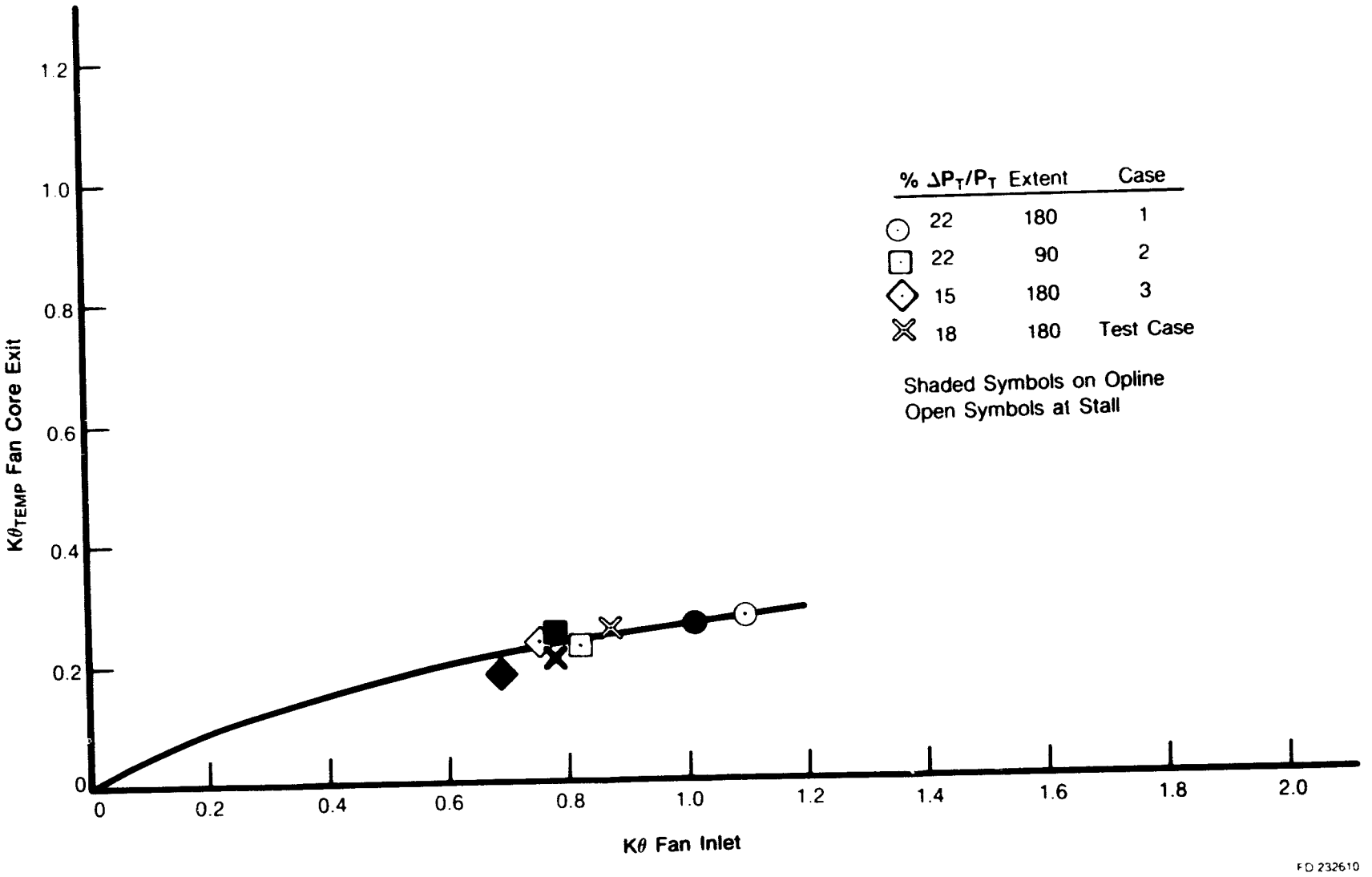

Figure 29. Predicted F100(3) Proximate Splitter Fan Temperature Distortion Generation: $K\theta_{TEMP}$

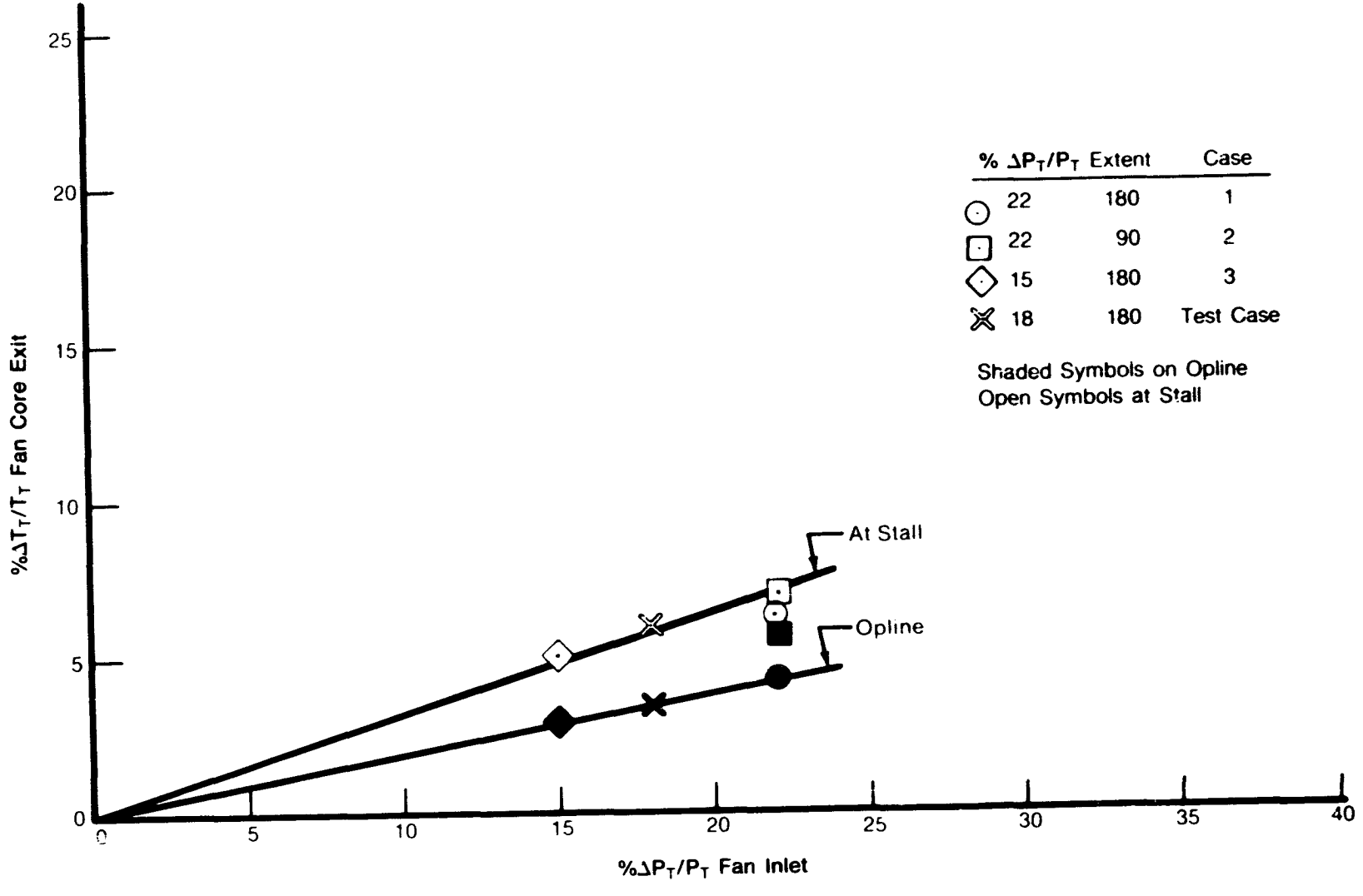

Figure 30. Predicted F100(3) Proximate Splitter Fan Temperature Distortion Generation: $\Delta T_T/T_T$

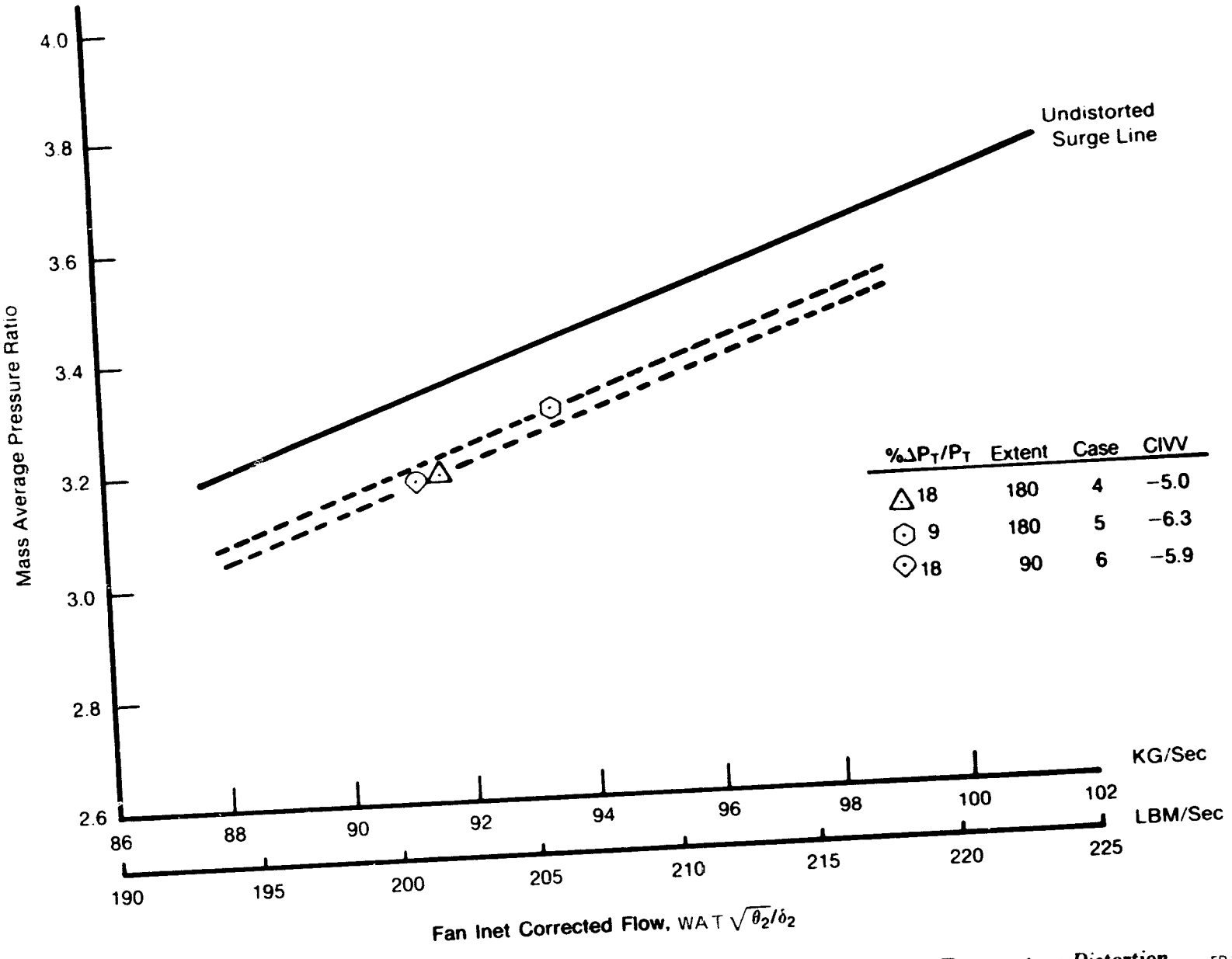

Figure 31. Predicted F100(3) Proximate Splitter Fan Surge Lines With Temperature Distortion

Figures 32 and 33 show the model-predicted sensitivity to inlet temperature distortion. The F100(3) fan has not been tested with temperature distortion so there is no data that can be used to judge the quality of these predictions. Figure 32 shows the predictions using the F100(3) system $K\theta_{TEMP}$. Although Figure 31 showed a lower surge line for 18% $\Delta T_T/T_T$ distortion than the 9% distortion of the same extent, Figure 32 shows that for a given amount of $K\theta_{TEMP}$ the 9% $\Delta T_T/T_T$ distortion results in a higher sensitivity. Figure 33 shows the predicted sensitivity to temperature distortion in terms of the $\Delta T_T/T_T$ min-max-avg system.

The distortion transfer characteristics of the fan when operating with temperature distortion were also predicted. Figures 34, 35, and 36 show the predicted attenuation of temperature distortion by the proximate splitter fan. The $K\theta$ system predicts no attenuation by the fan for all cases except Case 4 at stall. Figures 34 and 35 show this case has the highest level of inlet distortion ($K\theta_{TEMP}$=0.92), and that 13% of the distortion is attenuated by the fan. Figure 36 shows the $\Delta T_T/T_T$ max-min system which indicates that distortion amplitude is reduced about one-quarter as the temperature distortion is passed through the fan.

The proximate splitter fan is also predicted to generate an exit total pressure distortion. This pressure distortion results from the fan operating at different corrected speeds and flowrates in high- and low-temperature regions. Since the fan was assumed to have a constant exit static pressure, the varying flowrate caused by the temperature distortion results in an exit total pressure distortion.

Figures 37, 38, and 39 show that significant levels of exit pressure distortion are predicted to be generated due to temperature distortion. Figures 37 and 38 indicate the 18% $\Delta T_T/T_T$ 90-degree case generated more pressure distortion per $K\theta_{TEMP}$ than the 180-degree cases. On a $K\theta$ basis, the 180-degree cases generated a pressure distortion that is slightly less than half of the inlet temperature distortion. Figure 39 shows that there is no difference in the amplitude of pressure distortion generated for 90- or 180-degree distortions of the same amplitude. This means that a change in distortion extent is responsible for the differences in $K\theta$ seen with 90-degree and 180-degree distortions.

This analysis indicates temperature distortion is a stability threat both to the fan and high compressor in the F100(3) engine.

3. Detailed Flow Field Analysis

The MSPC model provides both a row-by-row and major station definition of the flow field through the engine compression system. In modeling the F100(3) engine, the fan was divided into a core and bypass stream as mentioned previously. For each stream, static and total pressure and total temperature circumferential profiles were calculated at each row except the inlet and exit. Total pressure and total temperatures profiles must be input at the inlet, and static pressure profiles at the exit. Additionally, the model calculates the angular displacement of a fluid particle and the acoustic path of each parallel segment. The parallel segments are rotated by the average angular displacement of all segments and this displacement is denoted as "flow swirl."

The swirl through the fan is determined by rotor speed and the rotor/stator mean flow angles. A fluid particle entering the fan will experience greater circumferential translation than a segment due to its slower throughflow velocity. Thus, a particle entering in one segment, such as a low pressure segment, may exit the fan in a high pressure segment. This mixing of fluid particles results in out of phase attenuation and generation of distortion through the component. For the F100(3) fan a fluid particle is translated about 65 degrees while the translation of the segments averages 35 degrees for a 102% corrected fan speed.

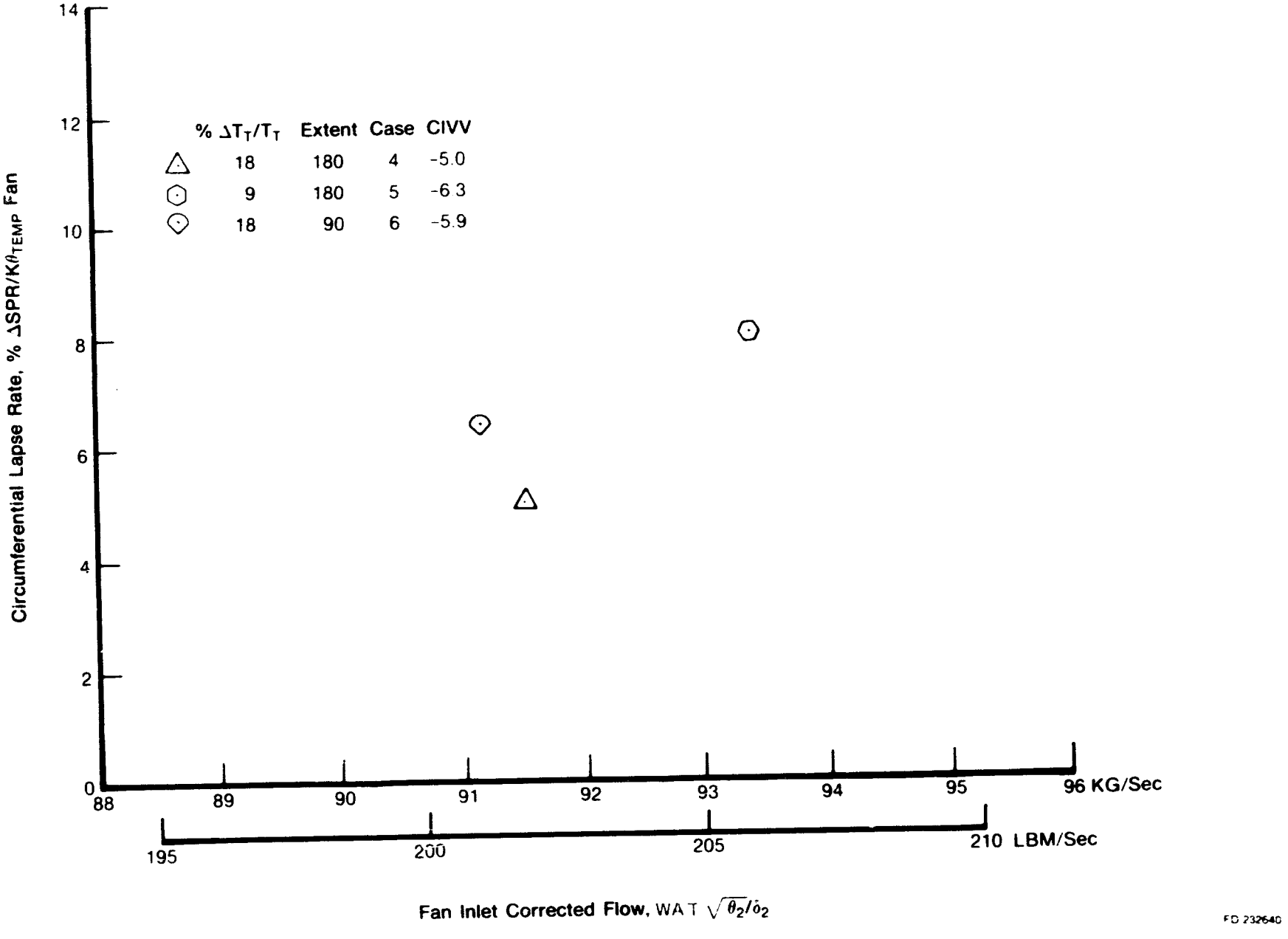

Figure 32. Predicted F100(3) Proximate Splitter Fan Circumferential Temperature Distortion $K\theta_{TEMP}$ Sensitivity

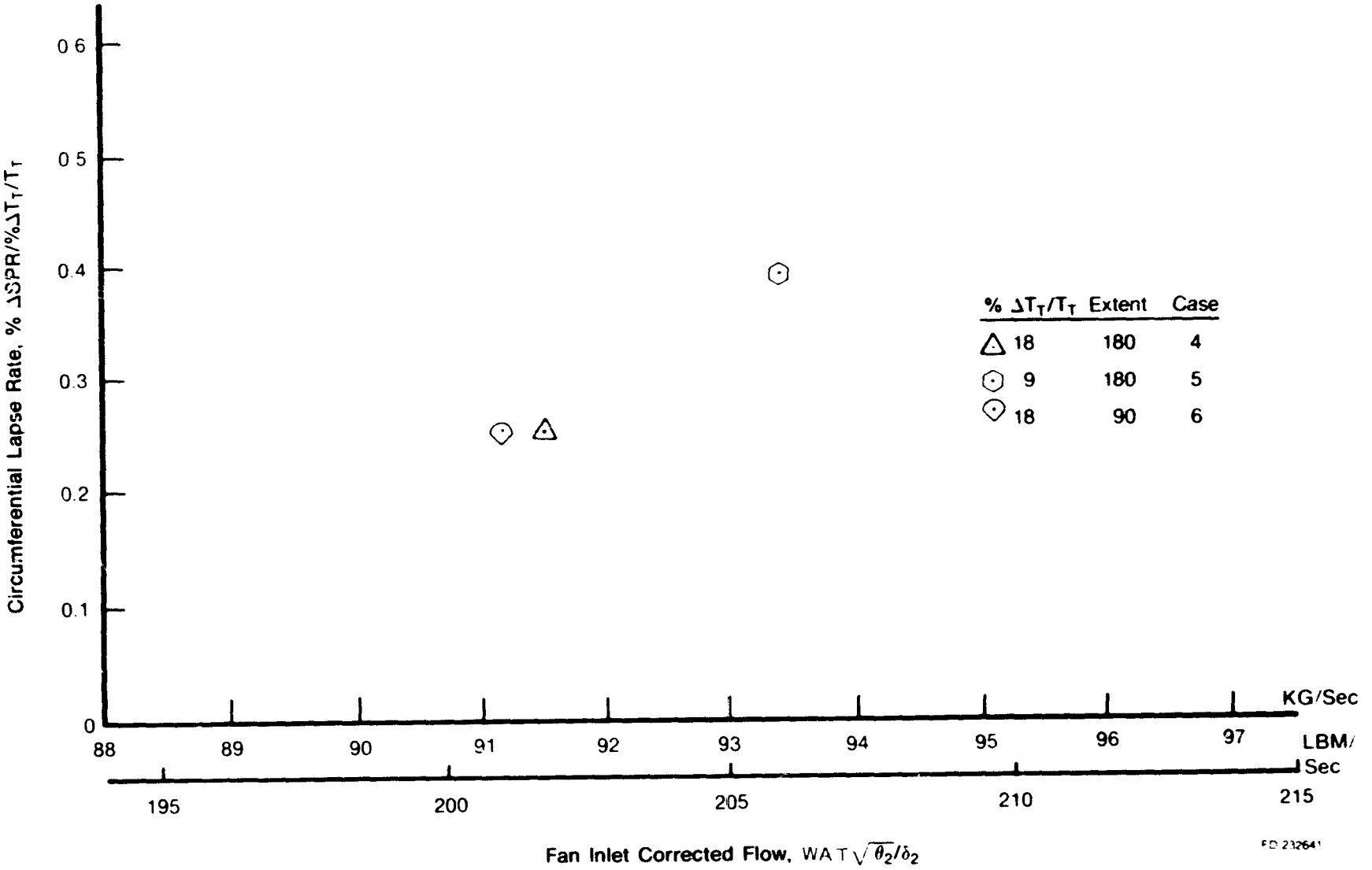

Figure 33. Predicted F100(3) Proximate Splitter Fan Circumferential Temperature Distortion $\Delta T_T/T_T$ Sensitivity

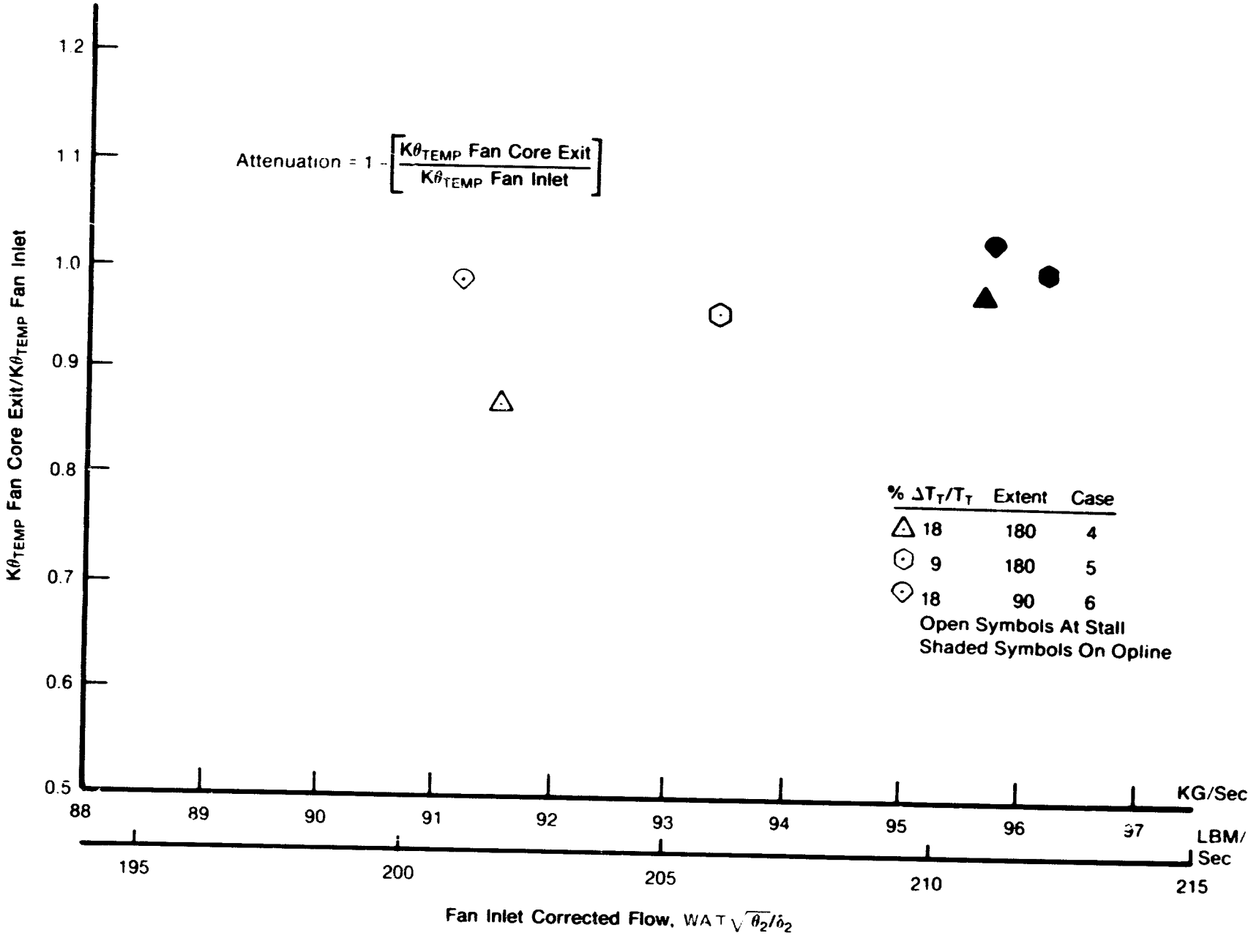

Figure 34. Predicted F100(3) Proximate Splitter Fan Temperature Distortion Attenuation

FD 232642

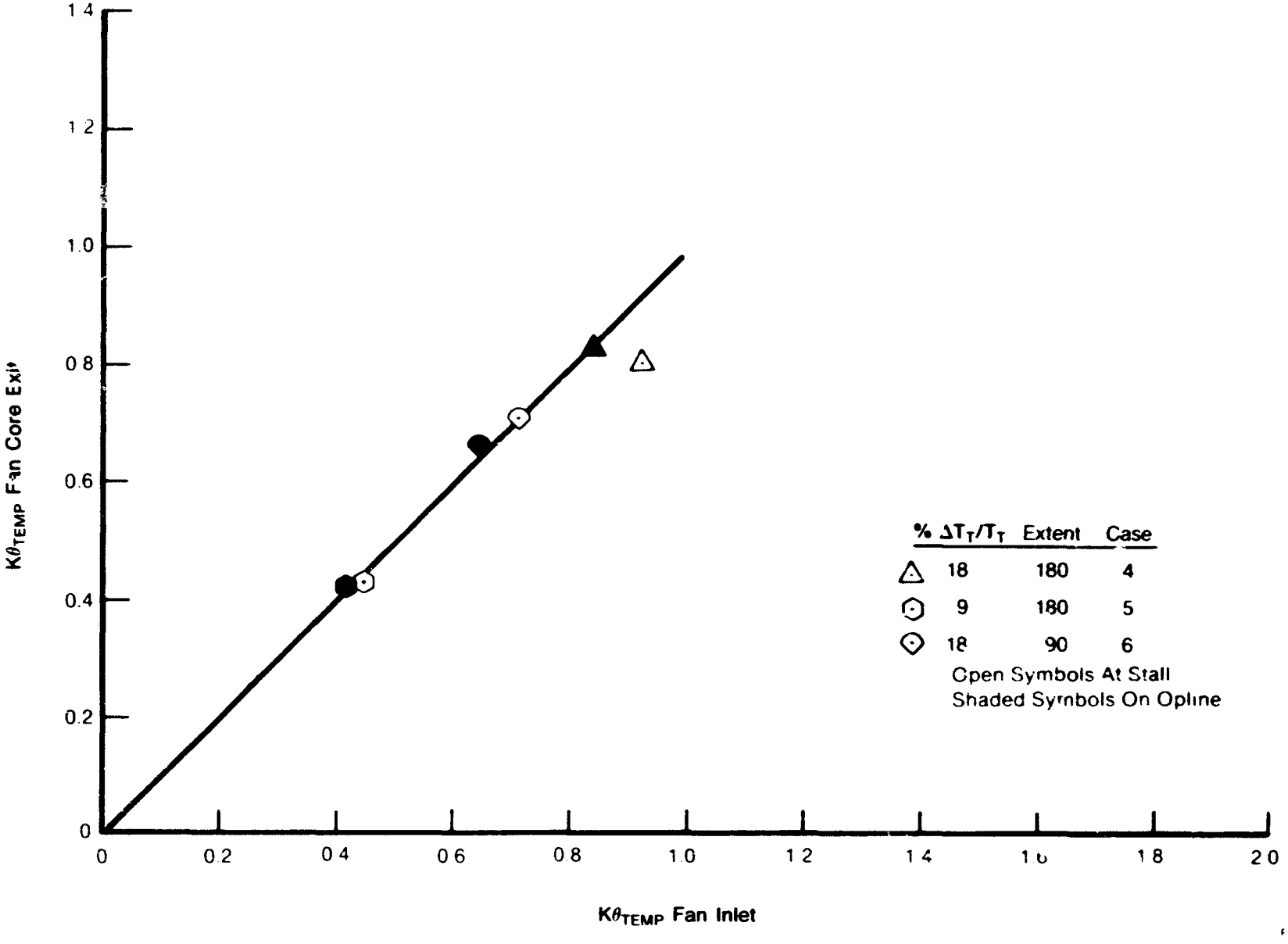

Figure 35. Predicted F100(3) Proximate Splitter Fan Temperature Distortion Attenuation: $K\theta_{TEMP}$

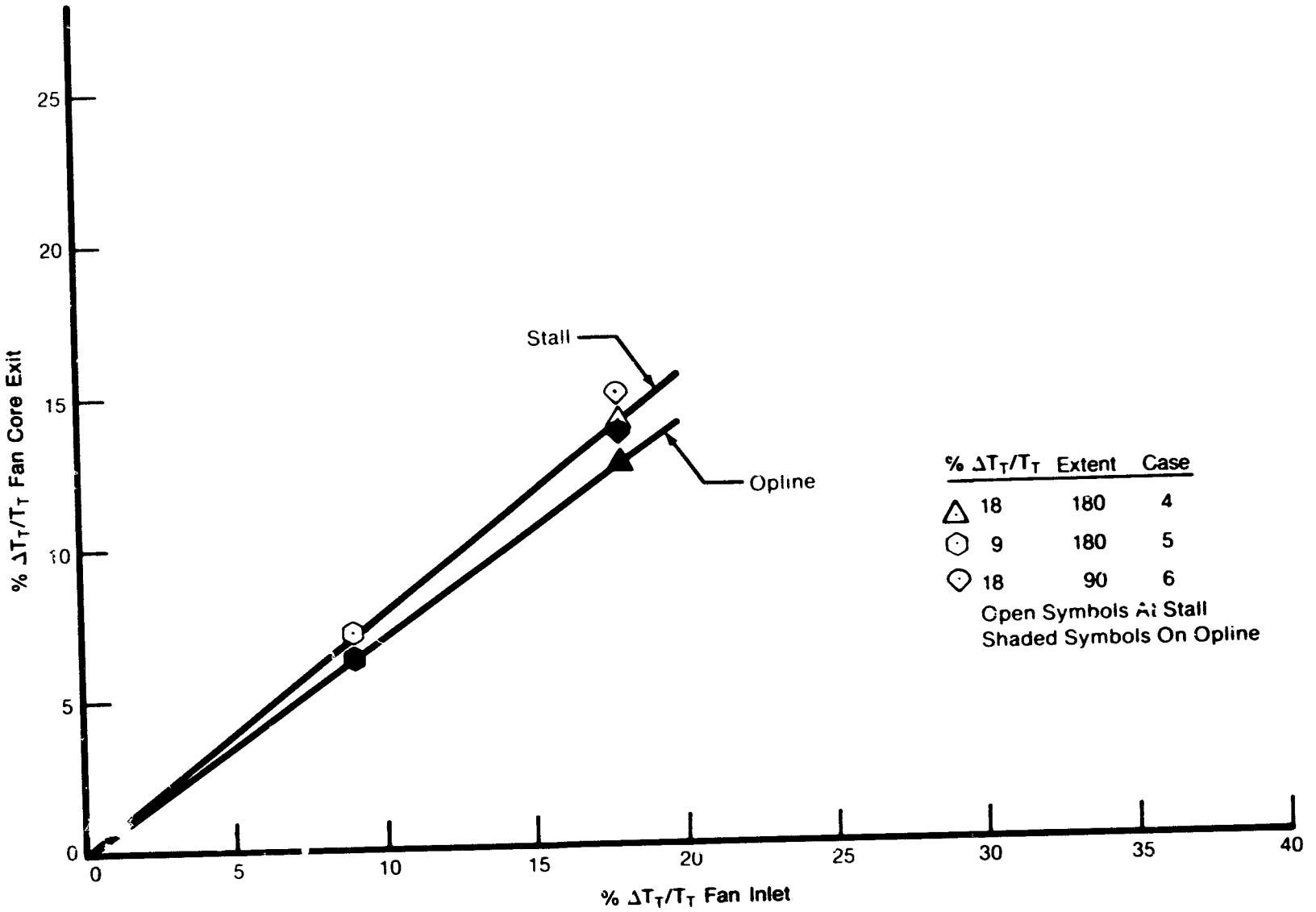

Figure 36. Predicted F100(3) Proximate Splitter Fan Temperature Distortion Attenuation: $\Delta T_T/T_T$

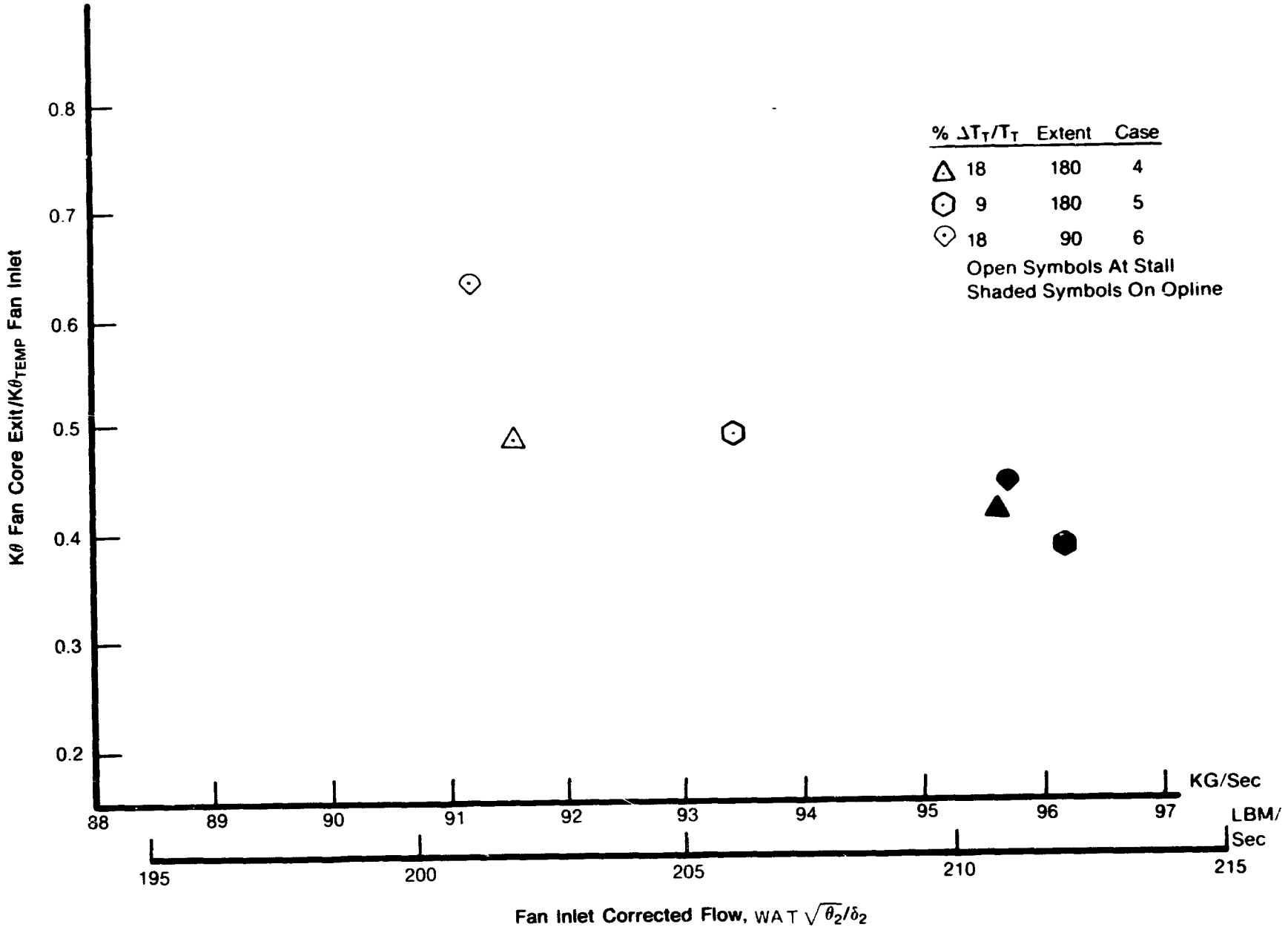

Figure 37. Predicted F100(3) Proximate Splitter Fan Pressure Distortion Generation

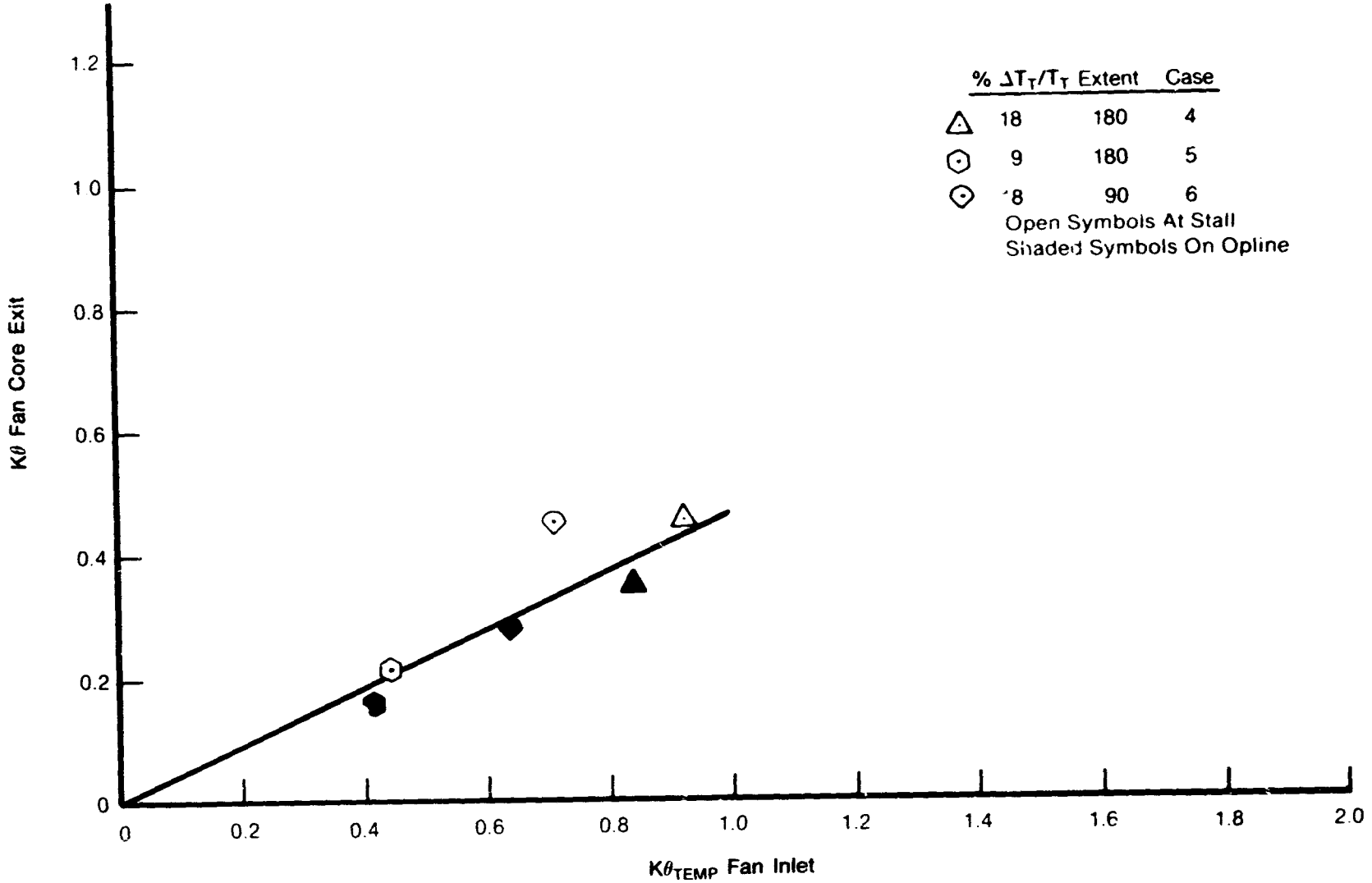

Figure 38. Predicted F100(3) Proximate Splitter Fan Pressure Distortion Generation: Kθ

FD 232614
820802
bt2 983

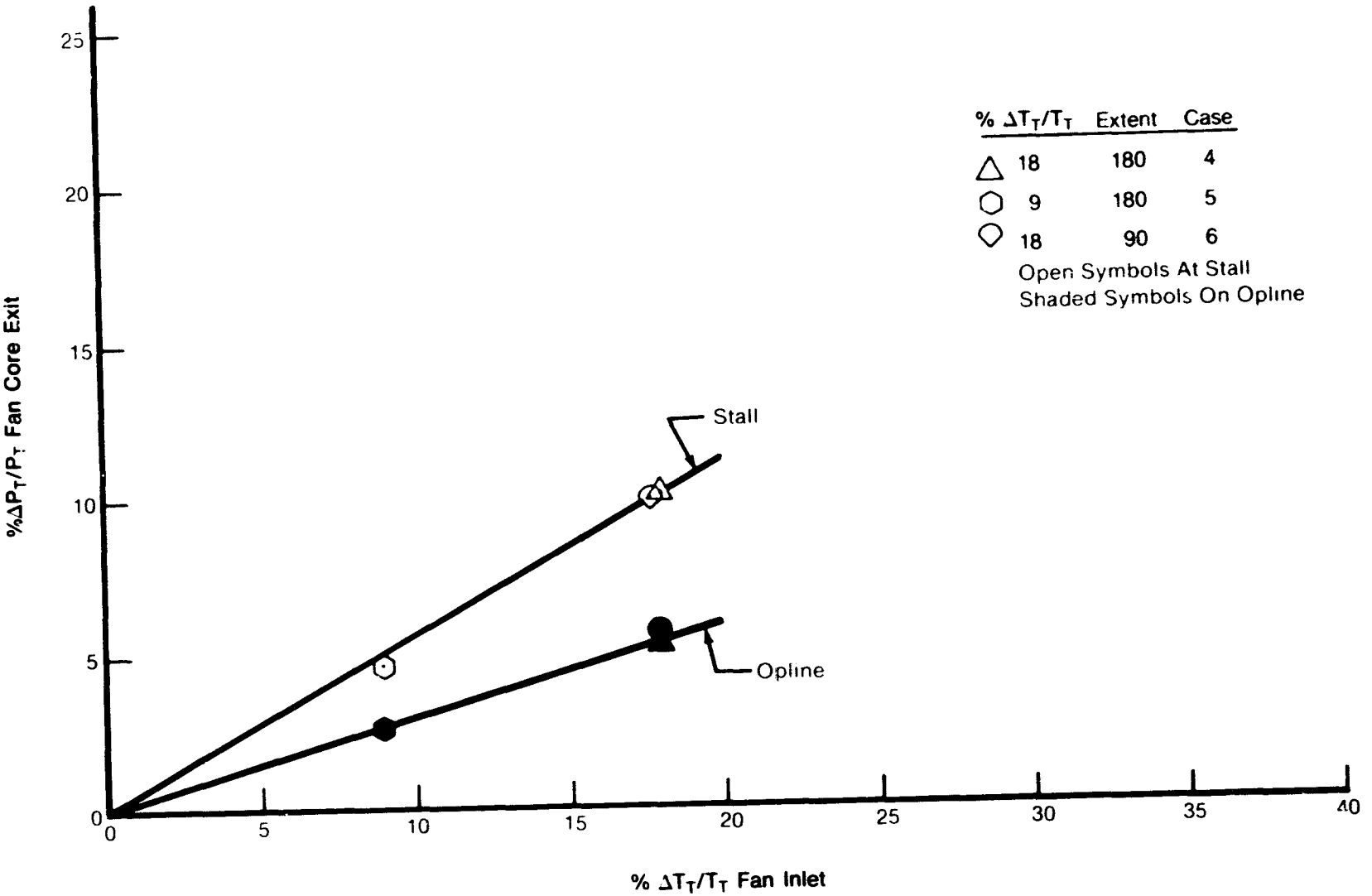

Figure 39. Predicted F100(3) Proximate Splitter Fan Pressure Distortion Generation: $\Delta P_T/P_T$

Predicted proximate splitter fan core exit total pressure and total temperature circumferential profiles are plotted in Figures 40, 41, and 42. Figures 40 and 41 present inlet pressure distortion Cases 1 and 2, respectively. Figure 42 shows the exit profiles for Case 4 temperature distortion. All cases show overlapping low-pressure and high-temperature regions at the fan exit due to distortion transfer characteristics of the fan. Previous work with MSPC model predictions of high-pressure compressor response to combined distortions of this type indicated that this orientation will cause the greatest loss in HPC stall margin.

Figures 43 through 51 show total and static pressure and total temperature circumferential profiles predicted by the model at the fan inlet and exit. Three cases were plotted: Case 1 and 2 pressure distortions and Case 4 temperature distortion. Also included on those figures are the segment flow swirl and fluid particle swirl angular displacements. Figures 43 and 46 show the total pressure profiles for the 22% $\Delta P_T/P_T$ 180-degree and 90-degree cases. Both show $\Delta P_T/P_T$ much more attenuation of the pressure distortion by the fan OD than the ID. Comparisons also show the circumferential extent of the pressure distortion increased 35% at the fan core exit for the 90-degree distortion while the increase was predicted to be 7% for the 180-degree case. Figure 50 shows the 18% $\Delta T_T/T_T$, 180-degree temperature distortion case. No significant difference is seen in the attenuation of the inlet temperature profile by the fan core side and fan duct side. Both show a similar decrease in distortion amplitude and no change in distortion extent.

4. Comparison of Distortion Response for Engines With Proximate and Remote Splitters

The MSPC model was expanded under NASA Contract NAS3-20610 to analyze the distortion response of the F100(3) compression system. The response of the system to various inlet pressure and temperature distortions was predicted under NASA Contract NAS3-20835. These predictions were shown in NASA Report CR-159754, Reference 3, to provide representative response characteristics to known F100(3) remote splitter fan test results. In this section those remote splitter predictions are compared to model results for the proximate splitter fan. The results are also evaluated by making similar comparisions to F100(3) stability correlations and available inlet pressure distortion data.

Table 2 presents the distortion response calculated for both proximate and remote splitter engines. The inlet distortions for each are identical except for the 90-degree extent temperature distortion. Case 6 for the proximate splitter has an 18% distortion amplitude, while the remote was executed with an amplitude of 9%. All temperature distortion cases were run with the low temperature region equal to 267.9°K (482.3°R) and located over the fan IGV temperature sensors. The different distortion amplitudes for Case 6 result in different average inlet temperatures and, since the IGV (CIVV) angle is set as a function of corrected speed, the proximate splitter CIVV is scheduled 0.9 degree more cambered than the remote.

The comparison of proximate and remote splitter engines distortion response was made using the F100(3) Kθ distortion descriptor system to evaluate fan stall line sensitivity and distortion transfer characteristics through the fan core. Figures 52 through 57 compare the model predictions for the proximate splitter configuration with the remote splitter fan results reported in CR-159754.

Figure 52 illustrates the circumferential pressure distortion lapse rates predicted for proximate and remote splitter fans and those used in the F100(3) stability audit system. The model predictions show the effect of fan exit splitter spacing on pressure distortion lapse rates to be minimal. All cases exhibit a slightly greater sensitivity to pressure distortion with the proximate splitter than the remote, but this difference is small, ranging from 1% ΔSPR/Kθ for Cases 1 and 3 to 1.6% for Case 2. Compared to its stability correlation, the proximate splitter model lapse rate predictions are high while for the remote splitter the predictions are below its correlation. The details of the stability correlations were examined to better understand the different pressure distortion lapse rates for the proximate and remote splitter fans.

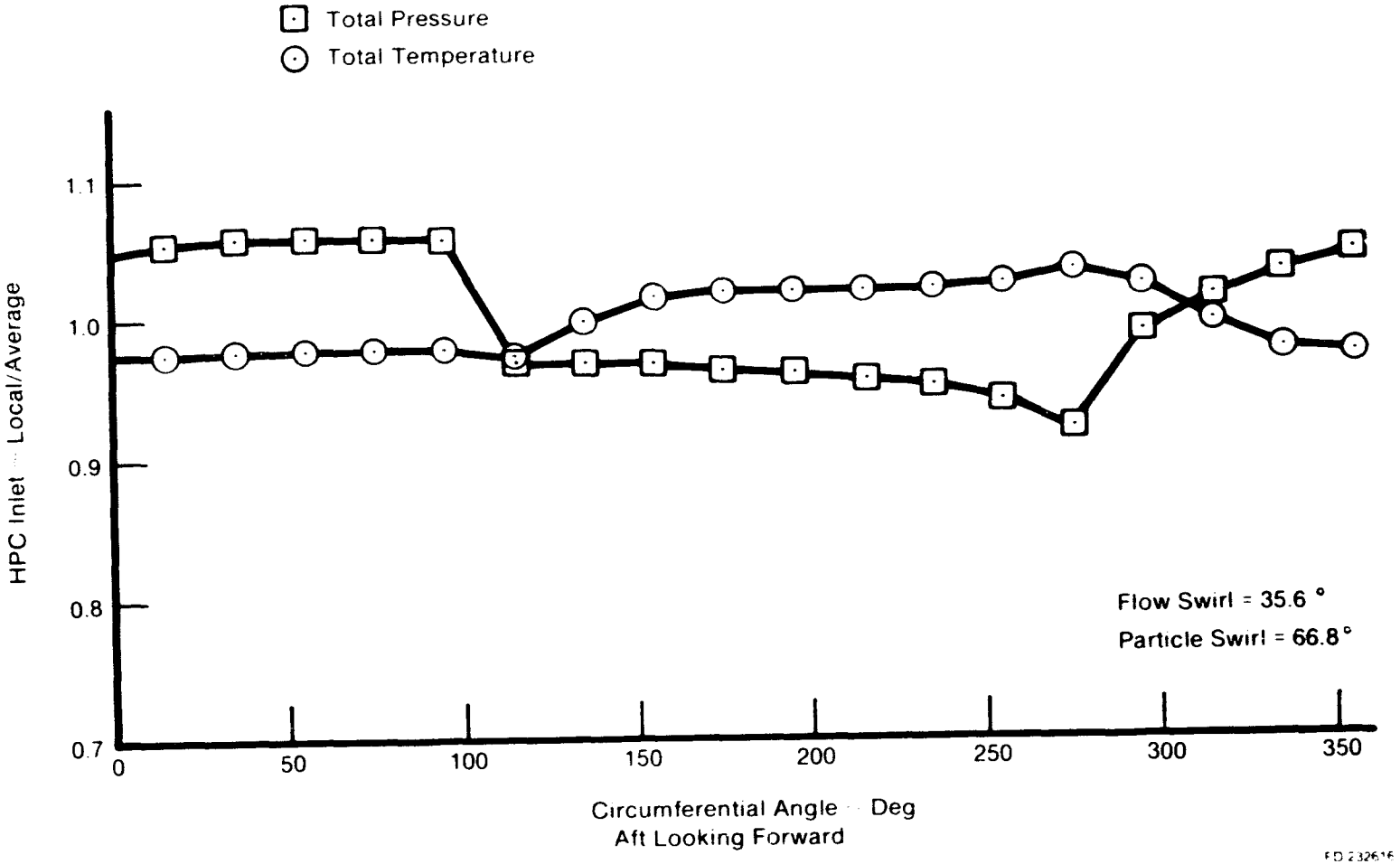

Figure 40. Predicted F100(3) Proximate Splitter Fan Core Exit Circumferential Profiles ~ Case 1 (22% $\Delta P_T/P_T$ / 180 Deg)

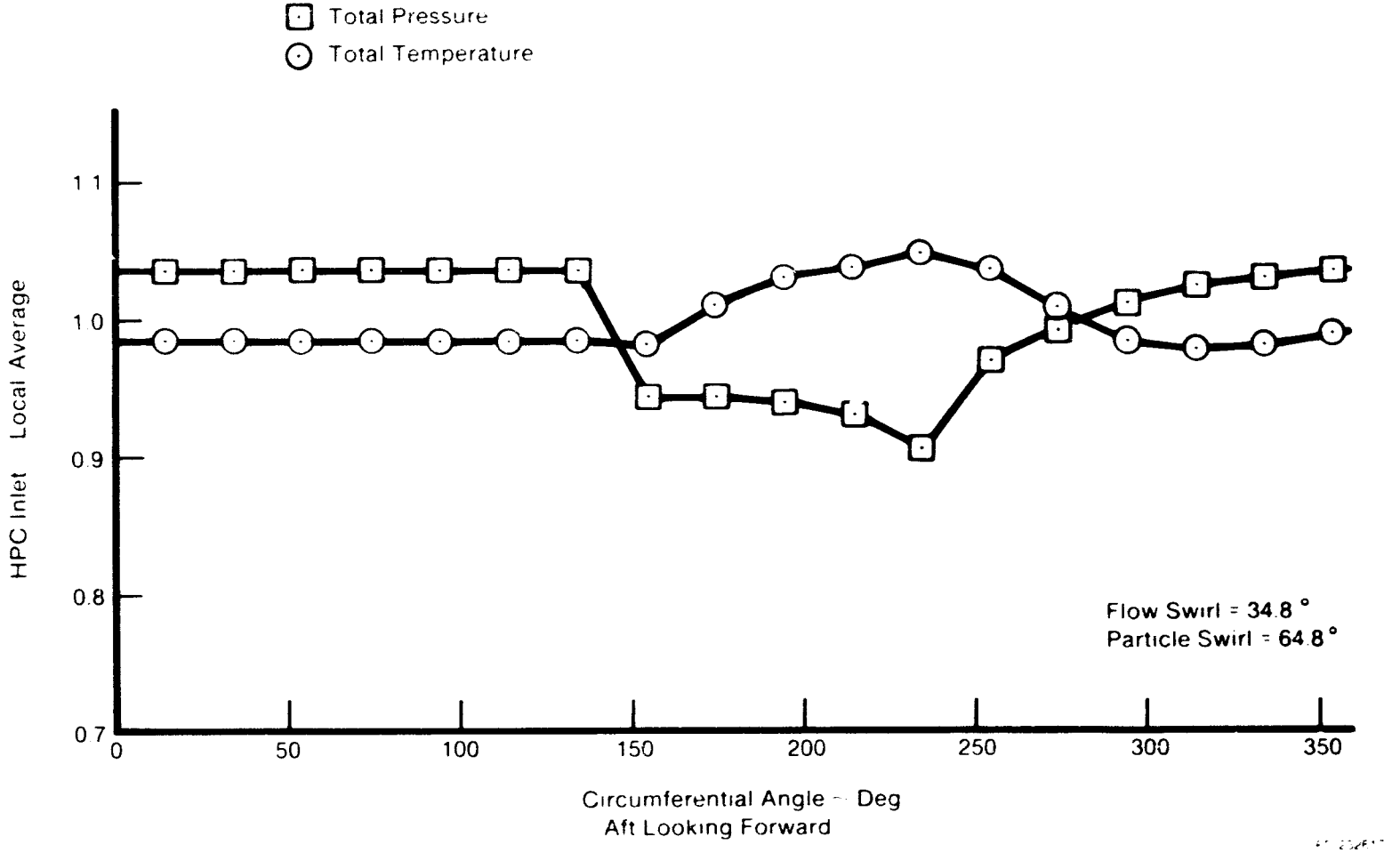

Figure 41. Predicted F100(3) Proximate Splitter Fan Core Exit Circumferential Profiles ~ Case 2 (22% $\Delta P_T/P_T$ 90 Deg)

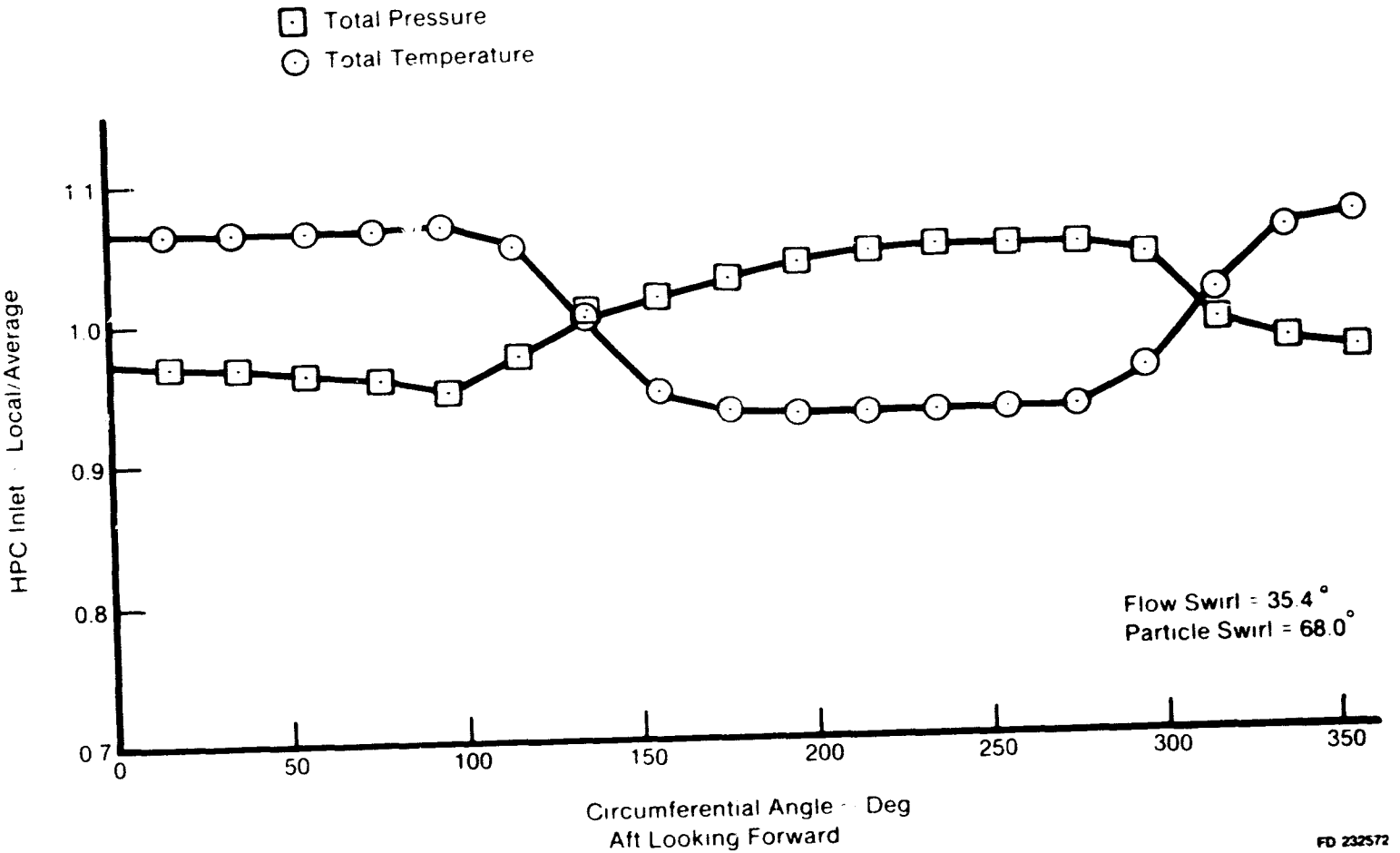

Figure 42. Predicted F100(3) Proximate Splitter Fan Core Exit Circumferential Profiles ~ Case 4 (18% $\Delta T_T/T_T$ /180 Deg)

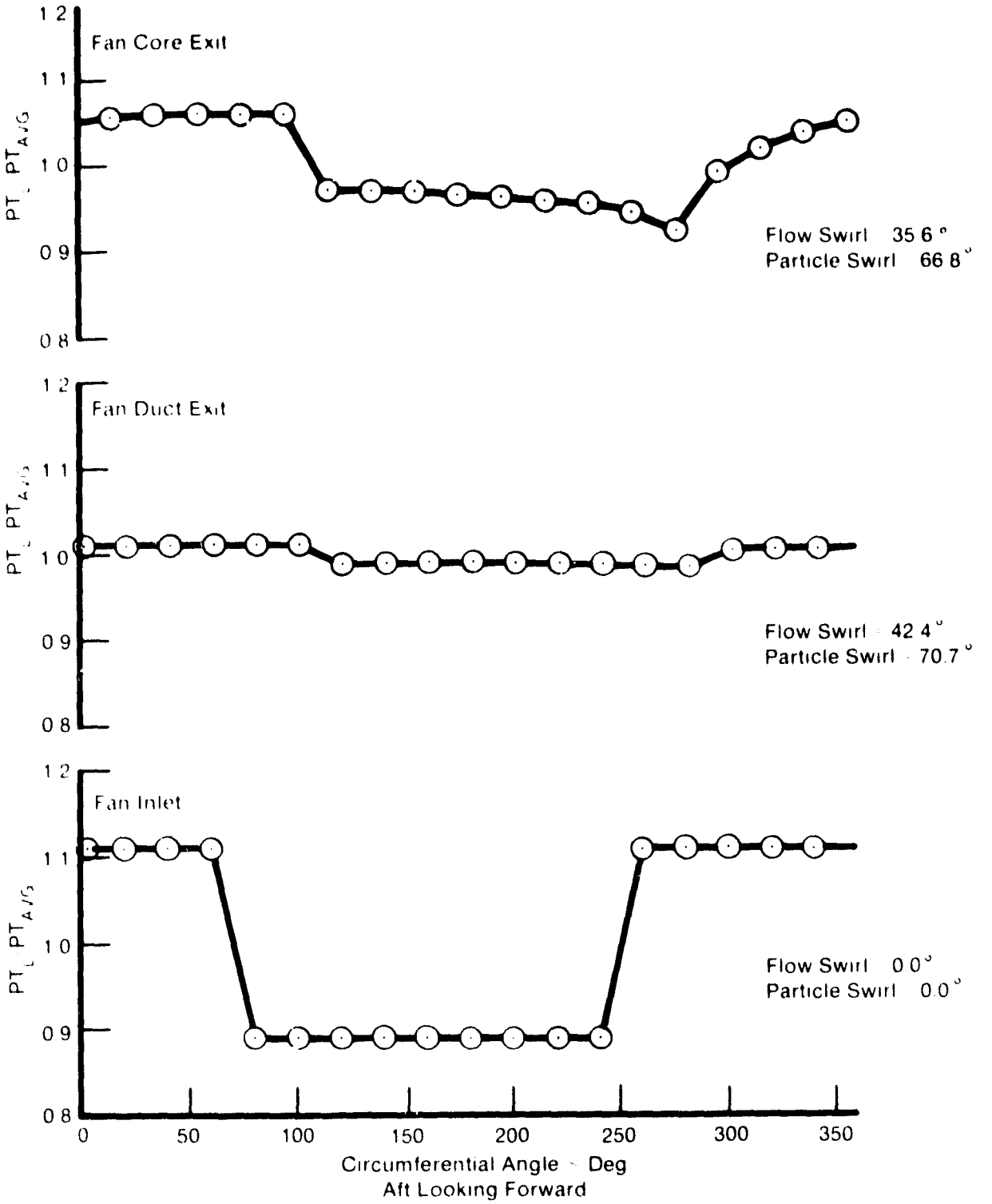

Figure 43. Predicted F100(3) Proximate Splitter Fan Total Pressure Profiles ~ Case 1 (22% $\Delta P_T/P_T$ /180 Deg)

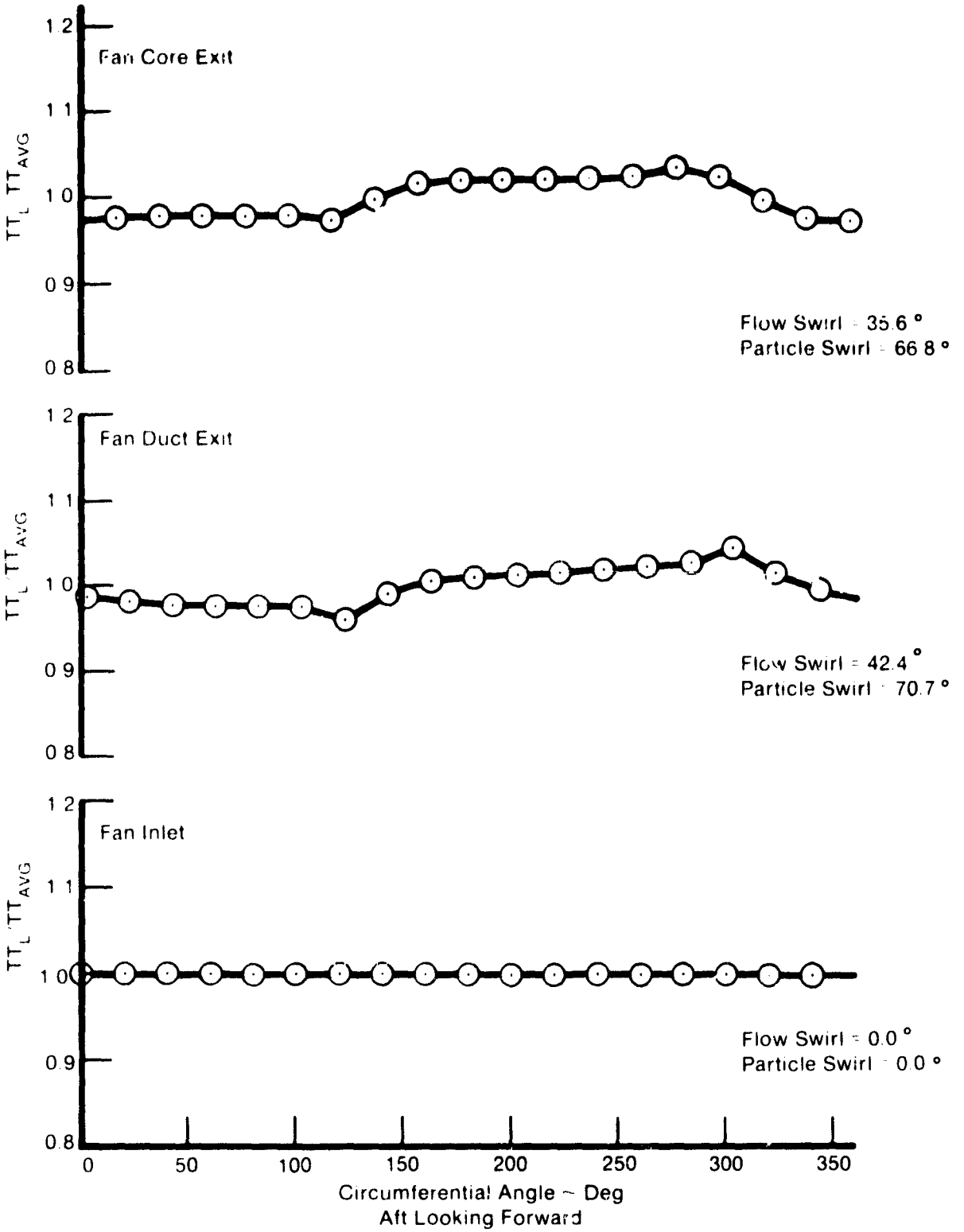

Figure 44. Predicted F100(3) Proximate Splitter Fan Total Temperature Profiles ~ Case 1 (22% $\Delta P_T/P_T$ /180 Deg)

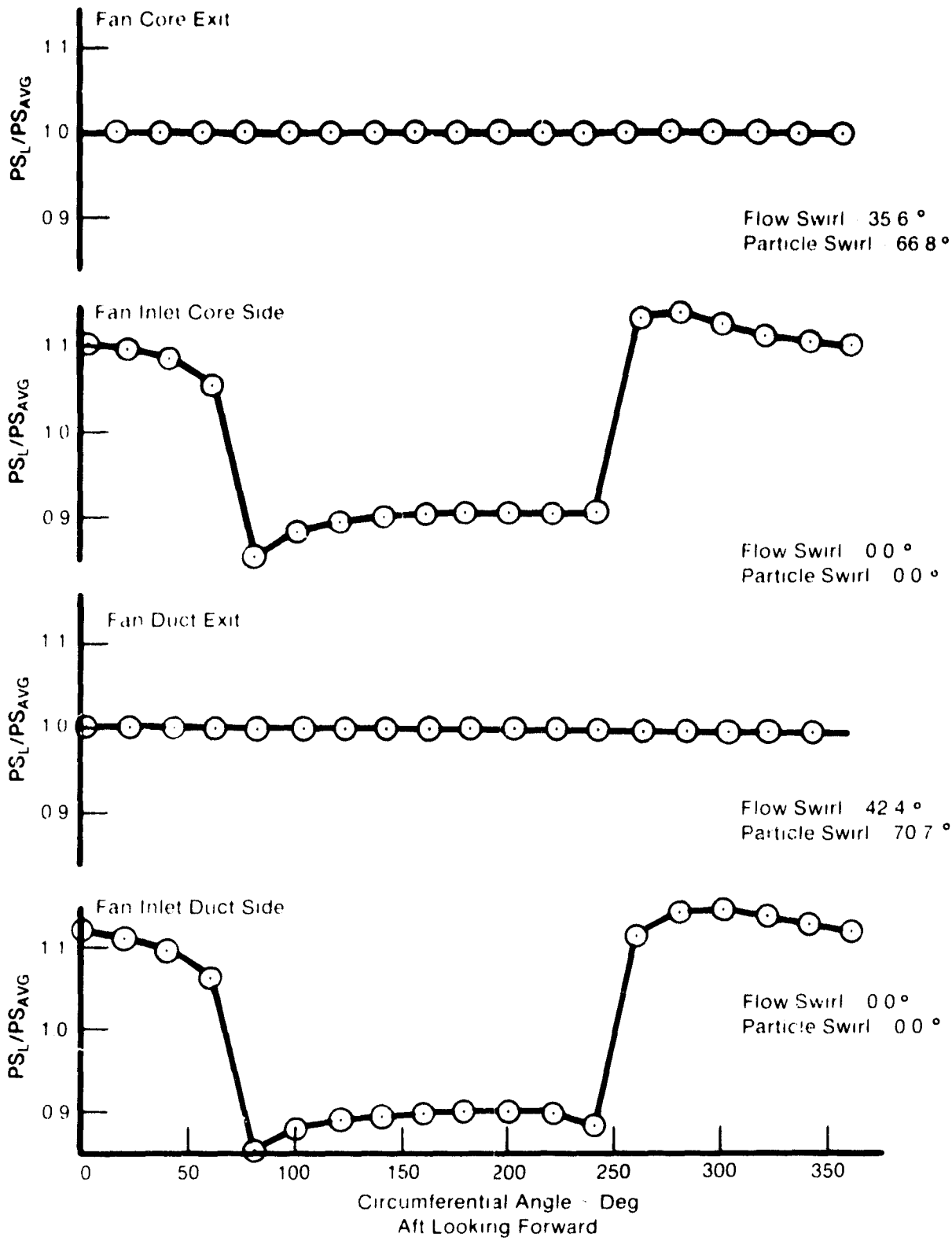

Figure 45. Predicted F100(3) Proximate Splitter Fan Static Pressure Profiles ~ Case 1 (22% $\Delta P_T/P_T$ /180 Deg)

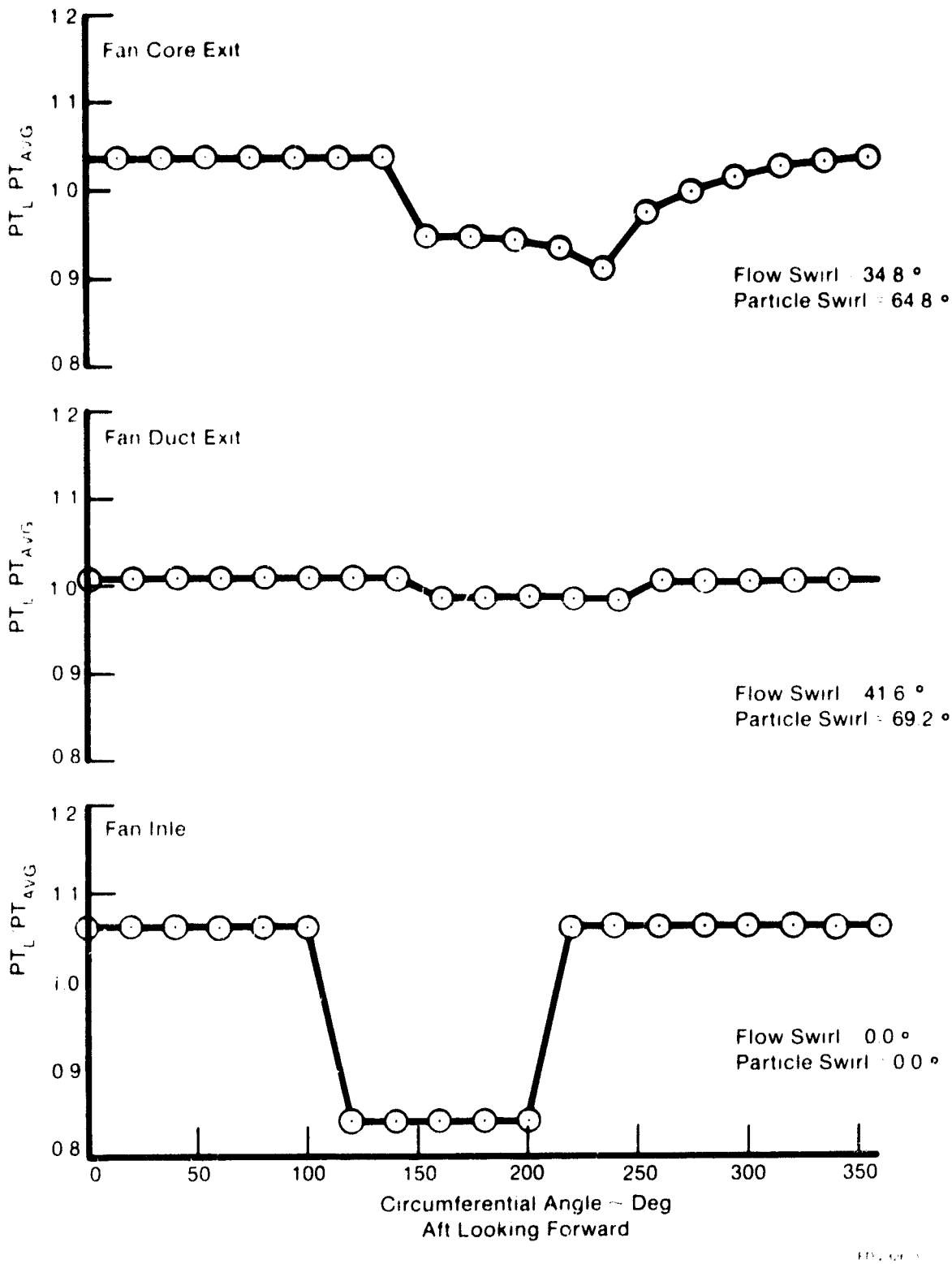

Figure 46. Predicted F100(3) Proximate Splitter Fan Total Pressure Profiles ~ Case 2 (22% $\Delta P_T/P_T$ 90 Deg)

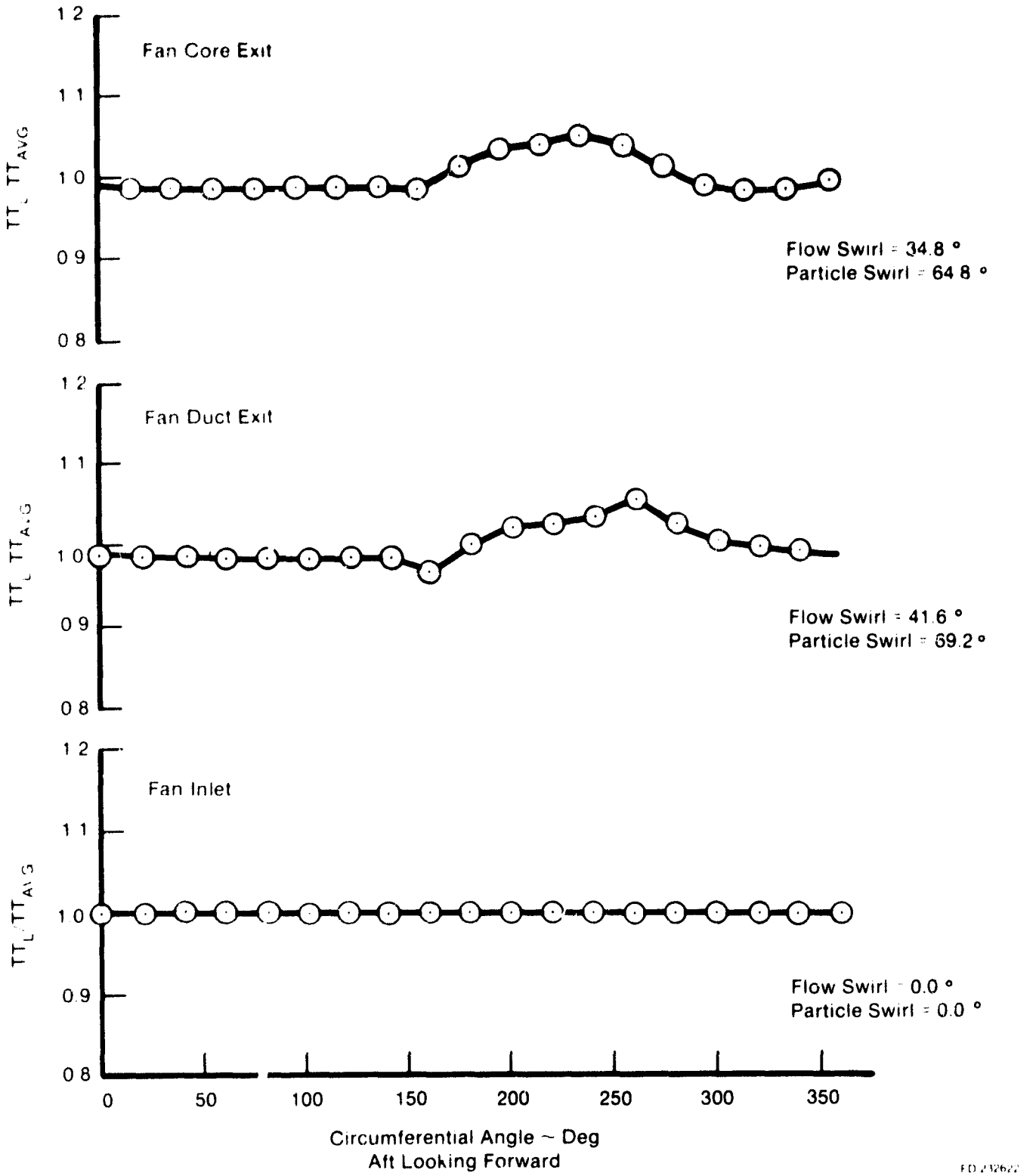

Figure 47. Predicted F100(3) Proximate Splitter Fan Total Temperature Profiles ~ Case 2 (22% $\Delta P_T/P_T$ /90 Deg)

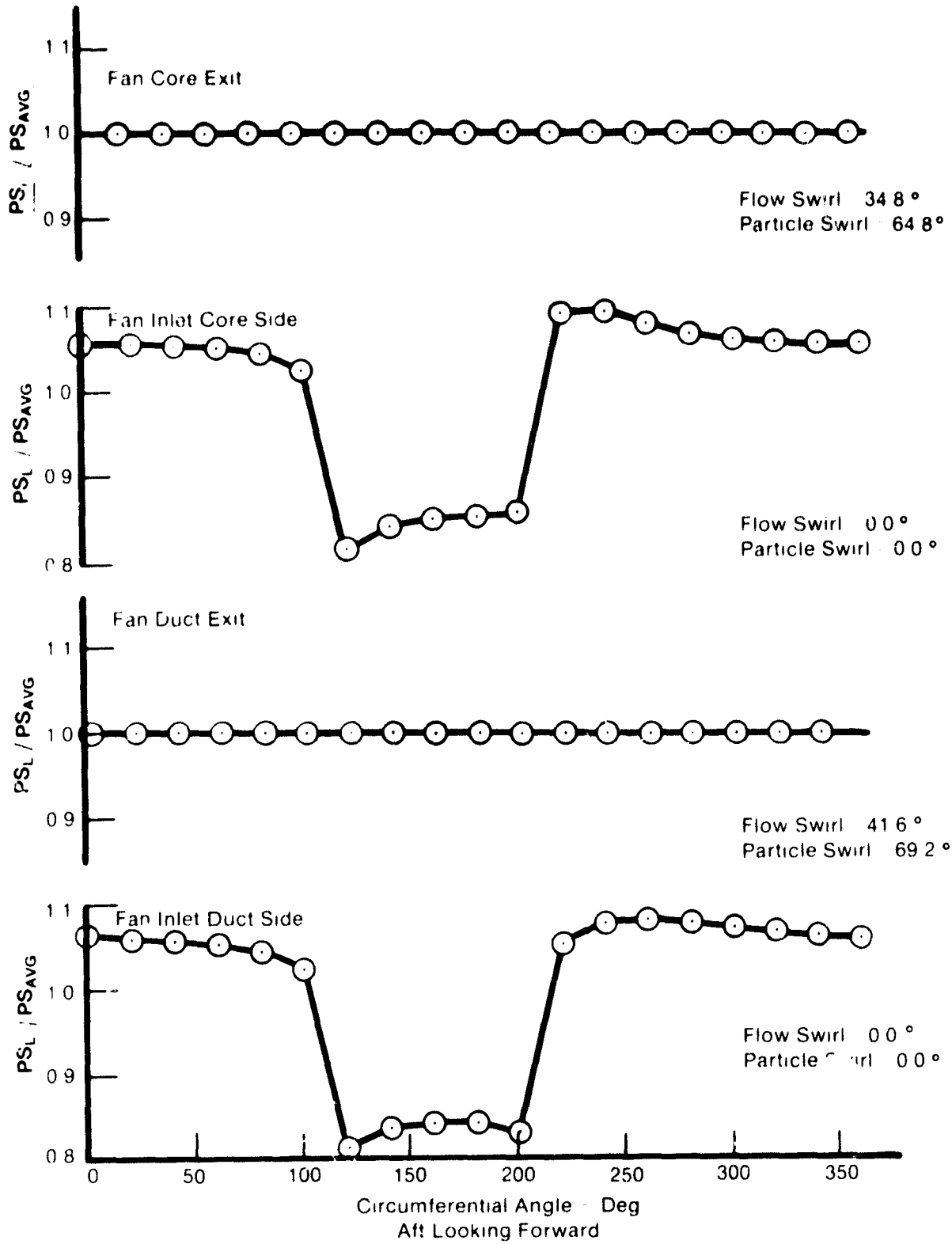

Figure 48. Predicted F100(3) Proximate Splitter Fan Static Pressure Profiles ~ Case 2 (22% $\Delta P_T/P_T$ 90 Deg)

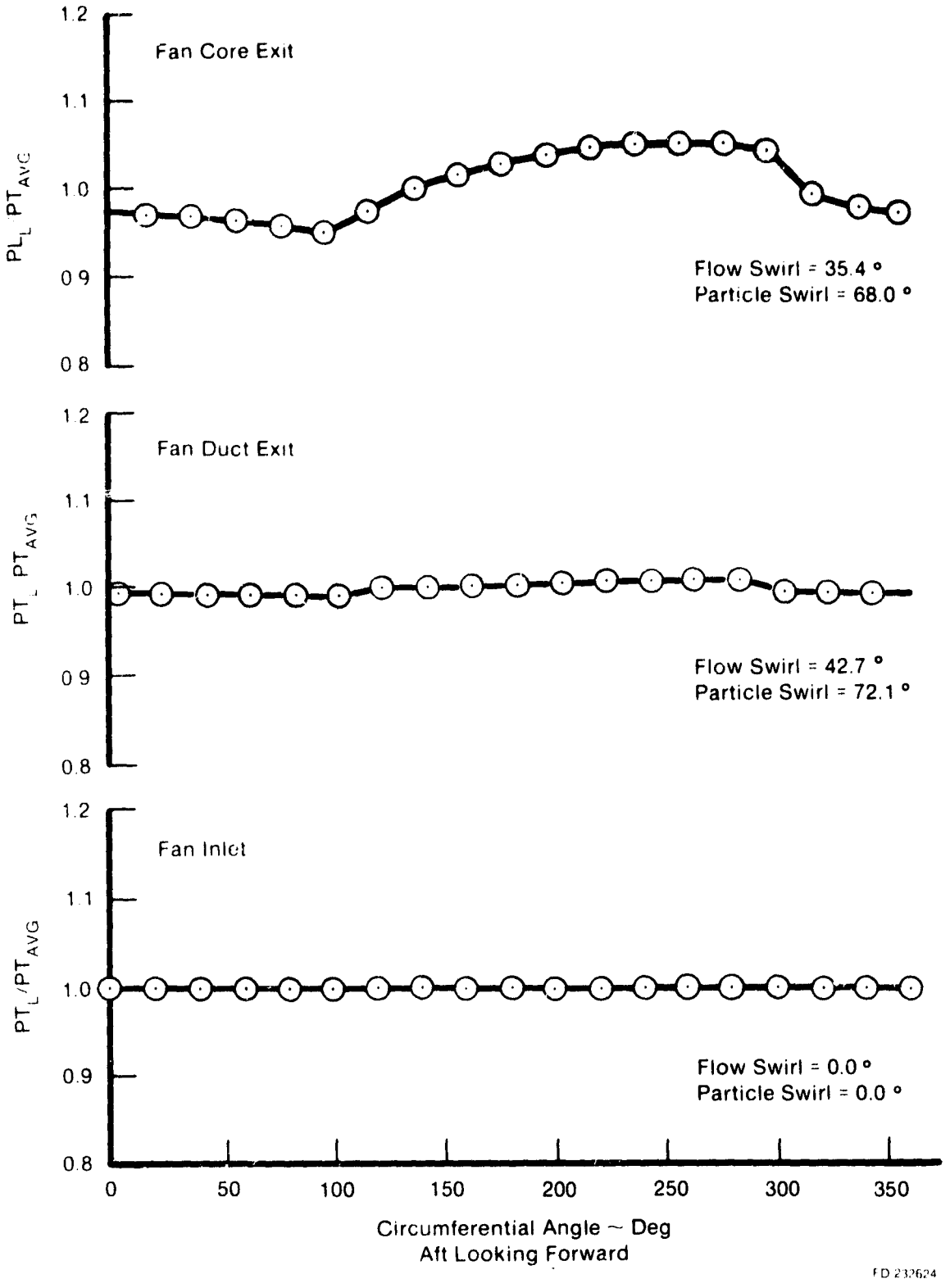

Figure 49. Predicted F100(3) Proximate Splitter Fan Total Pressure Profiles ~ Case 4 (18% $\Delta T_T/T_T$ /180 Deg)

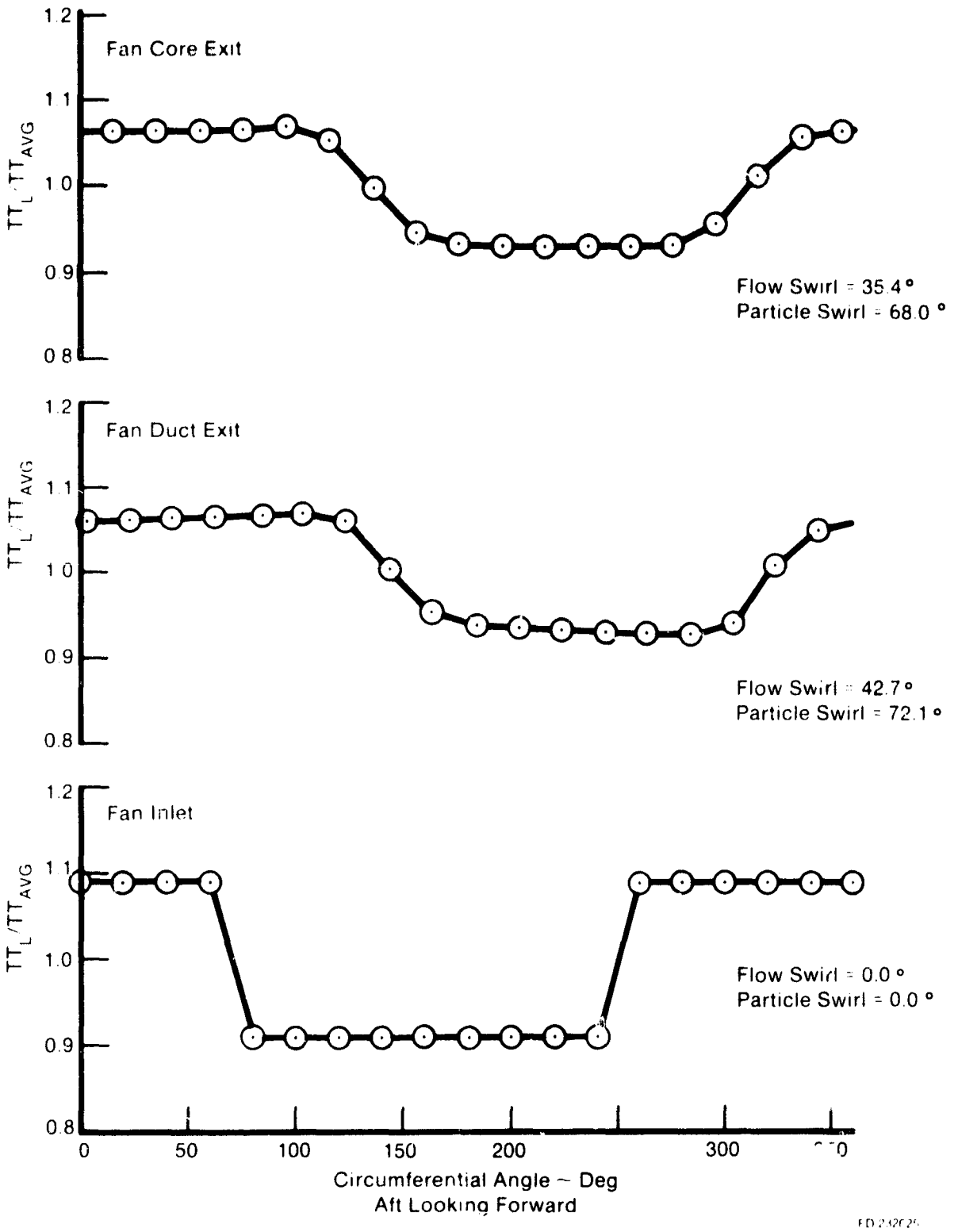

Figure 50. Predicted F100(3) Proximate Splitter Fan Total Temperature Profiles ~ Case 4 (18% $\Delta T_T/T_T$ /180 Deg)

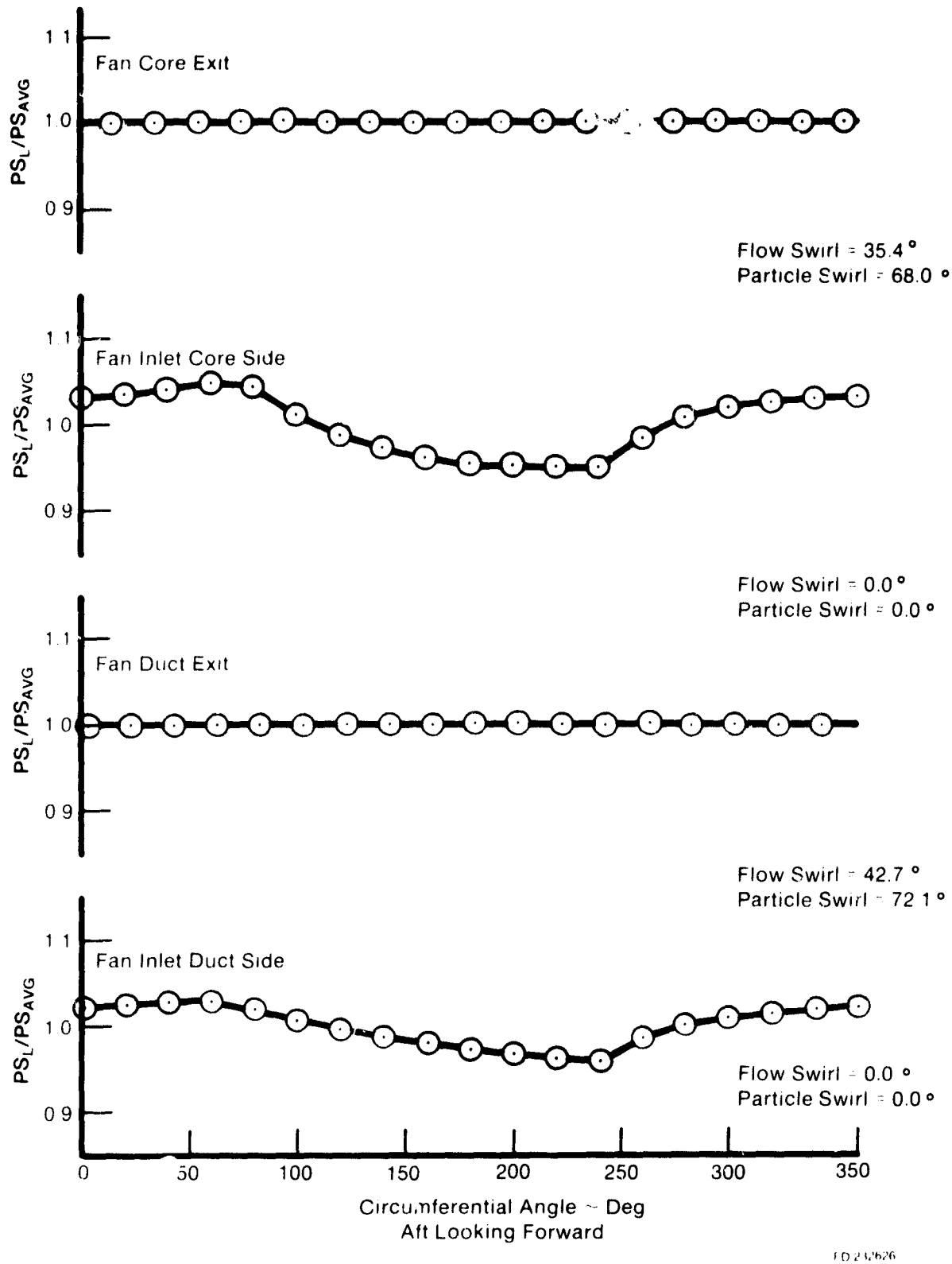

Figure 51. Predicted F100(3) Proximate Splitter Fan Static Pressure Profiles ~ Case 4 (18% $\Delta T_T/T_T$ /180 Deg)

TABLE 2. COMPARISON OF REMOTE AND PROXIMATE SPLITTER MSPC MODEL PREDICTIONS

Proximate Splitter

Distortion Type	*Amplitude (max-min)/avg*	*Extent of Distortion*	*Surge Flow*	*% ΔSPR*	$\Delta P_T/P_T$	$\Delta T_T/T_T$	*Kθ*	*Kp*
Pressure	22	180	204.46	6.40	13.68	6.25	0.561	0.271
Pressure	22	90	206.76	8.46	12.94	6.91	0.493	0.227
Pressure	15	180	203.53	3.81	9.99	5.00	0.393	0.232
Temperature	18	180	201.78	4.62	10.04	13.97	0.450	0.802
Temperature	9	180	205.88	3.52	4.67	7.13	0.214	0.422
Temperature	18	90	200.98	4.53	9.90	14.85	0.450	0.701

Remote Splitter (CR-159754)

Pressure	22	180	204.2	5.41	13.01	7.12	0.550	0.288
Pressure	22	90	206.1	7.14	11.75	7.90	0.485	0.242
Pressure	15	180	205.8	2.99	9.00	4.96	0.365	0.201
Temperature	18	180	206.2	3.56	9.70	15.60	0.404	0.890
Temperature	9	180	209.3	0.59	6.15	7.45	0.238	0.440
Temperature	9	90	208.5	1.17	4.35	7.80	0.166	0.325

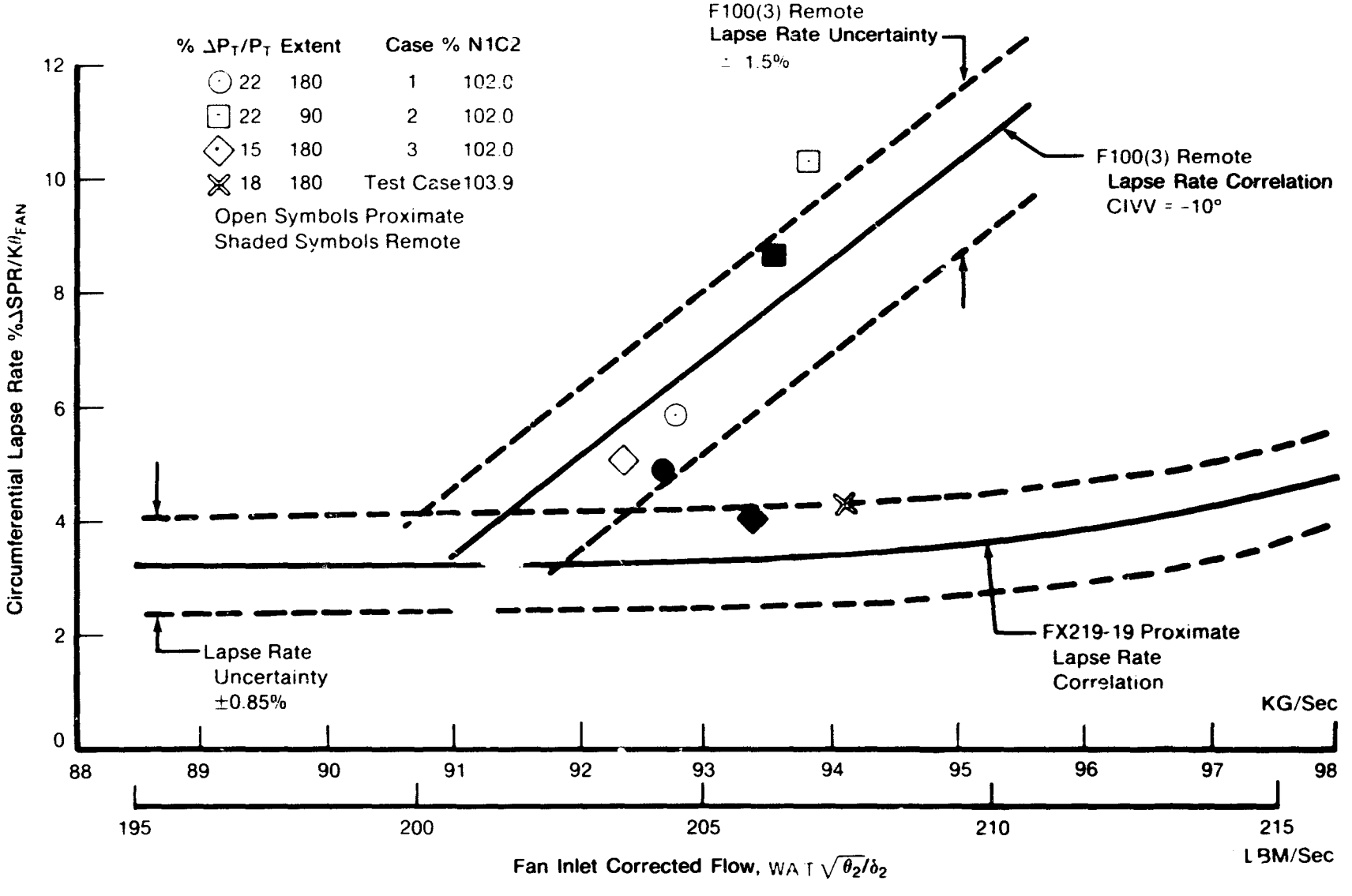

FD 232644
820802
bt2 987

Figure 52. Predicted F100(3) Proximate Splitter Fan Circumferential Pressure Distortion Kθ Sensitivity, Compared to Remote Splitter Predictions (CR-159754)

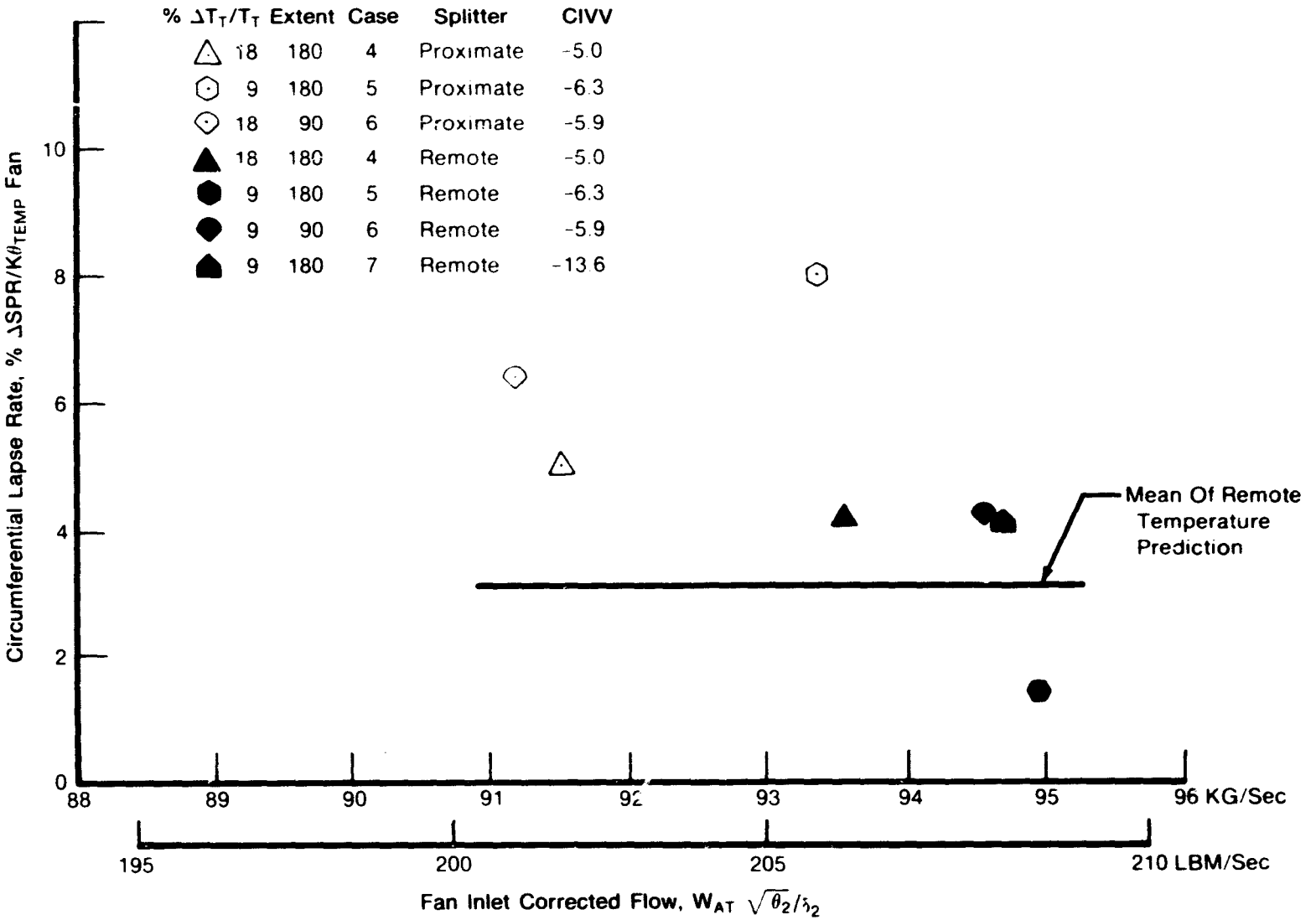

FD 232645
820802
bt2 988

Figure 53. Predicted F100(3) Proximate Splitter Fan Circumferential Temperature Distortion Kθ Sensitivity, Compared to Remote Splitter Predictions (CR-159754)

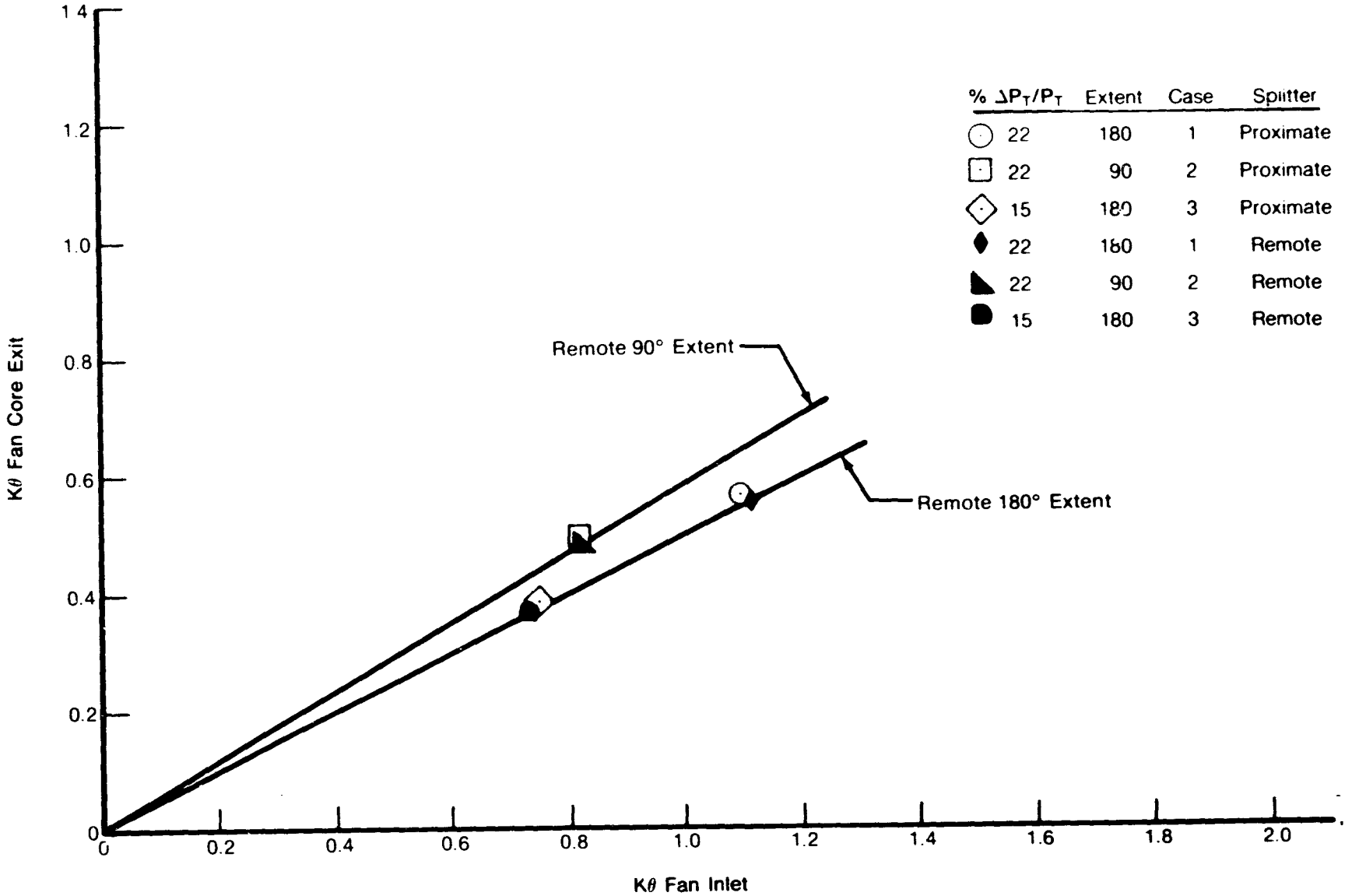

FD 232627
820802
bt2 988

Figure 54. Predicted F100(3) Proximate Splitter Fan Pressure Distortion Attenuation: Kθ, Compared to Remote Splitter Predictions (CR-159754)

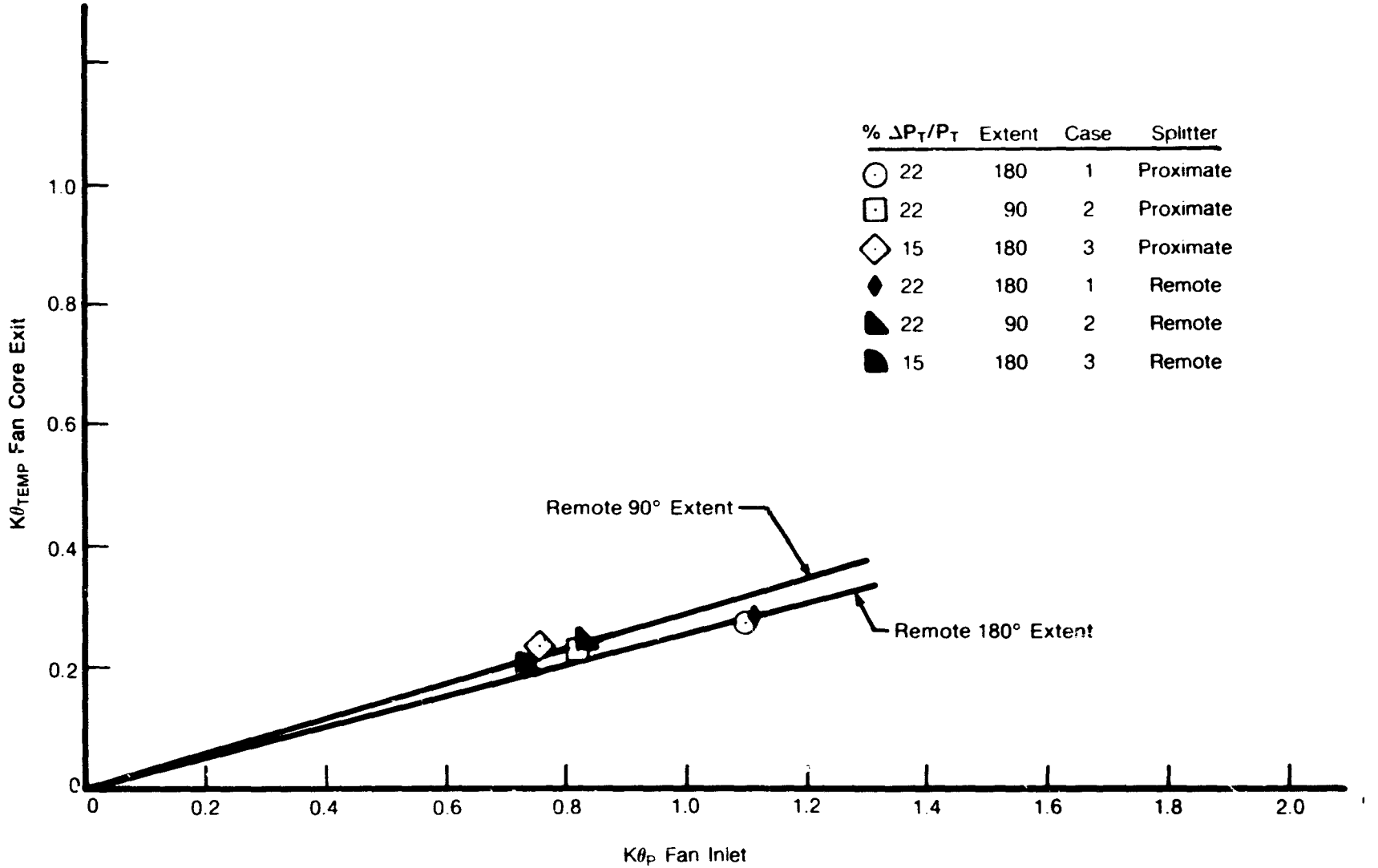

Figure 55. Predicted F100(3) Proximate Splitter Fan Temperature Distortion Generation: $K\theta_{TEMP}$ Compared to Remote Splitter Predictions (CR-159754)

FD 232626
820802
bk2 980

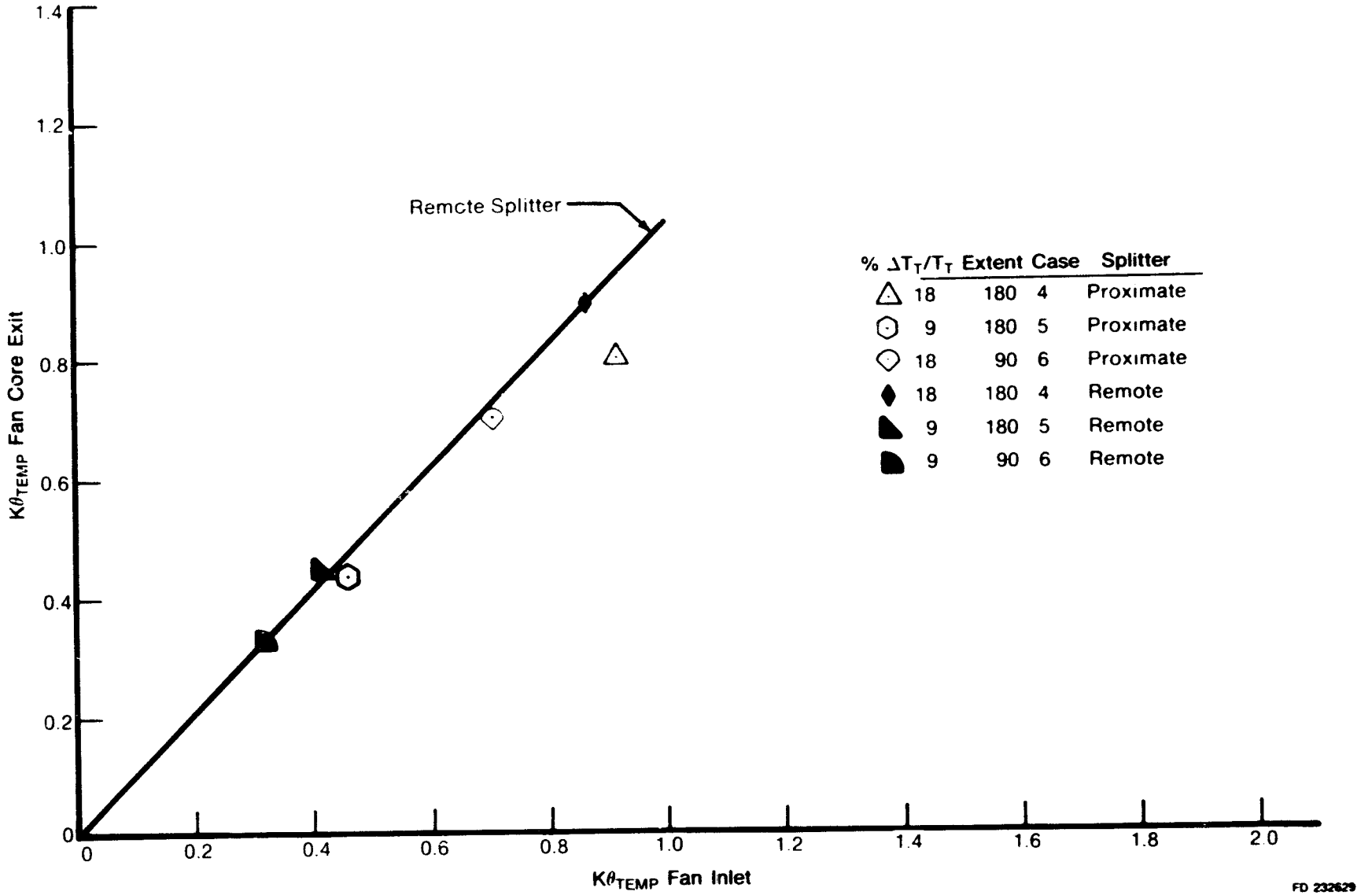

Figure 56. Predicted F100(3) Proximate Splitter Fan Temperature Distortion Attenuation: $K\theta_{TEMP}$, Compared to Remote Splitter Predictions (CR-159754)

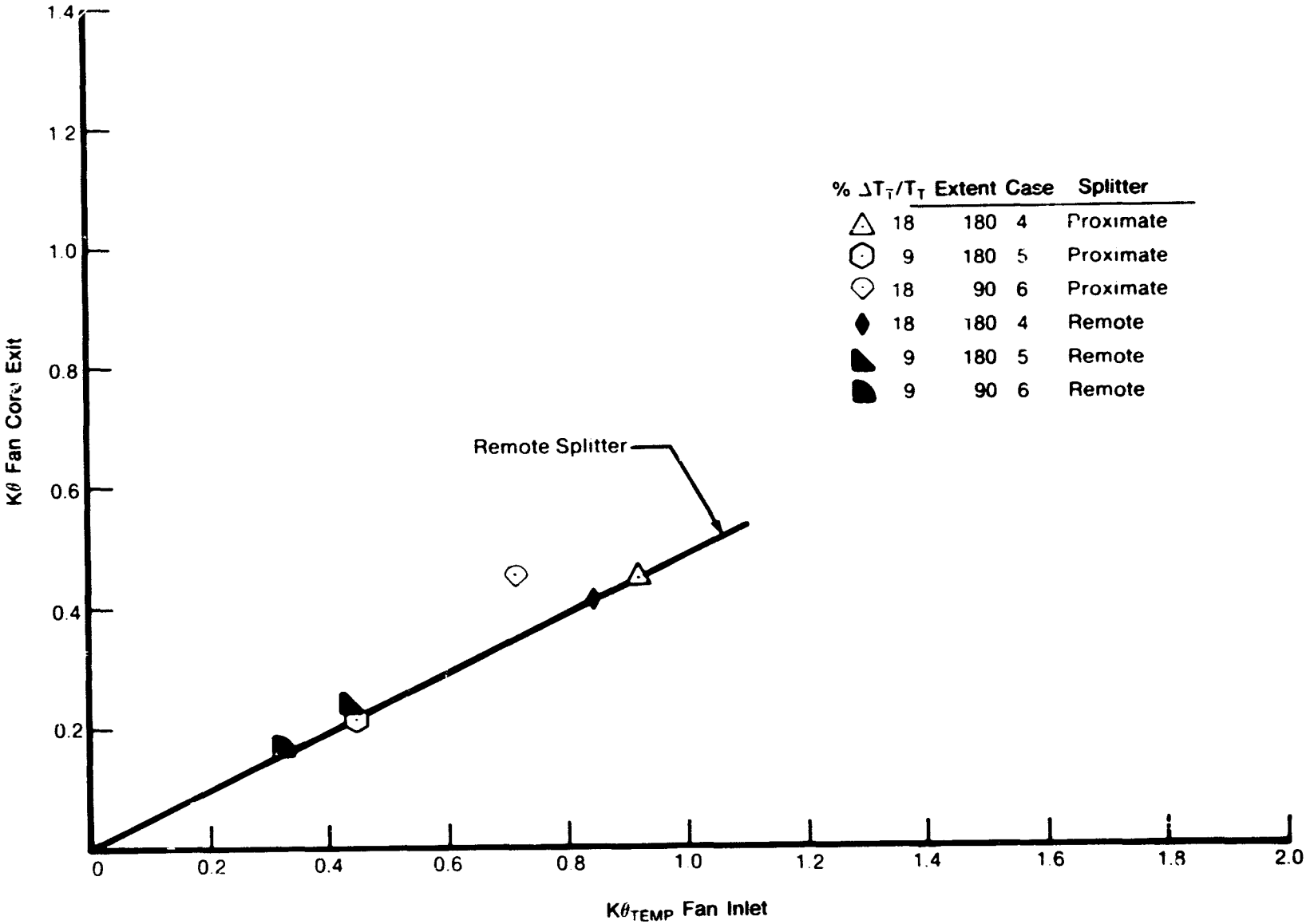

FD 232630
820802
bt2 992

Figure 57. Predicted F100(3) Proximate Splitter Fan Pressure Distortion Generation: Kθ, Compared to Remote Splitter Predictions (CR-159754)

The proximate splitter lapse rate correlation was derived from experimental testing conducted with engine FX219-19 at Arnold Engineering Development Center. As part of a test program designed to document fan stability characteristics with a proximate splitter, the circumferential lapse rate was determined by testing behind a 180-degree moderate intensity screen ($5^1/_2 \times 5^1/_2 \times 0.063$). The surge line was defined by running constant speedlines to stall along the variable IGV scheduled by the engine control as a function of corrected fan speed. Figure 58 shows the undistorted and 180-degree distortion surge lines which were adjusted to omit intermediate case losses. With the surge lines established, the percentage of loss in surge margin was calculated and divided by the inlet pressure distortion $K\theta$, Figure 59, to give the circumferential lapse rate to pressure distortion as a function of corrected air flow shown in Figure 60. The proximate splitter lapse rate correlation given in Figures 23 and 52 is the appropriate part of that curve.

In contrast to the proximate splitter stability audit which is limited to the nominal F100(3) CIVV schedule, the remote audit was formulated with off-schedule CIVV capability. It was generated from data acquired on Build 1 of P&WA's Improved Stability — Bulged ID Flowpath, F100 fan. The F100(3) fan has blading differences from that build and demonstrated in a brief experimental program somewhat less sensitivity to inlet pressure distortion than Build 1.

The off-schedule CIVV capability required surge lines to be generated at fixed CIVV angles when operating behind a circumferential distortion screen. The remote splitter stability audit correlates the pressure distortion circumferential lapse rate for nine lines of constant CIVV ranging from −30 degrees to 0 degrees. Figure 61 shows the lapse rate used for a constant CIVV equal to −10 degrees. This angle corresponds to the vane angle of the three pressure cases and that line is the remote splitter stability correlation shown in Figure 52.

Therefore, while it is valid to compare the proximate and remote splitter lapse rate predictions to their respective correlations as is done in Figure 49, a direct comparison between the correlations can be misleading because the proximate correlation represents a varying CIVV angle and the remote splitter line only one CIVV angle of the total remote correlation. Even with this difference considered, the inconsistency between the model predictions and the correlations remain; the F100(3) lapse rate correlation for a remote splitter configuration is significantly higher than for a proximate splitter, while the model predicts marginally greater sensitivity to inlet circumferential pressure distortion for a proximate splitter.

The model-predicted response to inlet temperature distortion is compared for proximate and remote splitters in Figure 53. A lapse rate correlation for temperature distortion that could be used to evaluate the quality of the model predictions does not exist for the F100(3) fan. The proximate splitter cases are predicted to have a greater sensitivity to inlet temperature distortion than the remote splitter. For the 18% $\Delta T_T/T_T$ 180-degree case, the proximate splitter prediction is 0.8% $\Delta SPR/K\theta_{TEMP}$ greater than the remote splitter. Case 5, a 9% ΔT T_T 180-degree distortion, showed a significant difference in the calculated lapse rate; 8.0 for the proximate and 1.4 for the remote.

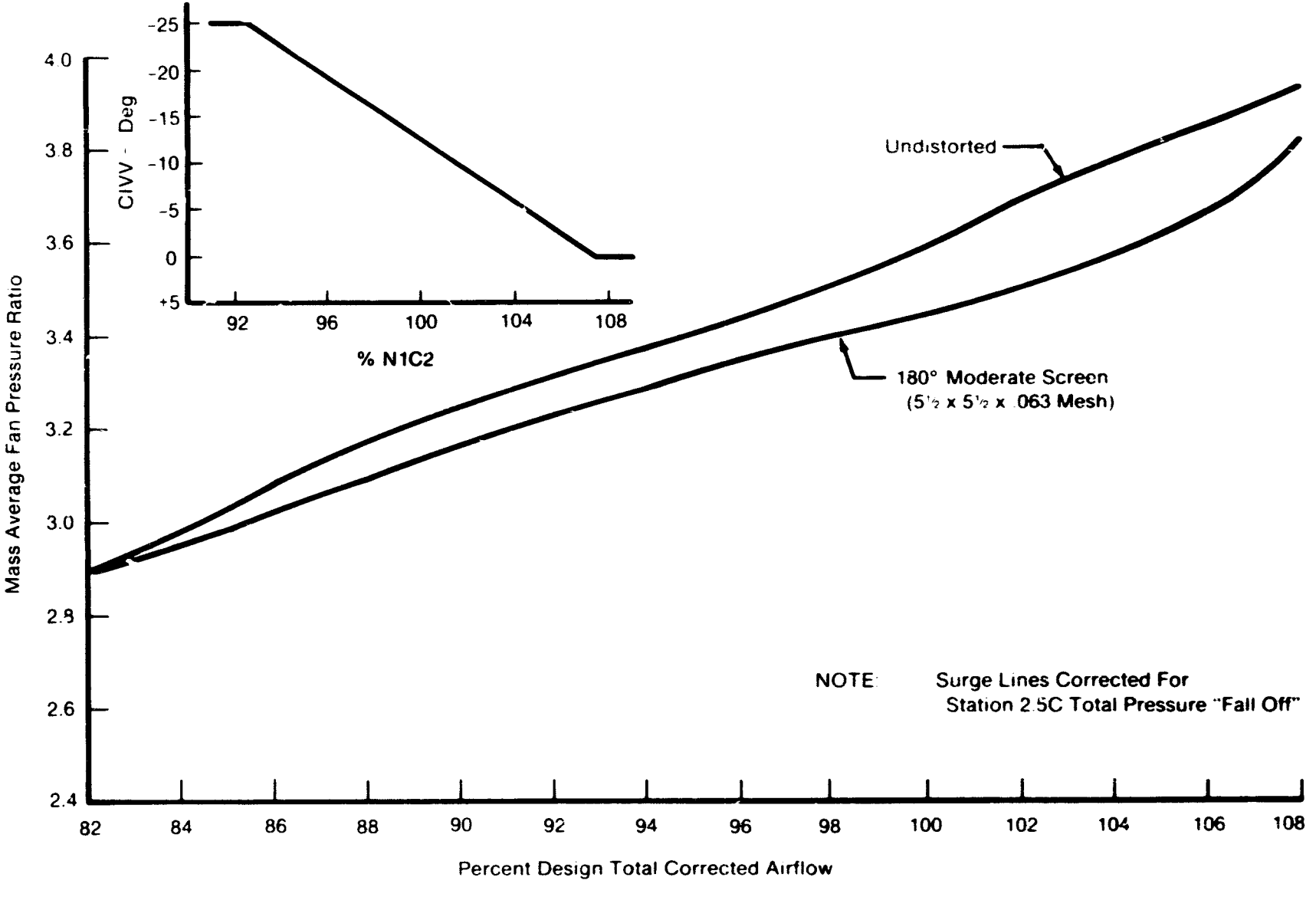

Figure 58. Comparison of FX219-19 Proximate Splitter Fan Undistorted and 180 Deg Distortion Surge Lines

FD 232646
820802
962 983

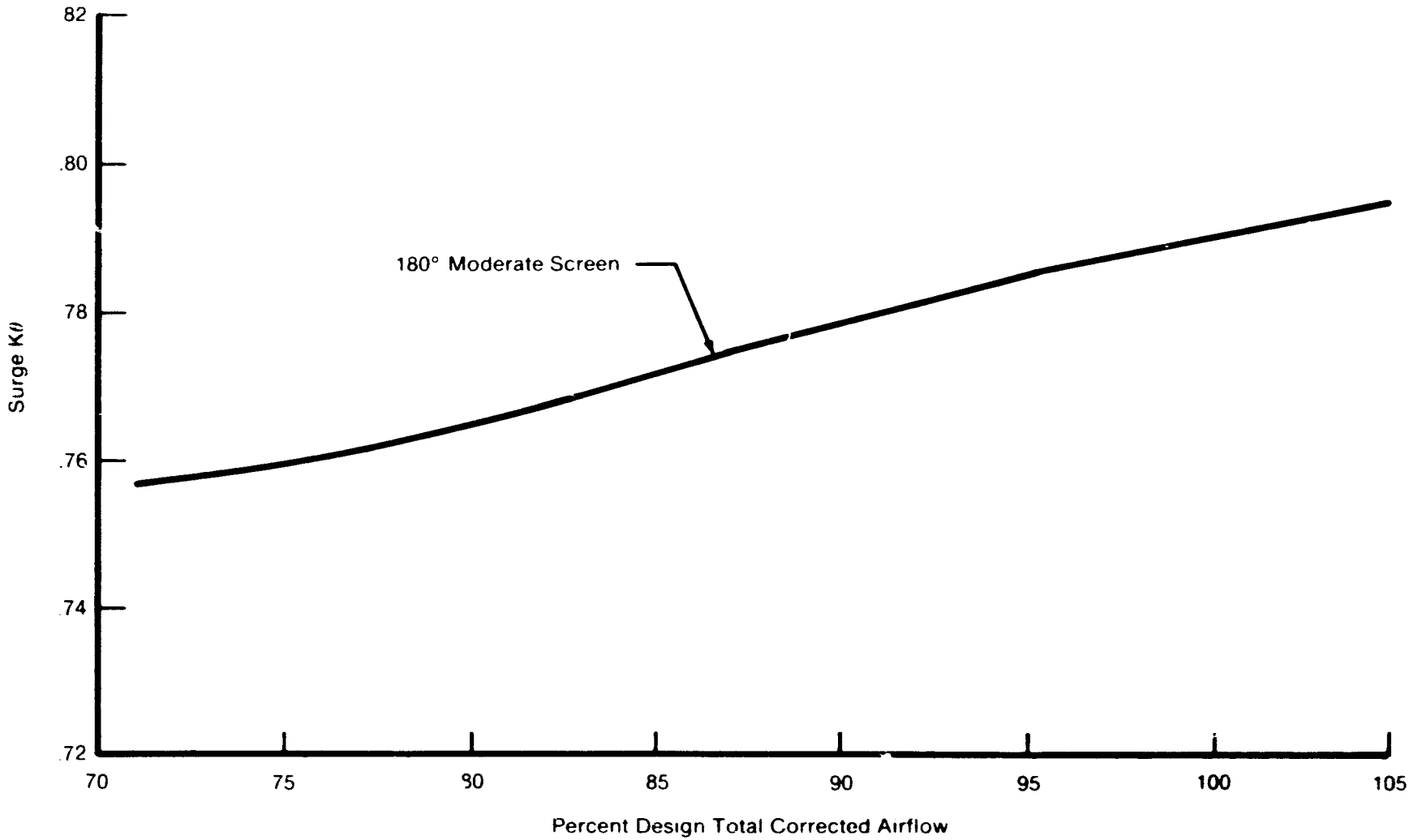

Figure 59. FX219-19 Proximate Splitter Fan Surge Kθ

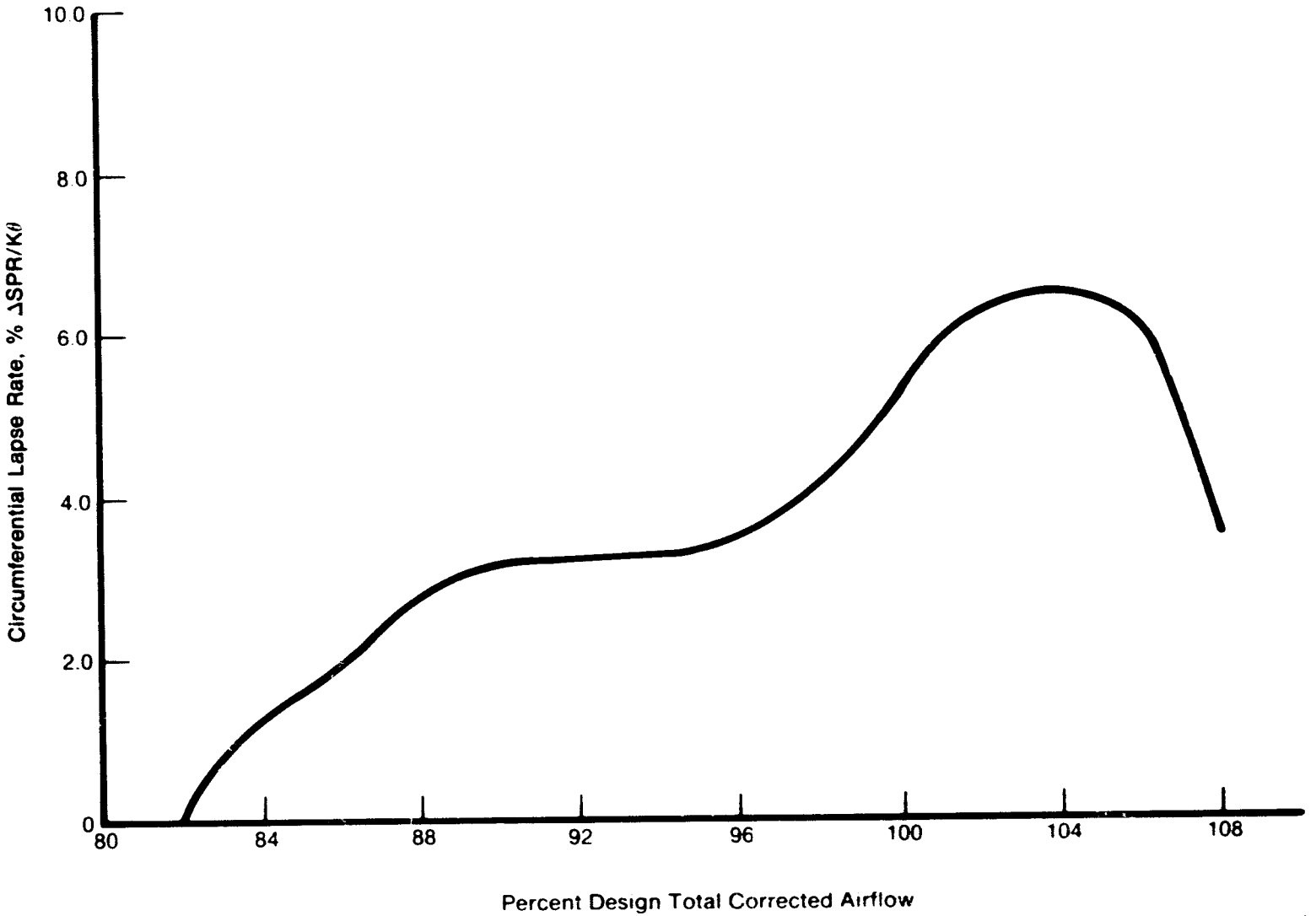

FD 232649
820802
042 994

Figure 60. FX219-19 Proximate Splitter Fan Circumferential Lapse Rate

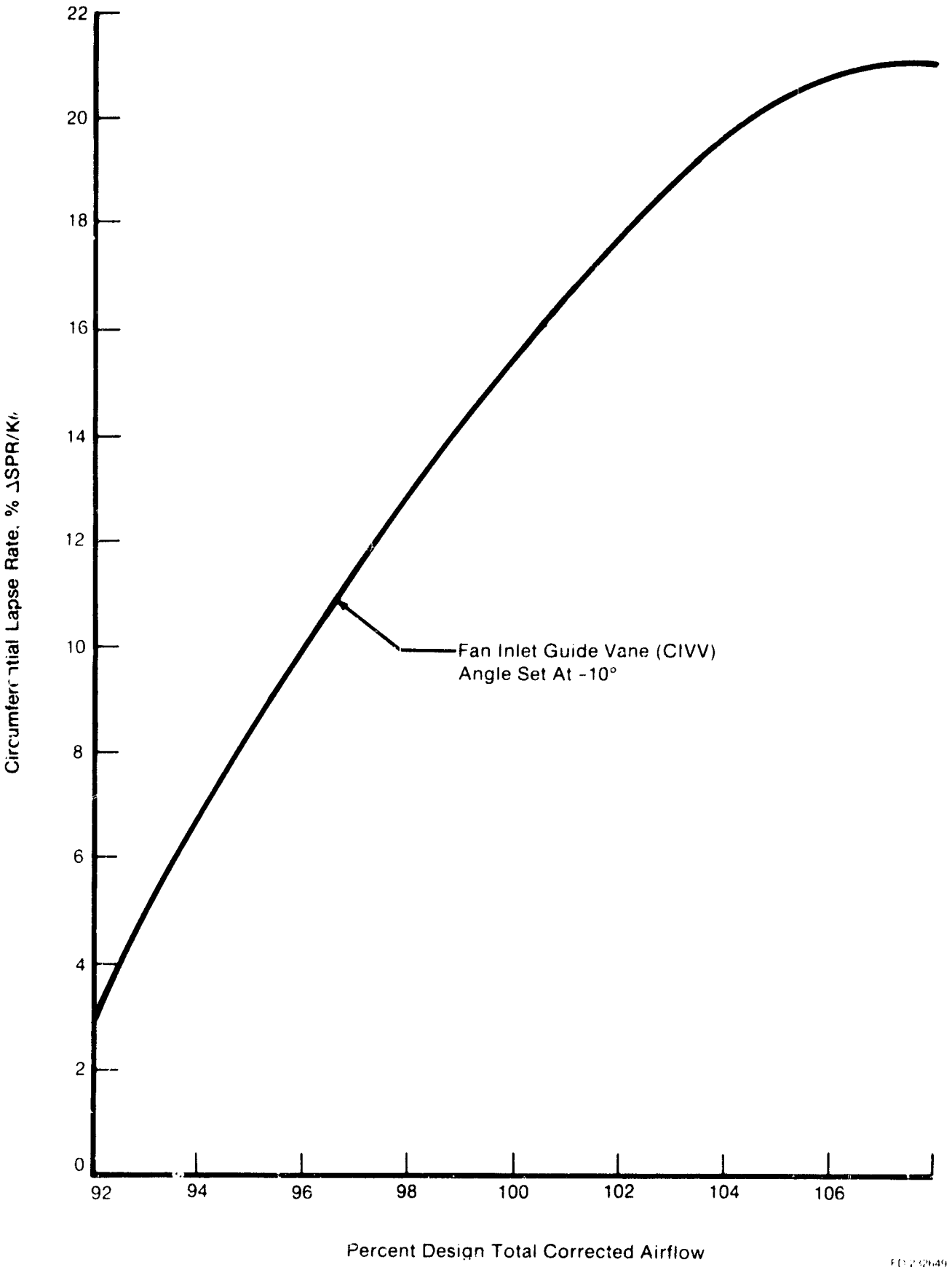

Figure 61. F100 Remote Splitter Fan Circumferential Lapse Rate

The reason for the scatter in the temperature distortion predictions has not been determined. The authors of the remote splitter final report (Reference 3) indicated that model accuracy when predicting fan response to low levels of temperature distortion (9% $\Delta T_T/T_T$ could be a source of scatter and recommended that cases be run at 18% $\Delta T_T/T_T$. Another possibility is the definition of the fan performance characteristics. The stall side pressure rise characteristics were adjusted so the pressure distortion test case model prediction gave good agreement with test data. It was impossible to use temperature distortion data as additional verification of performance characteristics because the F100(3) fan has not been tested with inlet temperature distortion. One obvious difference between the proximate and remote model predictions was which fan stream set the stall-limiting airflow. Table 3 shows the splitter configuration had no effect on the limiting stream for the pressure distortion cases; however, all the temperature distortion cases were predicted to be limited by the ID stream for a proximate splitter, while all remote splitter cases were limited by the fan OD stream.

TABLE 3. COMPARISON OF MODEL-PREDICTED STALL LIMITING FAN STREAM FOR PROXIMATE AND REMOTE EXIT SPLITTERS

Distortion Type	*Amplitude (max-min)/avg*	*Extent (deg)*	*Stall Limiting Fan Stream*	
			Proximate	*Remote*
Case 1 Pressure	22%	180	ID	ID
Case 2 Pressure	22%	90	ID	ID
Case 3 Pressure	15%	180	OD	OD
Case 4 Temperature	18%	180	ID	OD
Case 5 Temperature	9%	180	ID	OD
Case 6 Temperature	18%	90	ID	–
Case 6 Temperature	9%	90	–	OD
Case 7 Temperature	9%	180	–	OD

The calculated distortion transfer characteristics for the fan are compared in Figures 54 through 57. The proximate splitter predictions are plotted on figures documenting the remote splitter results reported in CR-159754. For both splitter configurations the distortion transfer characteristics are predicted to be very similiar. Figure 54 compares the predicted pressure distortion attenuation across the fan ID. The attenuation of the pressure distortion results in the generation of a fan exit temperature distortion. As with the pressure distortion attenuation, the temperature distortion generation is shown in Figure 55 to be virtually identical for proximate and remote splitters. Figure 56 compares the predictions for the attenuation of inlet temperature distortion.

The remote splitter is predicted to provide no attenuation of temperature distortion across the fan ID. Like the remote, the proximate splitter shows no attenuation, except at very high levels of inlet temperature distortion where the proximate splitter begins to show a small amount of attenuation. Figure 57 compares the pressure distortion generated by the inlet temperature distortion. Both splitter configurations show the same characteristics, generating a $K\theta$ of 0.48 for an inlet $K\theta_{TEMP}$ of 1.0.

CONCLUSIONS

1. The P&WA Multiple Segment Parallel Compressor Model predicts that the stall margin loss of an F100(3) proximate splitter fan is approximately the same for equal levels of pressure and temperature circumferential distortion.

2. The model predicts a greater sensitivity to inlet pressure distortion than was calculated based on proximate splitter engine distortion data.

3. Distortion of different circumferential extents should be tested since the model indicates significantly different fan response for pressure distortions of 180 and 90 degrees.

4. The F100(3) fan splitter configuration is predicted to have minimal effect on circumferential pressure distortion sensitivity with $\Delta SPR/K\theta$ about 1 to 1½% greater for a proximate splitter fan.

5. The F100(3) fan is predicted to be more sensitive to circumferential temperature distortion with the proximate splitter configuration than the remote.

6. The F100 fan splitter configuration has no effect on the predicted fan distortion transfer characteristics and these characteristics, agree well with test data.

7. The ability of the model to predict distortion response depends upon the accurate definition of blade row performance characteristics. This requires interstage data of high quality for both pre- and post-stall operation.

8. The MSPCM is a development tool which can be used to assist in planning experimental test programs.

RECOMMENDATIONS

NASA-LeRC should consider the following recommendations in their planned F100(3) distortion test program.

(1) Instrument the fan exit case and compressor exit with multiple static pressure taps to determine the exit boundary conditions.

(2) A minimum of two circumferential extent, and two distortion amplitudes should be tested.

(3) A bolt-on proximate splitter should be tested to verify the splitter spacing sensitivity in a controlled back-to-back test.

(4) Interstage instrumentation should be available to verify the independence of IGV through stator 2 to splitter configuration.

(5) High response instrumentation will be required to evaluate the stalling criteria, and excursions of individual rows beyond their undistorted match conditions in the presence of inlet distortion.

APPENDIX I

Blade Row Performance Characteristics

The blade row performance characteristics for an F100(3) proximate splitter fan are contained in this appendix. The parameters have been defined separately for the fan ID and OD. This is possible since the flow per unit area is approximately equal for the ID and OD. Each rotor and stator is represented by a static pressure rise characteristic, PSI. Each rotor is also represented by a total temperature rise characteristic, LAMBDA. These are defined as a function of mass flow parameter divided by area, PHI/A, for lines of constant "speed parameter" in each of the figures. The characteristic parameters are defined as follows:

$$\text{PSI} = \frac{PS_{out} - PS_{in}}{PS_{in}} \cdot \frac{(N/\sqrt{\theta})^2_{DES}}{(N/\sqrt{\theta})^2}$$

$$\text{LAMBDA} = \frac{TT_{out} - TT_{in}}{TT_{in}} \cdot \frac{(N/\sqrt{\theta})^2_{DES}}{(N/\sqrt{\theta})^2}$$

$$\text{PHI/A} = \frac{W\sqrt{\theta}}{\delta A} \cdot \frac{(N/\sqrt{\theta})_{DES}}{(N/\sqrt{\theta})}$$

The characteristics use lines of constant "speed parameter" as opposed to typical corrected speed values as a method of accounting for the effects of variable geometry. The reason is that a wide variation in vane angle accompanies the change in corrected speed. The "speed parameter" represents both a corrected speed and the inlet guide vane angle. The relationship between corrected speed and "speed parameter" is of the following form:

Speed parameter = corrected speed/[a + b (IGV angle)]

In this equation a and b are empirical constants determined from F100(3) fan rig data. A separate set of constants has been defined for the fan ID and OD. A detailed explanation of the treatment of variable geometry effects by the MSPC model is given in Reference 1.

The F100(3) high-pressure compressor performance characteristics are defined using the above definitions and presented in Reference 6.

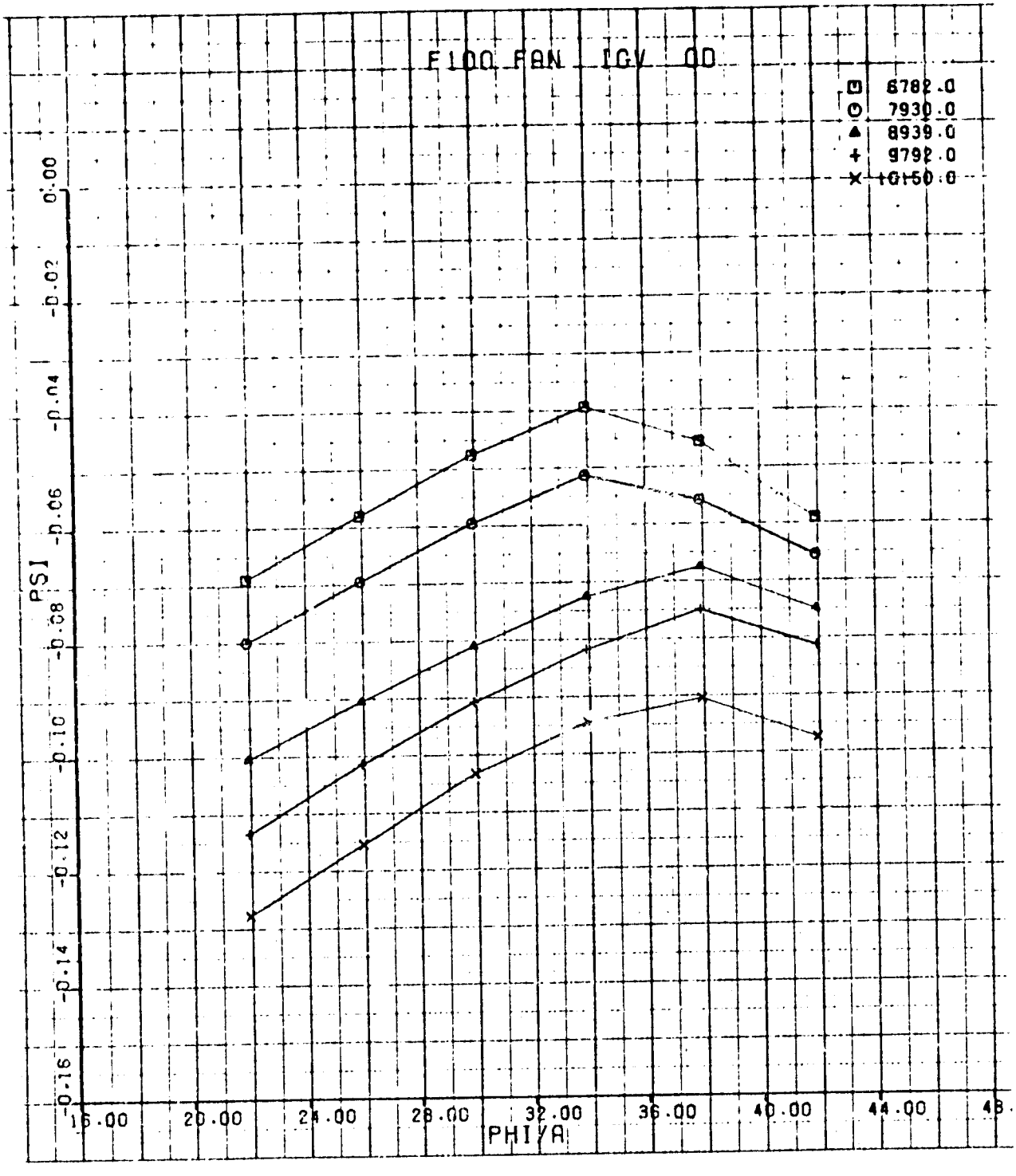

ORIGINAL PAGE IS
OF POOR QUALITY

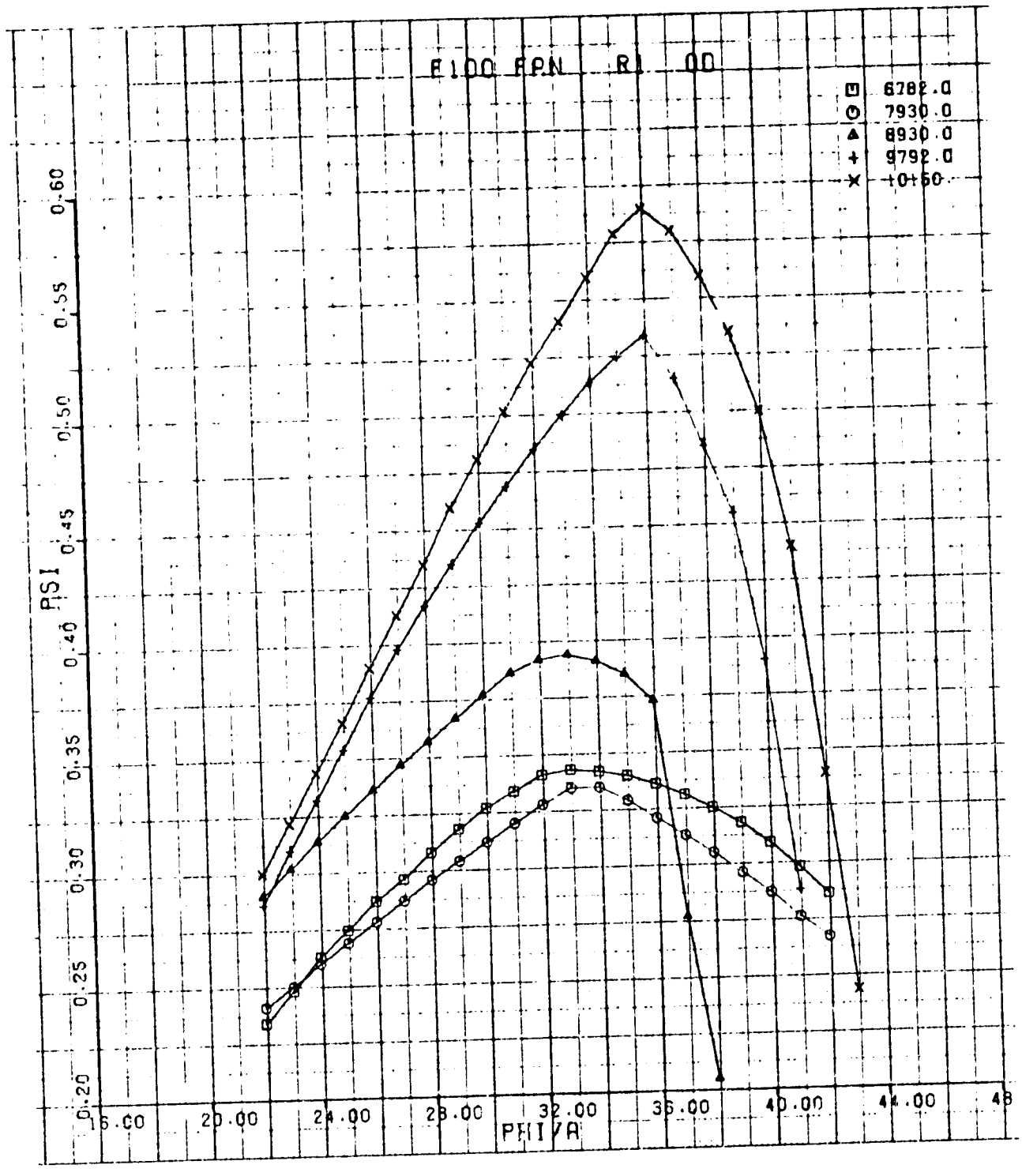

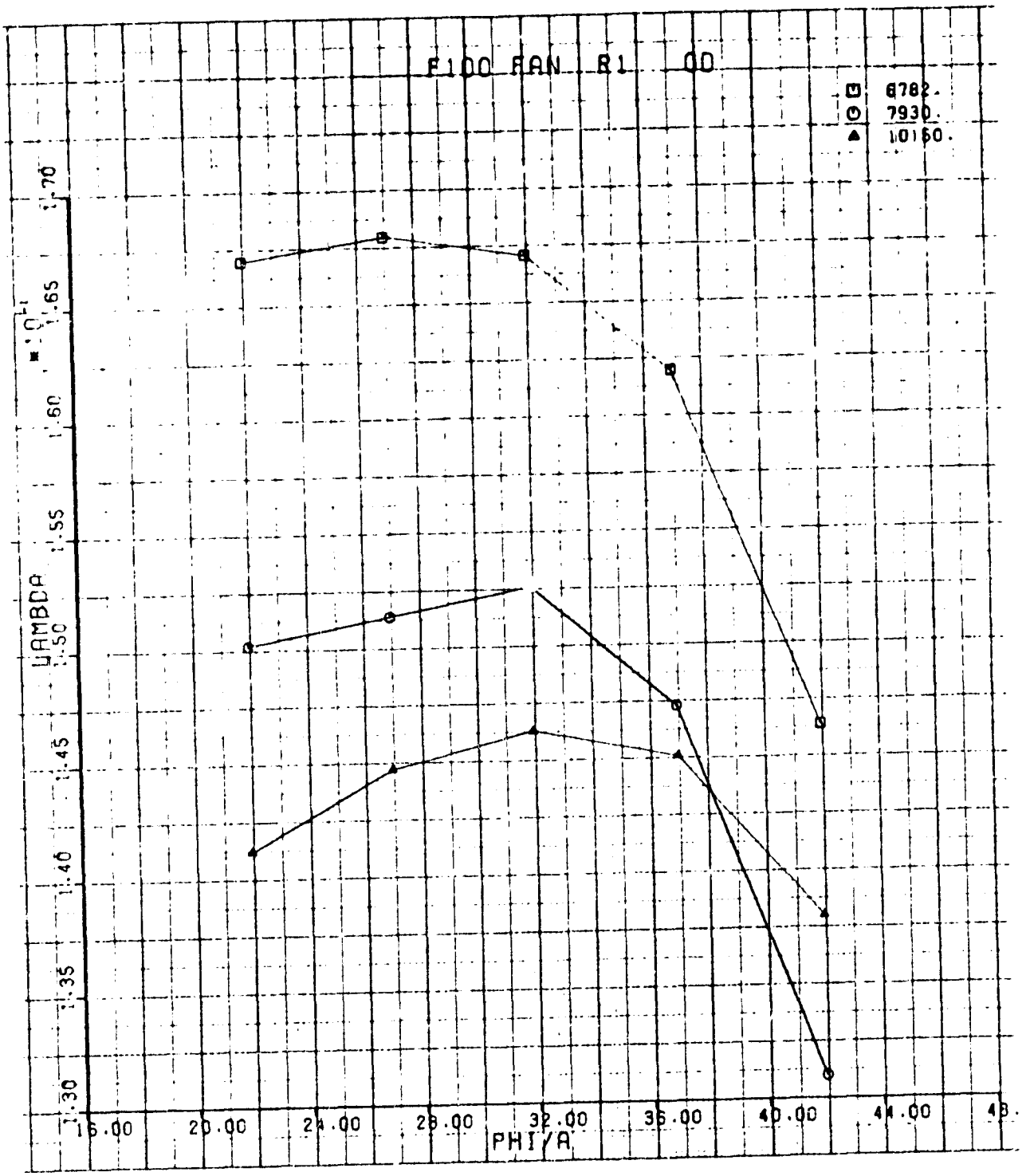

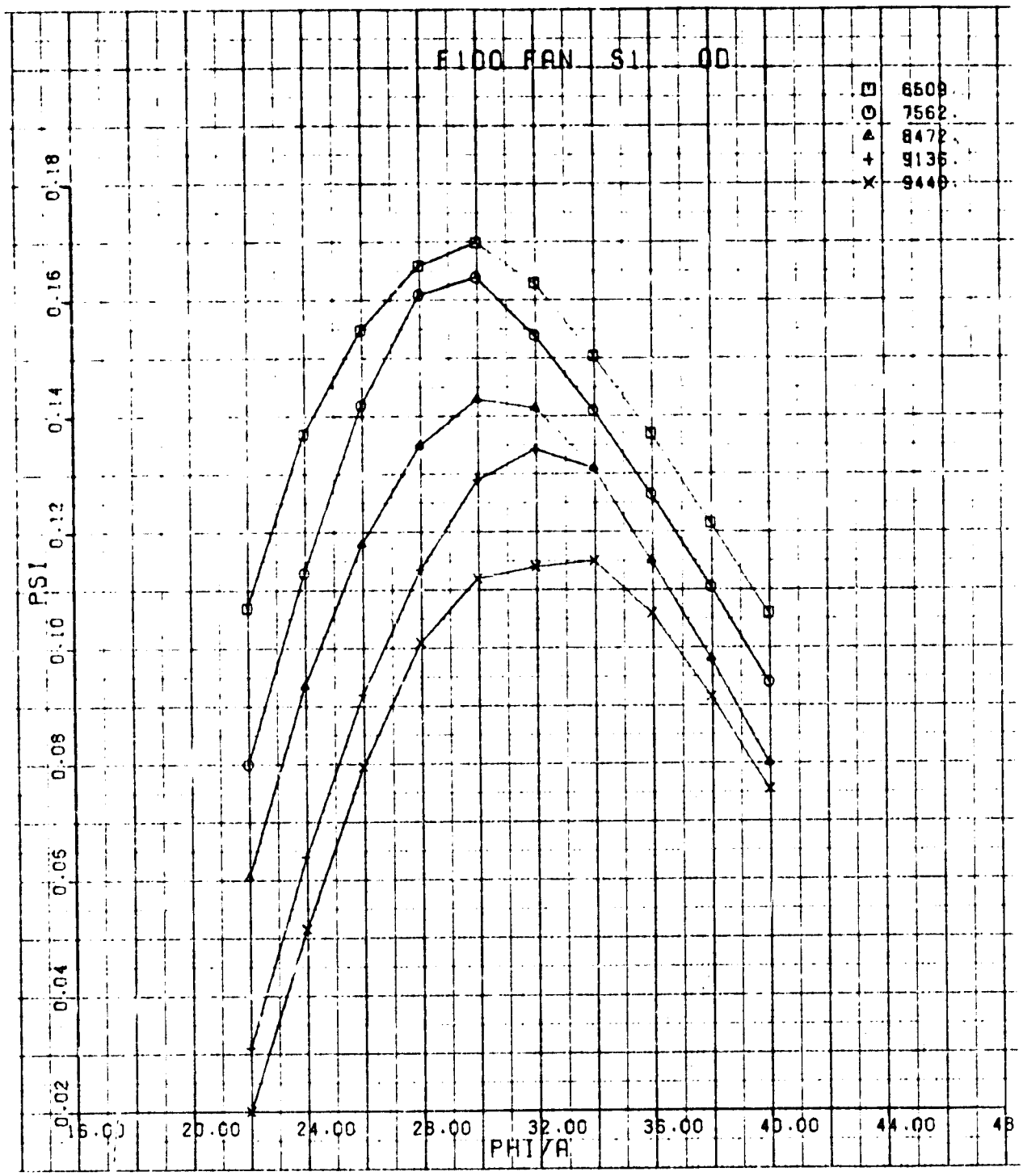

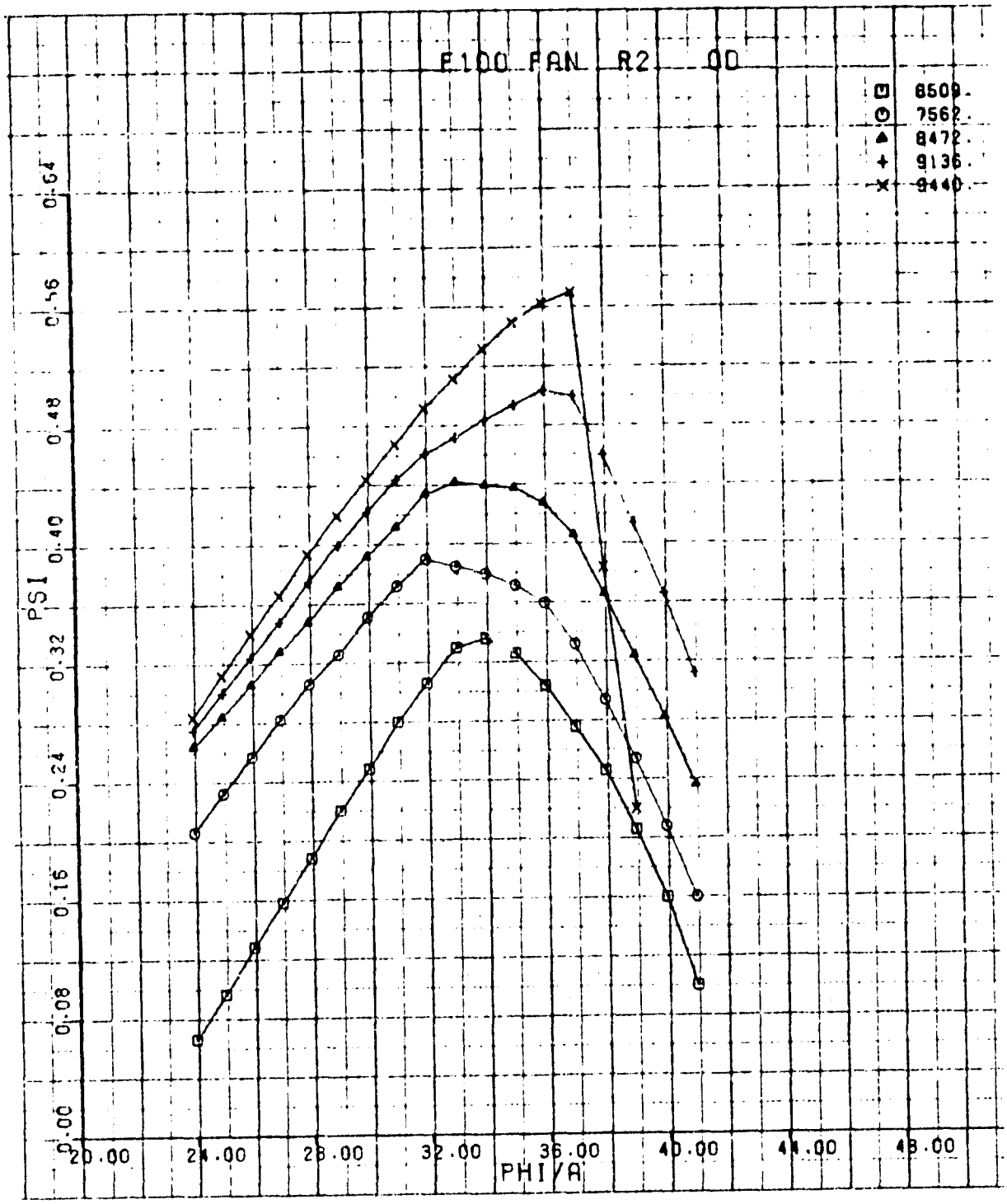

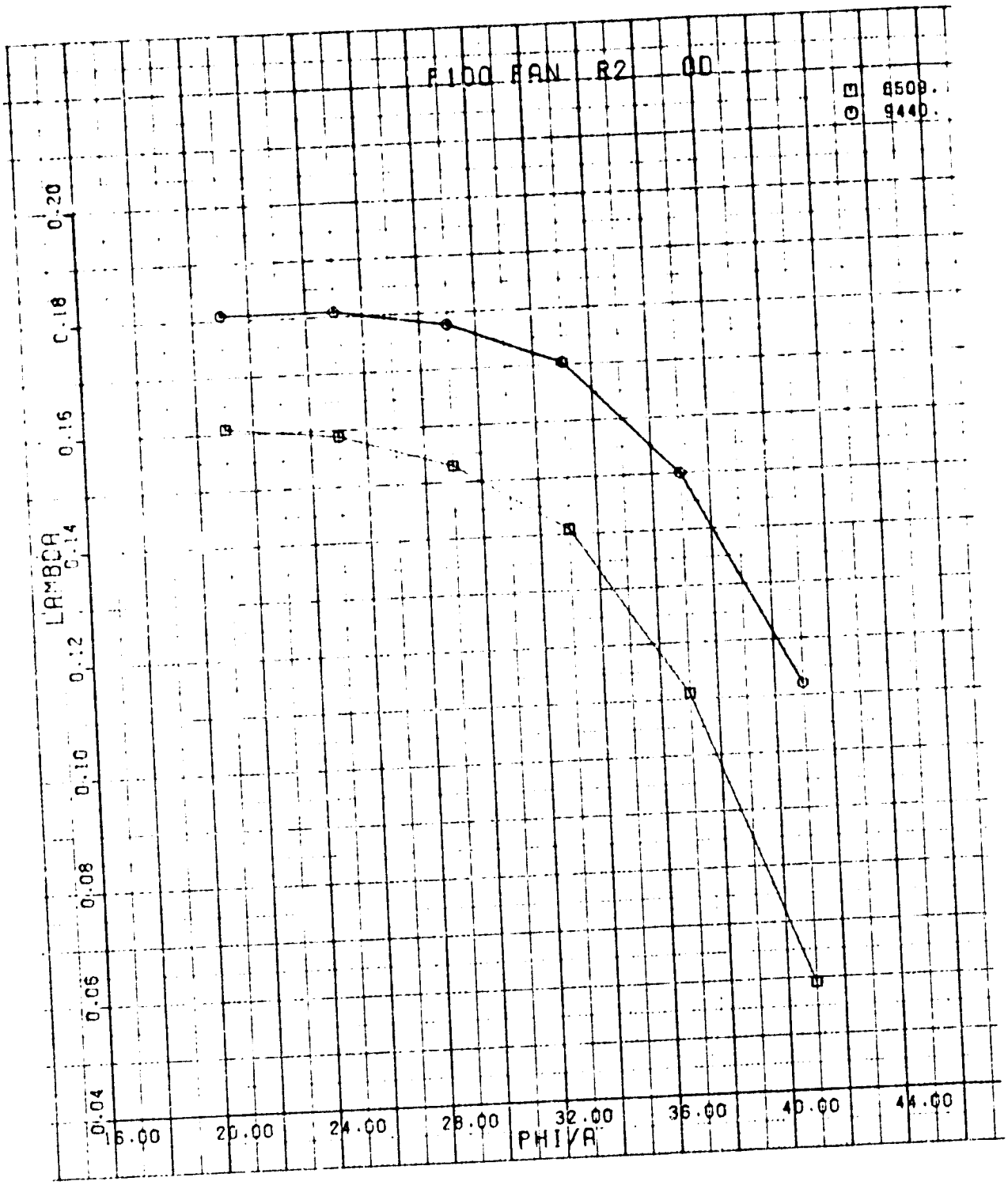

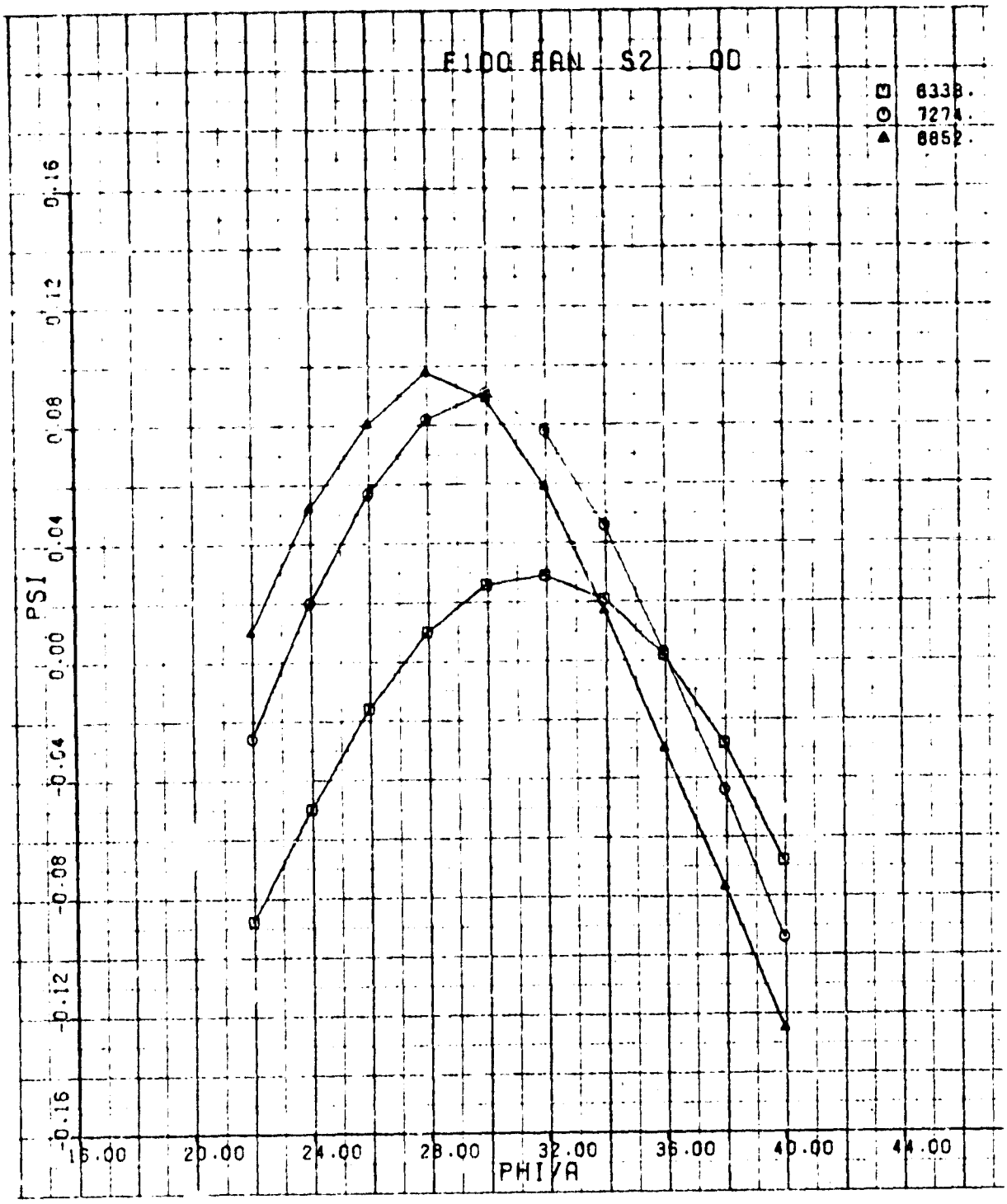

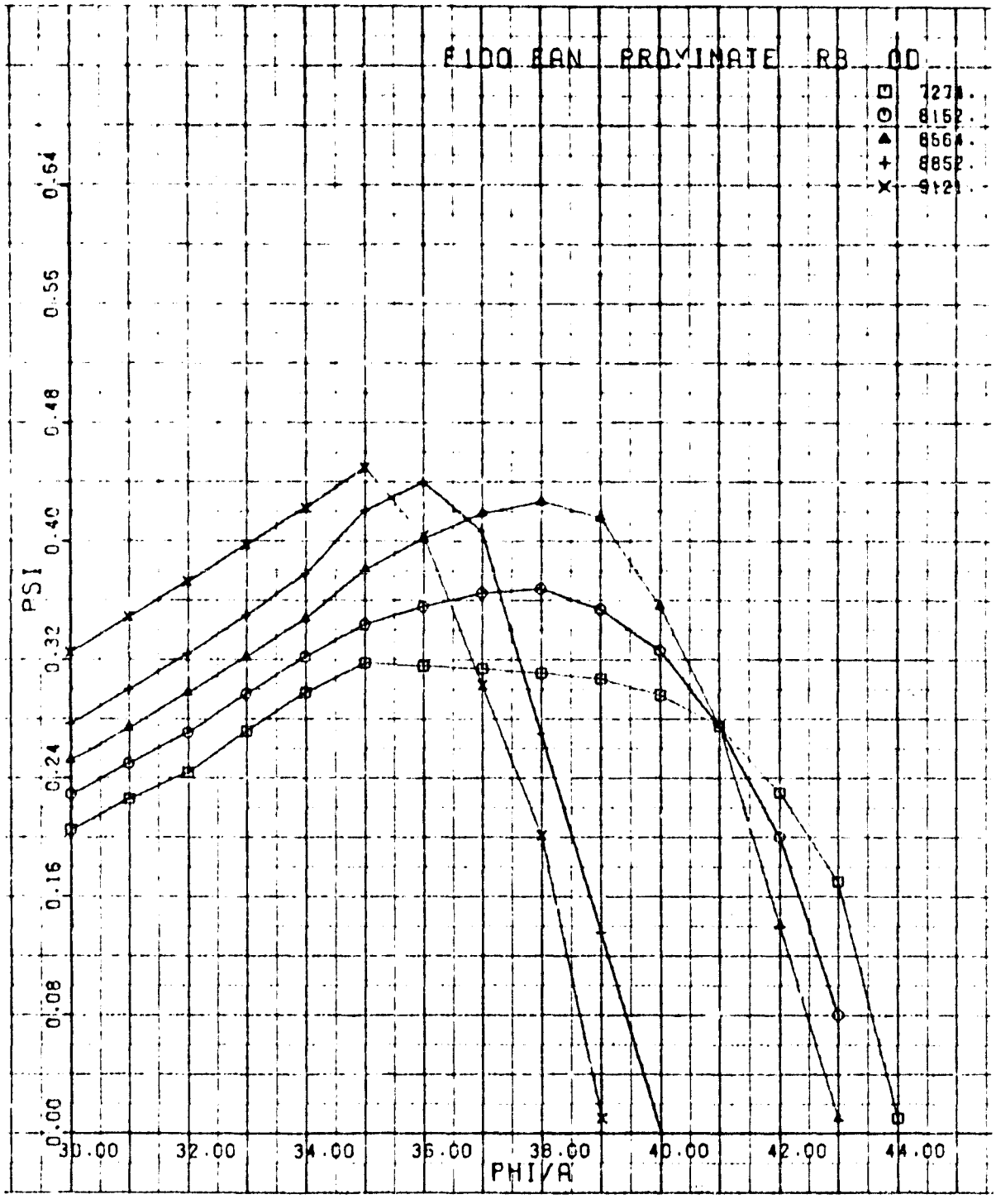

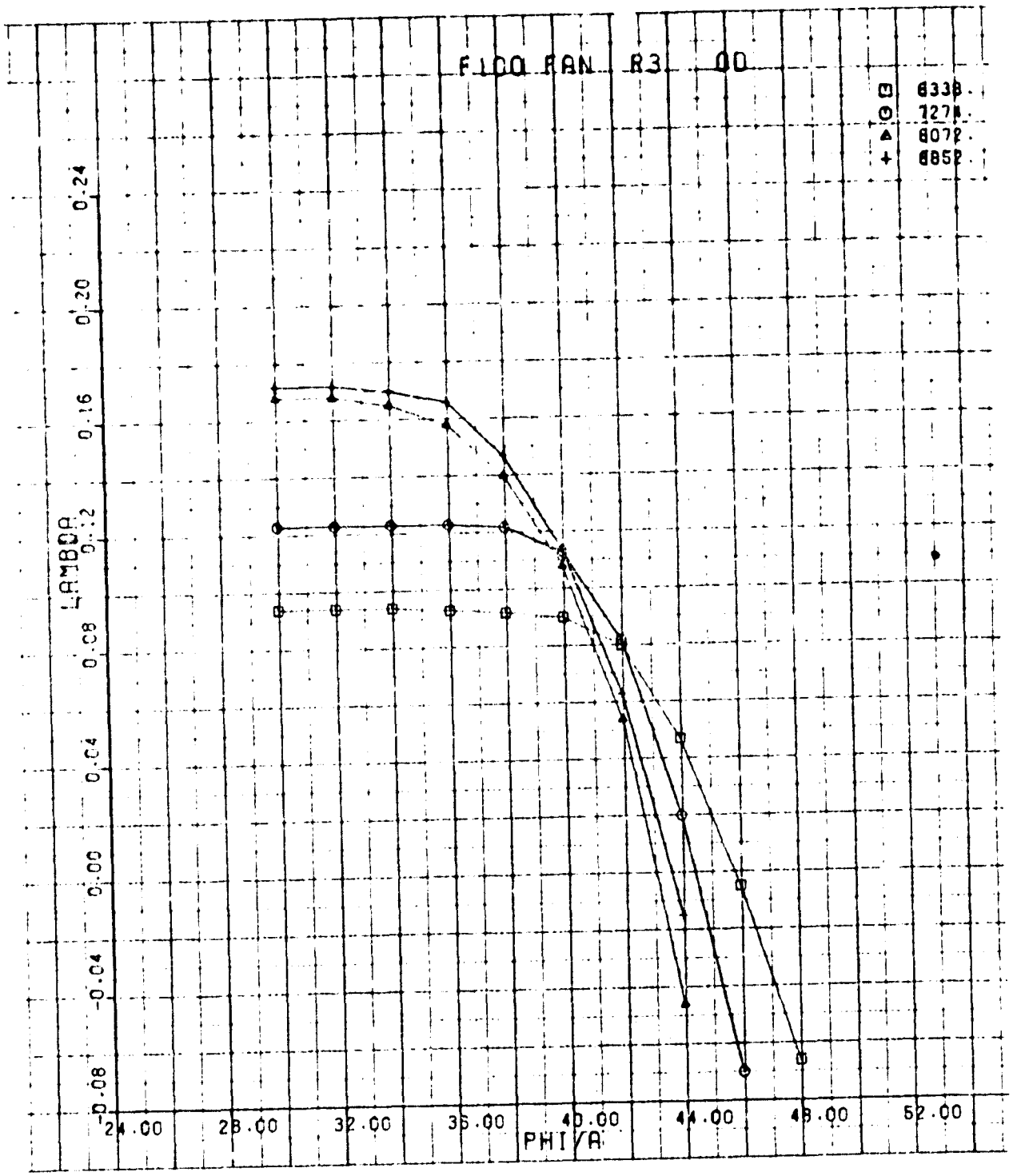

10

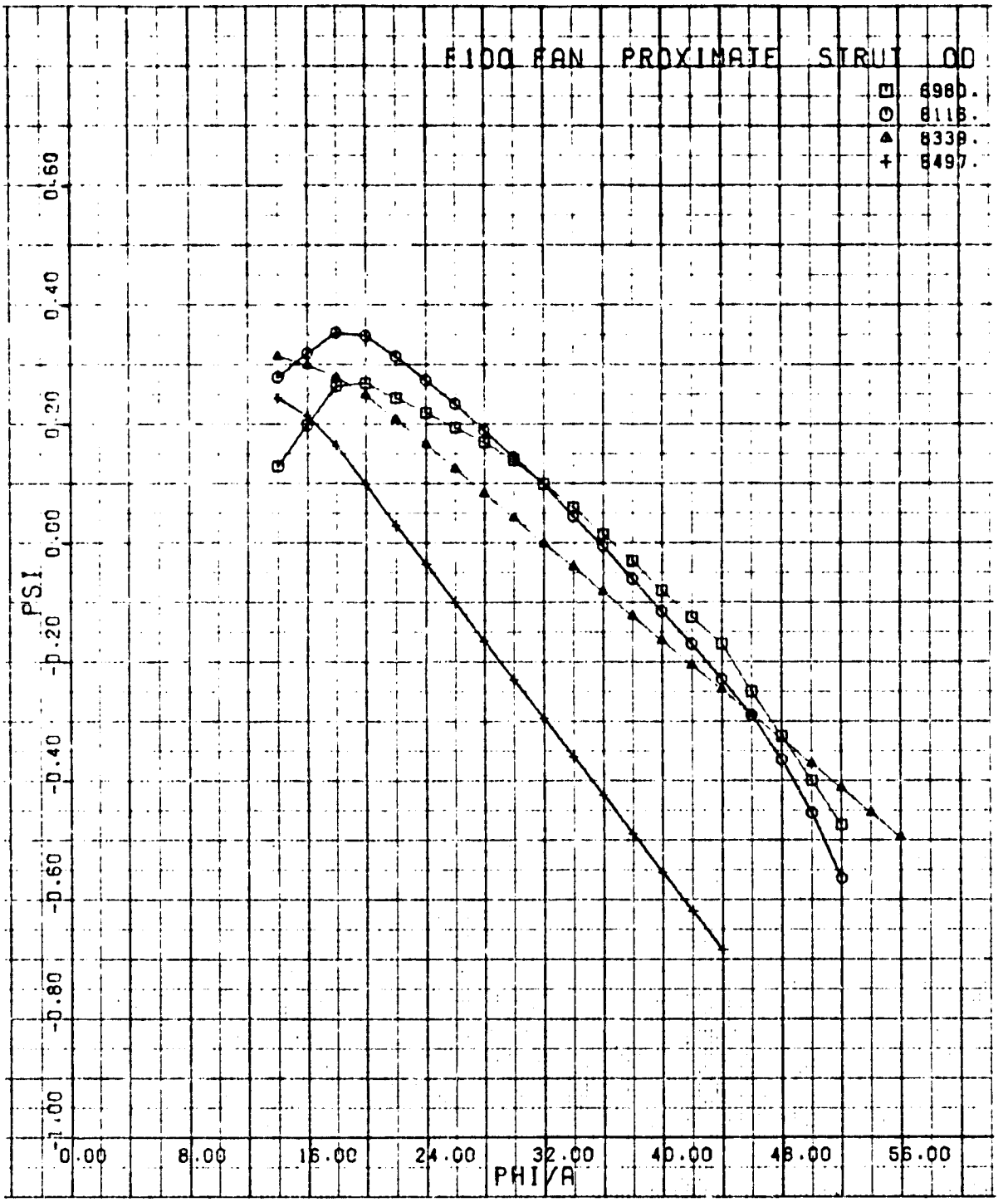
E100 FAN PROXIMATE STRUT OD
6980.
8118.
8339.
8497.
PSI
0.60
0.40
0.20
0.00
-0.20
-0.40
-0.60
-0.80
-1.00
0.00
8.00
16.00
24.00
32.00
40.00
48.00
56.00
PHI/A

C-2

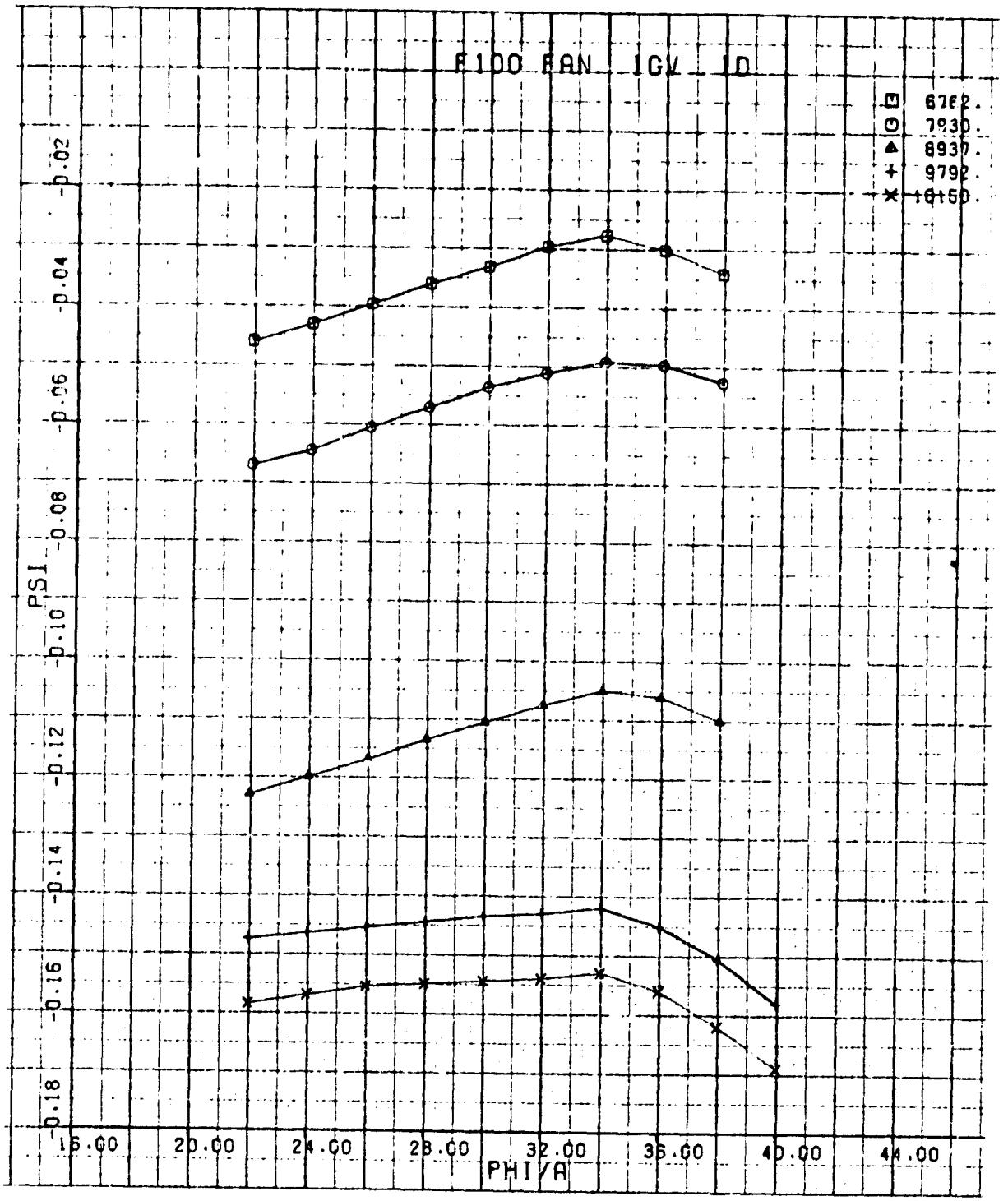

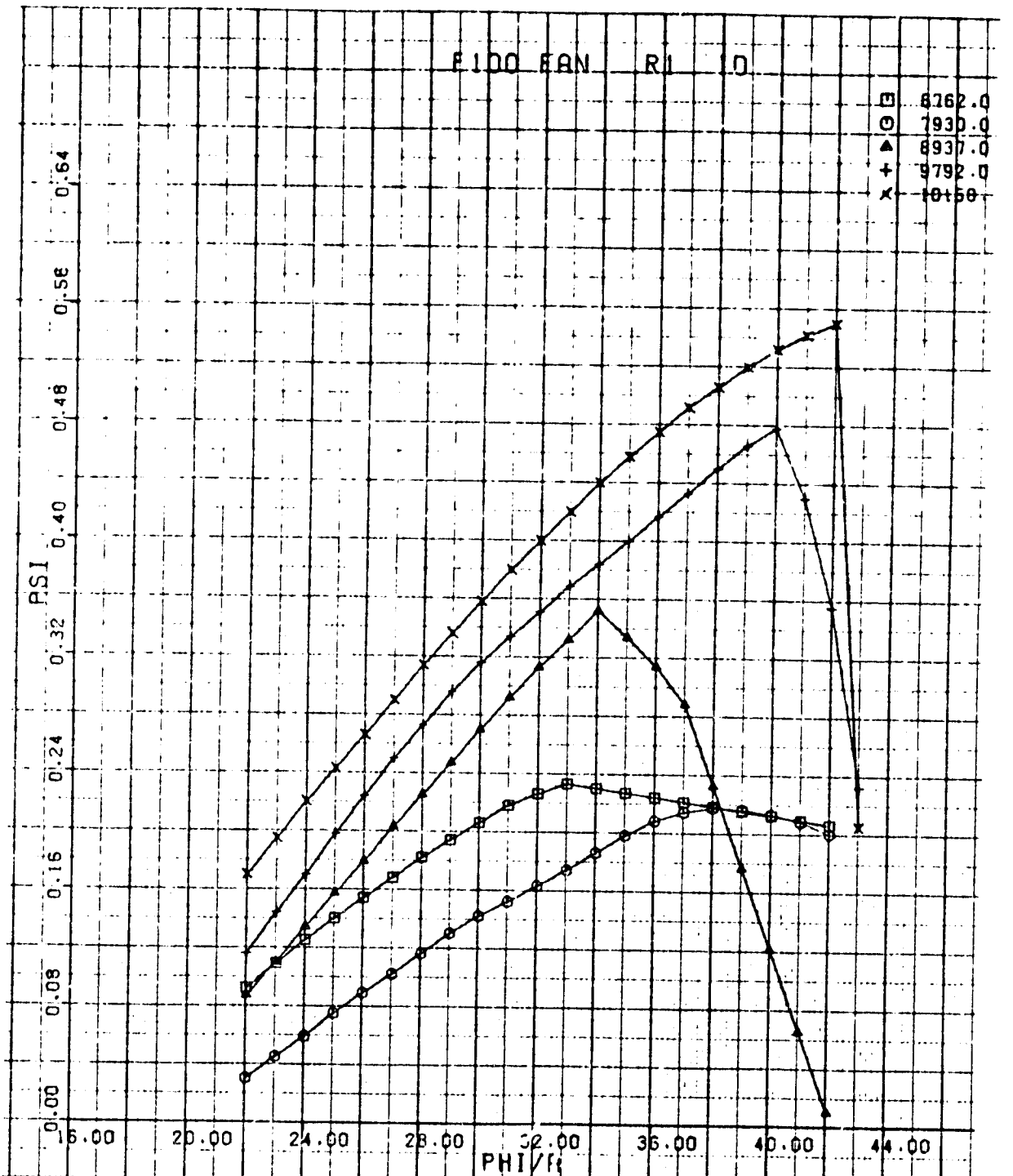

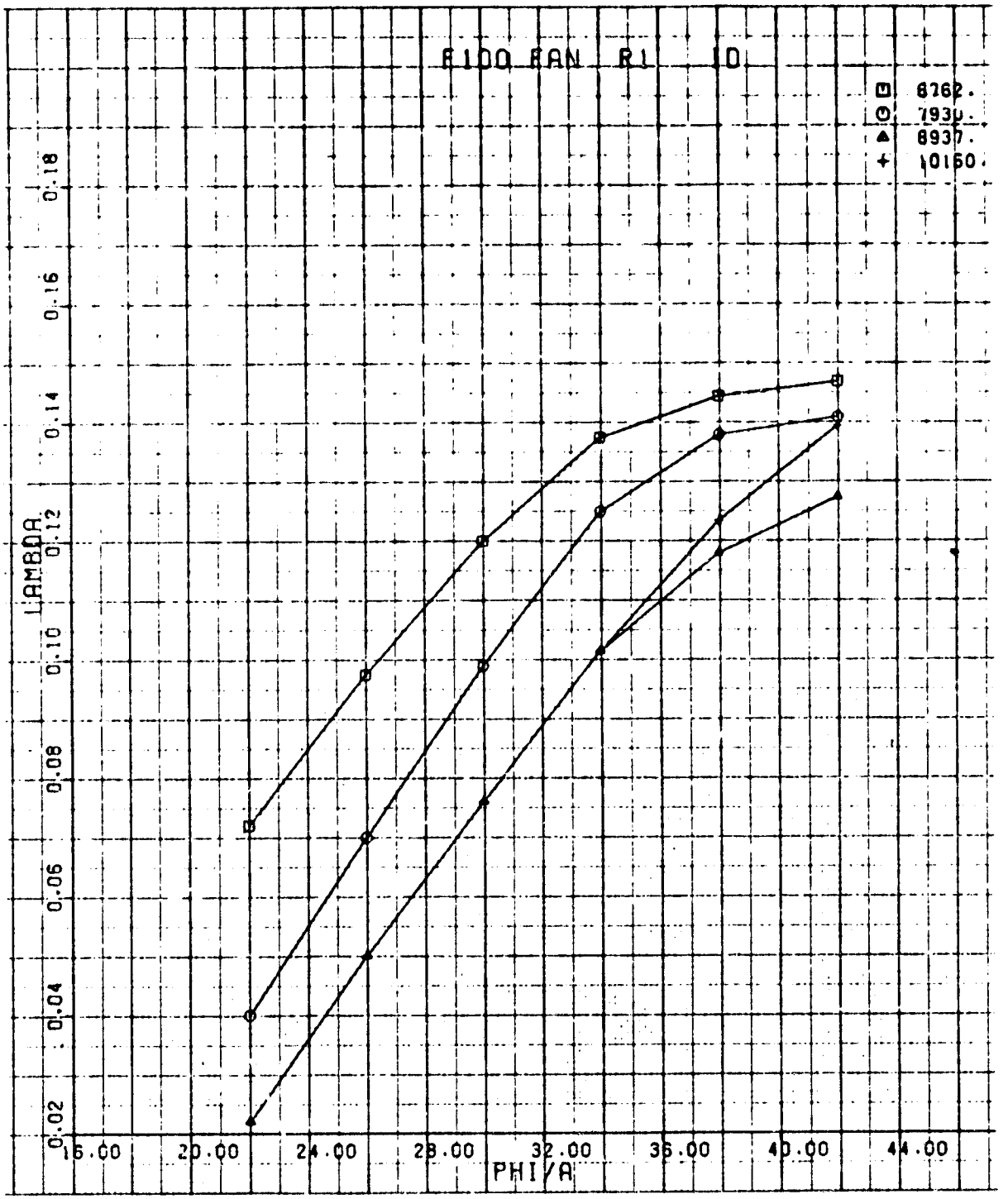

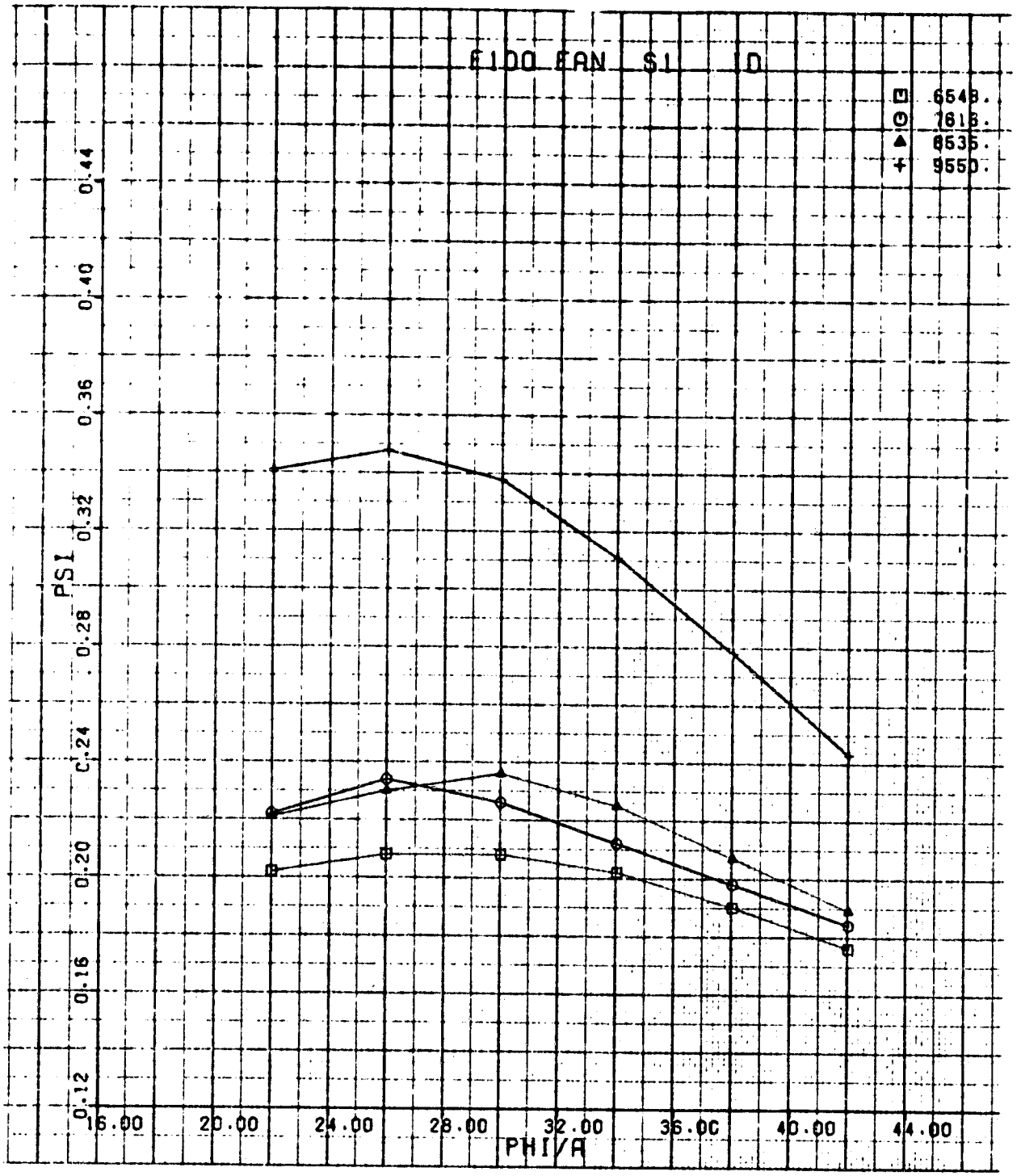

ORIGINAL PAGE IS
OF POOR QUALITY

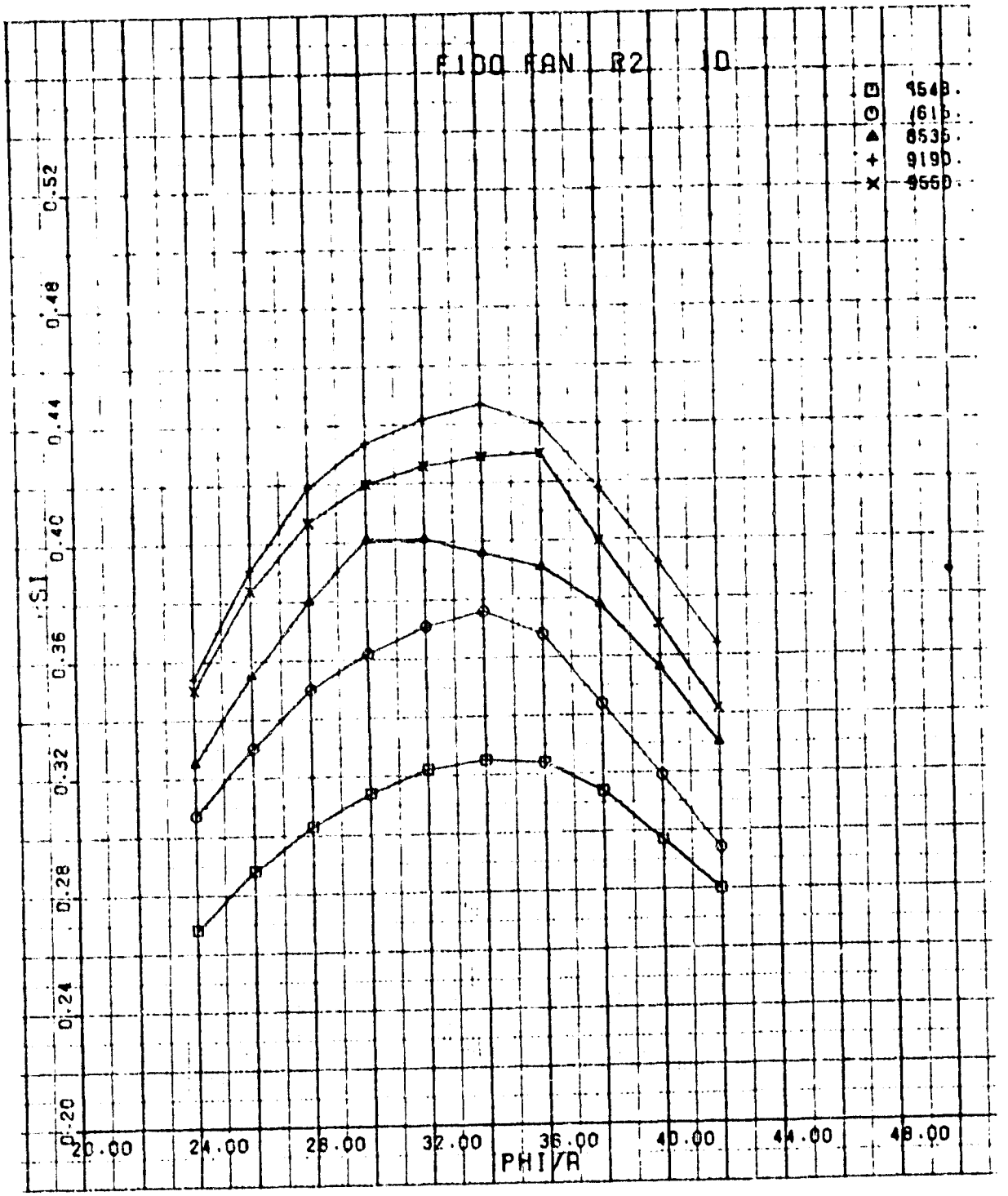

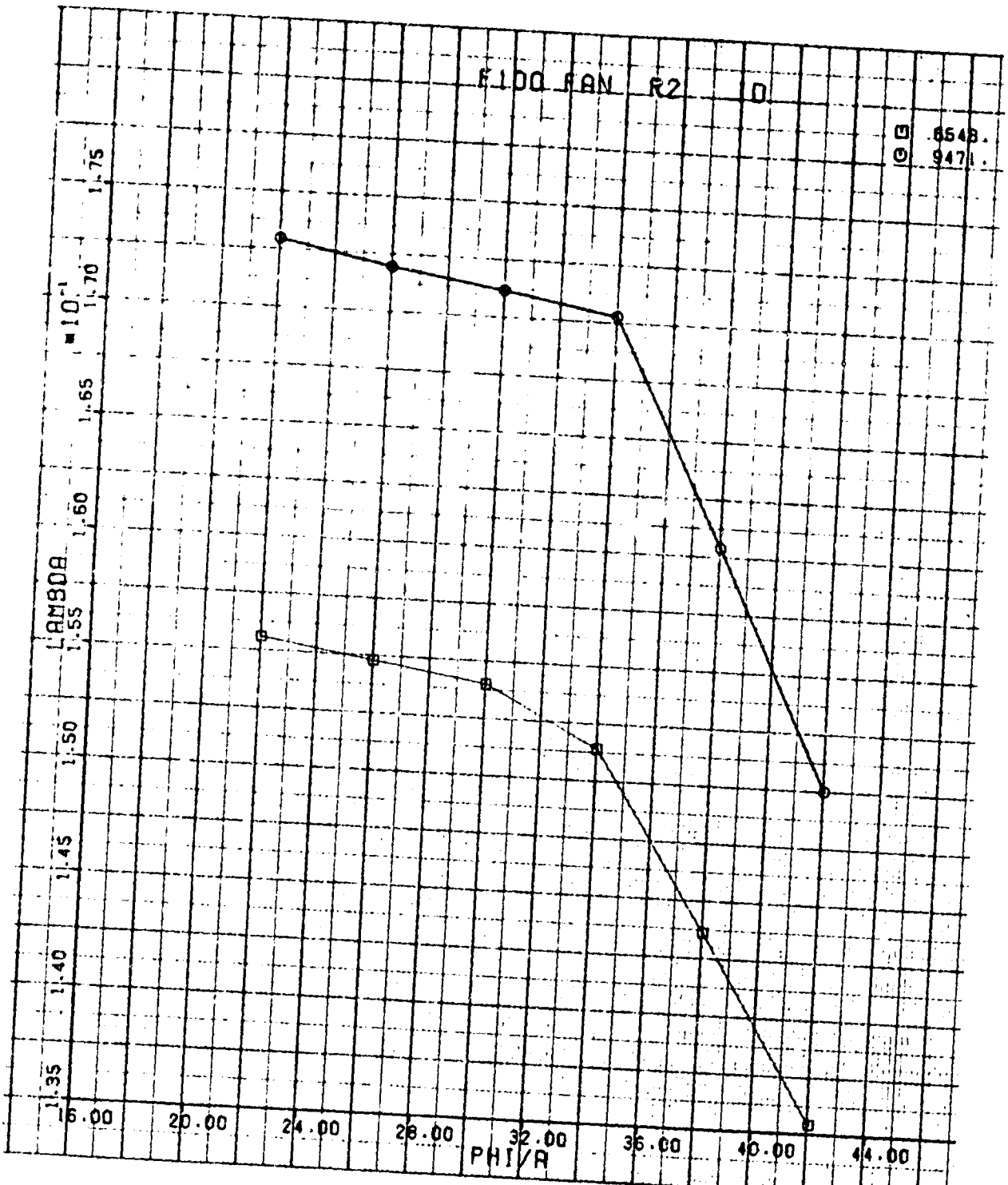

ORIGINAL PAGE IS
OF POOR QUALITY

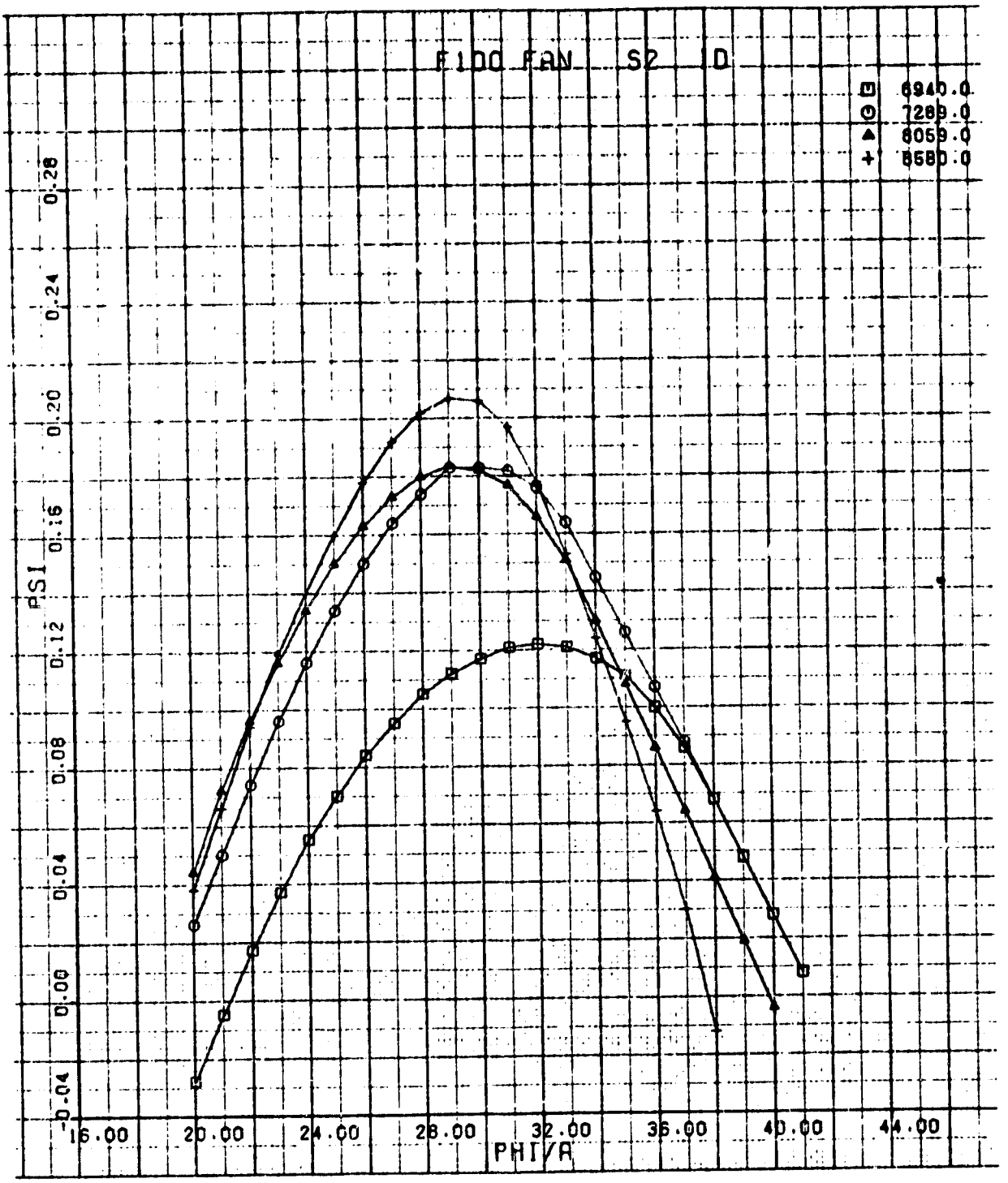

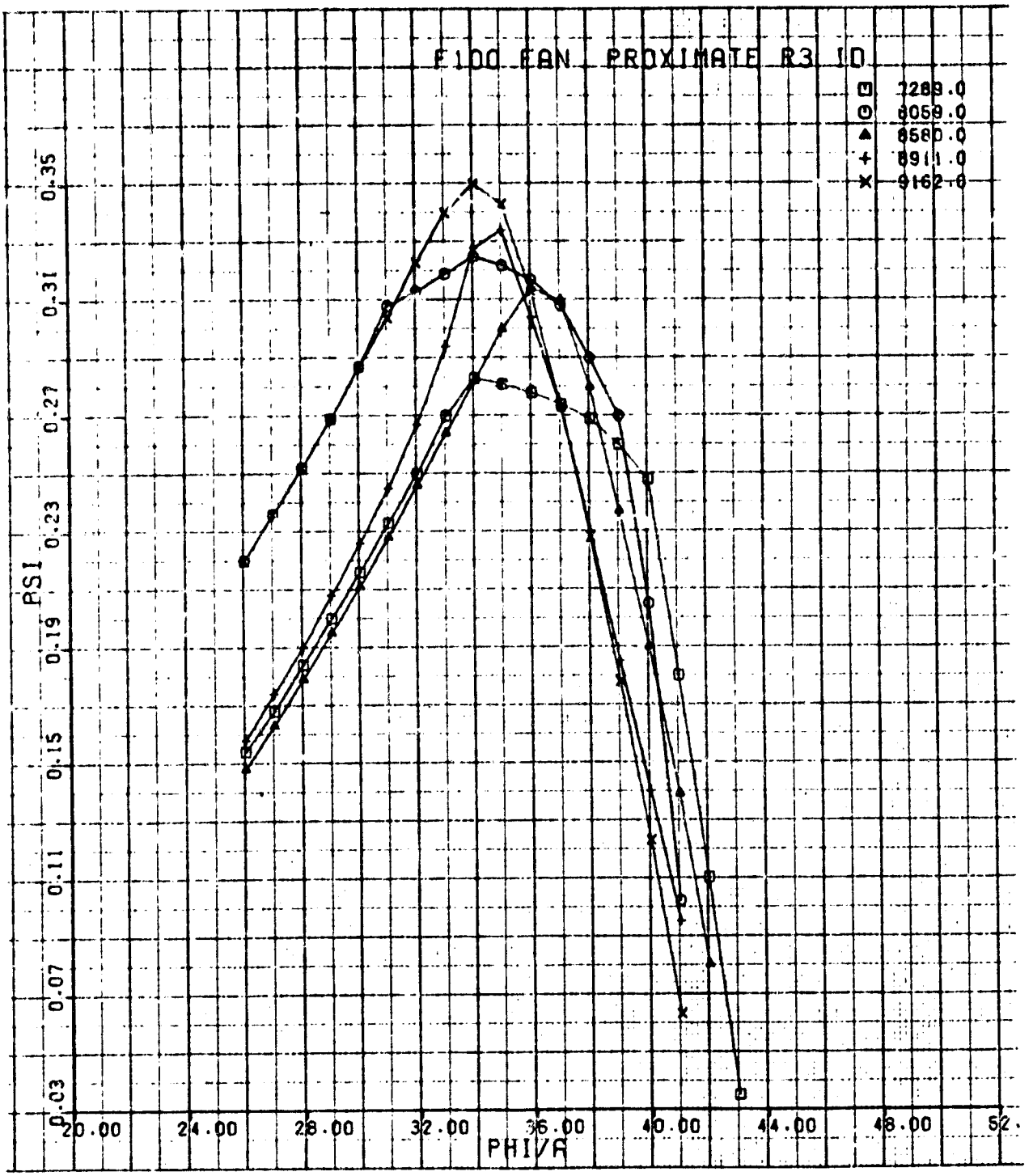

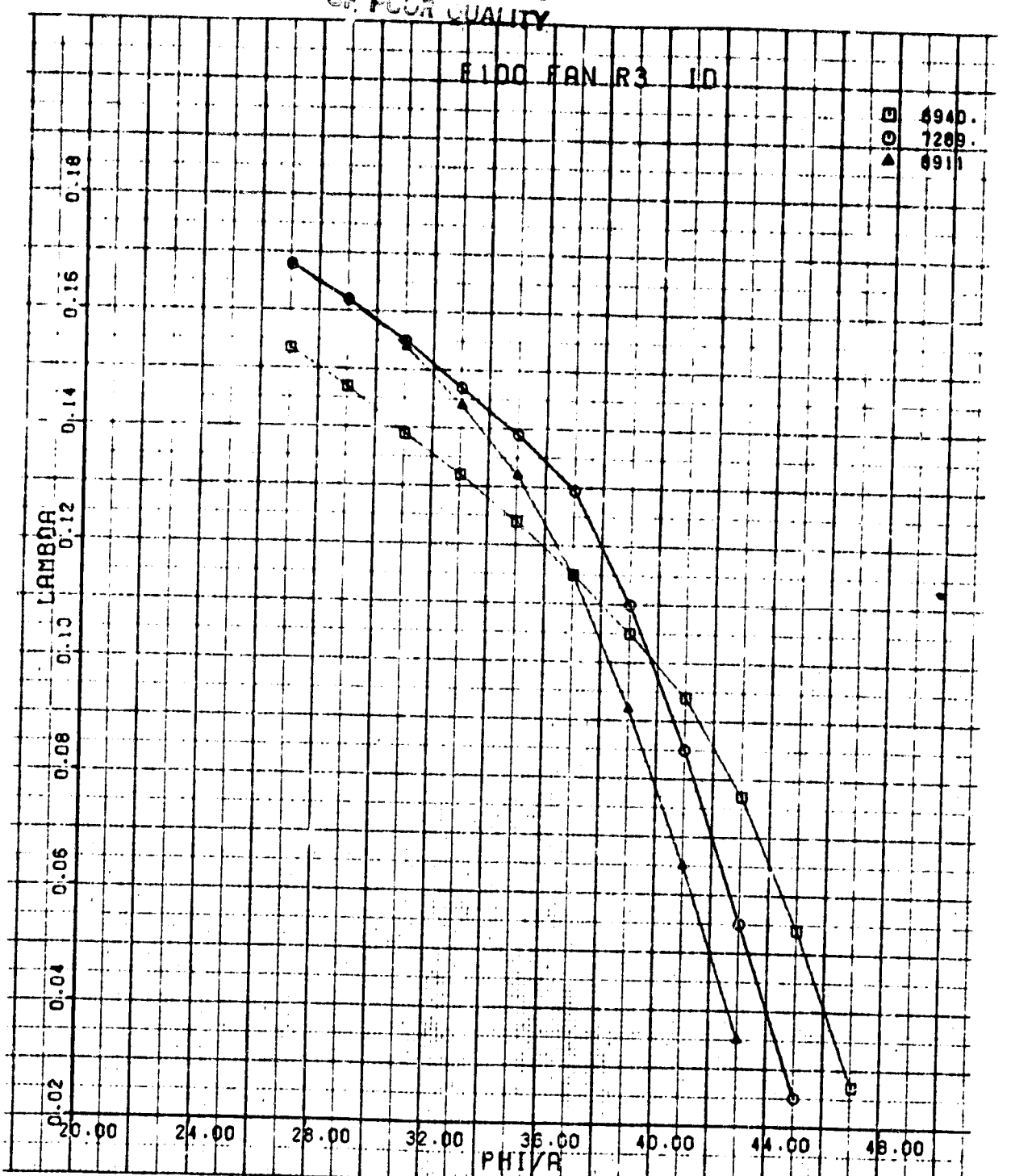

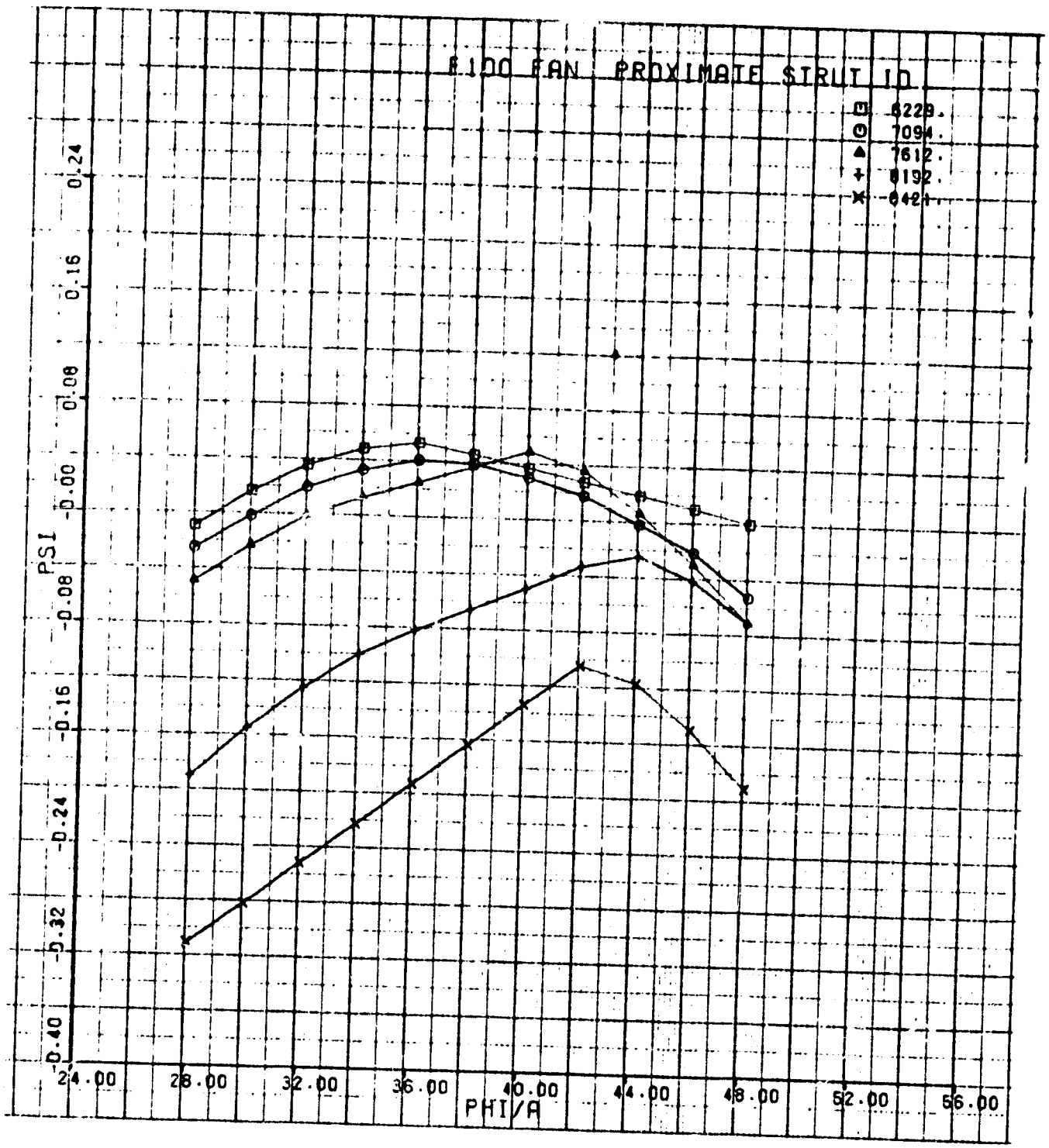

APPENDIX II

Definition of Model Input Parameter Values

The Computer Code and User's Manual, Reference 6, provides detailed input instructions. Because of the capability to analyze the TF30-P-3, and the F100(3) with either proximate or remote splitter configurations, additional input is required to specify the corresponding compression system geometry and blade row performance characteristics. The value (IX) is input on card 1, card column 80, and is defined as below.

IX=0 F100(3) remote splitter fan geometry. Fan performance characteristics as originally defined under NAS3-20610. F100(3) high-pressure compressor geometry and performance characteristics as defined under NAS3-20610.

IX=1 TF30-P-3 compression system geometry and performance characteristics as defined under NAS3-18535.

IX=2 F100(3) remote splitter fan geometry. Revised remote splitter fan performance characteristics defined to be independent of input BPR and compatible with modifications made as part of this contract, NAS3-22739. F100(3) high-pressure compressor geometry and performance characteristics as defined in NAS3-20610.

IX=3 F100(3) proximate splitter fan geometry. Proximate splitter fan performance characteristics defined to be independent of input BPR and compatible with modifications made as part of this contract, NAS3-22739. F100(3) high-pressure compressor geometry and performance characteristics as defined in NAS3-20610.

Based on the input value of IX, a message is printed out stating which fan performance characteristics are used. The input data set is also repeated as part of the program output. A sample of the program input for one pressure distortion case, and one temperature distortion case is shown on the following page.

The fan analysis was performed for classic 180- and 90-degree patterns, so it is possible to use only two values of inlet total pressure and temperature (ISQ=0 and IK3=0). The fan circumference was divided into 18 parallel segments (NSEG=18) equal to 20 degrees per segment. The fan exit static pressure profile is constant (IK2=0) and the deck calculation of upstream air angle is used (IKQ=0). A constant value of bypass ratio was used for all 18 segments (IBPR=0). In order to keep computing times to a minimum, the program calculated crossflow fractions for the first solution were maintained for succeeding solutions (KBLEED = −1, ABCON = 1). As recommended in Report CR-159754, the initial step size used in the exit static pressure backpressuring of the fan was set to one-tenth of a percent (STPS = 1.001). Program default values of the nondimensionalized unsteady rotor loss lag were used (TAUND=1.). In determining a fan stall point, a low value of total flow was specified (WCORR=200.0) and the calculations started at a higher flow and continue towards WCORR until stall is reached. The fan variable guide vane was scheduled as a function of low rotor corrected speed by a schedule built into the program. The scheduling temperature sensors (TPLH1 and TPLH2) were specified to be at 150 and 210 degrees.

The fan was analyzed using run option (IOPT) of 4 (parallel compressor + particle swirl + unsteady rotor + upstream swirl). The study was performed at 102% of design corrected speed (N1=9842). The average input pressure was 5.171×10^4 n/m^2 (7.5 psia), and average temperature for the 18% $\Delta T_T/T_T$ 180-degree distortion, Case 4, was 294.4°K (530°R). For subsequent temperature distortion cases, the low-temperature region was fixed at 267.9°K (482.3°R). The inlet Reynolds Index was approximately 0.5. Bypass ratio for the fan was set equal to 0.52 for alll cases.

INPUT LISTING

CARD COLUMN

```
         1111111111222222222233333333334444444444555555555566666666667777777778
1234567890123456789012345678901234567890123456789012345678901234567890123456789

CASE 1 20%P 102.0%    10   -1                                                -1013
1.                              1.001                                  1.0
   1    2                                      150. 210. 157. 157.
200.000   9842.    180.       0.3250   6.6750  482.3    482.3    0.5200   4
```

```
         1111111111222222222233333333334444444444555555555566666666667777777778
1234567890123456789012345678901234567890123456789012345678901234567890123456789
```

CARD COLUMN

INPUT LISTING

CARD COLUMN

```
         1111111111222222222233333333334444444444555555555566666666667777777778
1234567890123456789012345678901234567890123456789012345678901234567890123456789

CASE 4 18%T 102.0%    10   -1                                                -1013
1.                              1.001                                  1.0
   1    2                                      150. 210. 157. 157.
200.000   9842.    180.       7.5000   7.5000  577.700  482.300  0.5200   4
```

```
         1111111111222222222233333333334444444444555555555566666666667777777778
1234567890123456789012345678901234567890123456789012345678901234567890123456789
```

CARD COLUMN

APPENDIX III
F100(3) Kθ DISTORTION DESCRIPTOR SYSTEM

A distortion descriptor system has been defined and continually refined during the F100 engine development and component improvements program. The circumferential distortion factor, Kθ, is part of that system and is defined below.

Fan Circumferential Pressure Distortion Factor, K_θ

$$K_\theta = \frac{\sum_{ring\ 1}^{J} \left[\left(\frac{A_N}{N^2} \right)_{max} \times \frac{1}{D_{ring}} \right]_{ring}}{(q/P_{t2})_{ref} \sum_{ring\ 1}^{J} \left[\frac{1}{D_{ring}} \right]}$$

where:

J = Number of rings (probes per leg)
D = Ring Diameter
$\left(\frac{q}{P_{t2}} \right)_{ref}$ = Reference value of engine face dynamic pressure

$$A_n = \sqrt{a_N^2 + b_N^2},\ N = 1,2,3,4$$

where:

$$a_N = \frac{\Delta\theta}{180} \sum_{k=1}^{K} \frac{P_{t2}/P_{t0}\ (k\Delta\theta)}{P_{t2}/P_{t0}} \cos\ (Nk\Delta\theta)$$

$$b_N = \frac{\Delta\theta}{180} \sum_{k=1}^{K} \frac{P_{t2}/P_{t}\ (k\Delta\theta)}{P_{t2}/P_{t0}} \sin\ (Nk\Delta\theta)$$

and

$P_{t2}/P_{t0}\ (k\Delta\theta)$ = Local recovery at angle, $k\Delta\theta$
(P_{t2}/P_{t0}) = Face average recovery
K = Number of rake legs
$\Delta\theta$ = Angular distance between rake legs degrees

$\left(\frac{A_N}{N^2} \right)_{max}$ = maximum value for the four Fourier coefficients calculated; normally turns out to be A_1.

N = Number of the harmonic of the Fourier Series

The application of this definition can be seen by examining some symmetric distortion patterns. For these cases a simple equation results. The definition can be used to calculate $K\theta$ for either pressure or temperature distortion.

180° Square Wave

$$K\theta = \frac{0.635\ (\Delta P_T/P_T)}{Q/P_T}$$

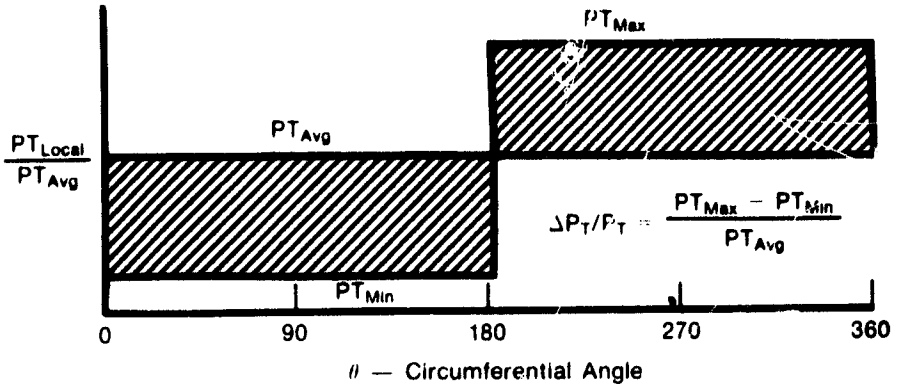

90° Square Wave

$$K\theta = \frac{0.448\ (\Delta P_T/P_T)}{Q/P_T}$$

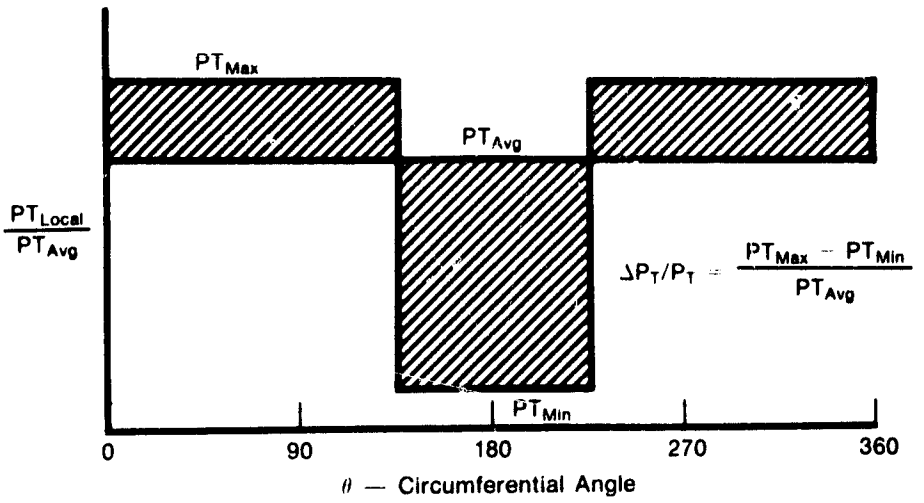

Sine Wave

$$K\theta = \frac{0.5\ (\Delta P_T/P_T)}{Q/P_T}$$

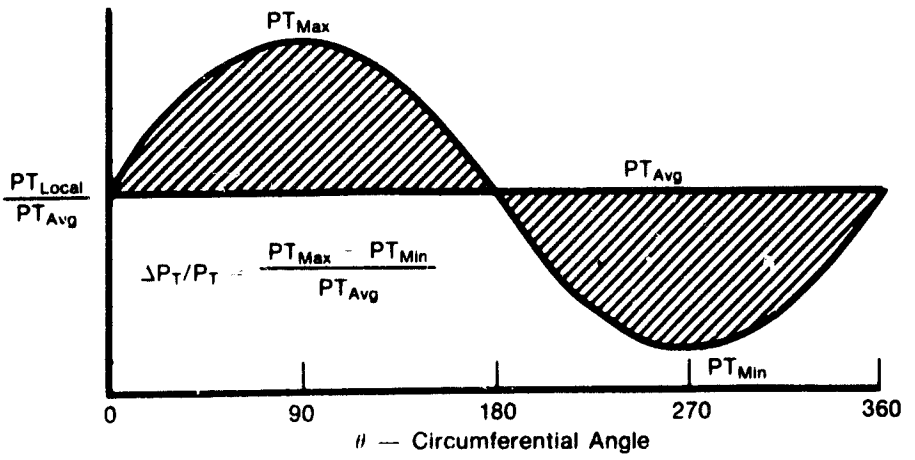

FD 238472
822002
BT3 466

REFERENCES

1. Mazzawy, R. S., D. A. Fulkerson, D. E. Haddad and T. A. Clark, "F100(3) Parallel Compressor Computer Code and User's Manual Final Report," NASA CR-135388, May 1978.

2. Mazzawy, R. S., "Multiple Segment Parallel Compressor Model for Circumferential Flow Distortion," *ASME Journal of Engineering for Power*, Vol. 99 No. 2, April 1977.

3. Walter, W. A. and M. Shaw, "Distortion Analysis for F100(3) Engine," NASA CR-159754, January 1980.

4. Mason, J. R., J. W. Park, R. F. Jaekel, "Extended Frequency Turbofan Model," NASA CR-165261, 15 December 1980.

5. Mazzawy, R S. and G. A. Banks, "Circumferential Distortion Modeling of the TF30-P-3 Compression System," NASA CR-135124, January 1977.

6. Mazzawy, R. S., Haddad and D. A. Fulkerson, "F100(3) Parallel Compressor Computer Code and User's Manual," PWA 5549-7, May 1978.

LIST OF SYMBOLS

A	Flow Area
BPR	Bypass Ratip; BPR = Duct Airflow/Core Airflow
CIVV	Fan Inlet Variable Vane; Degrees From Nominal Position
$\Delta E'$	Pressure Warpage; $\Delta E' = E'_{2.5C} - E'_{2.5H}$
E'	Warpage Parameter; $E' = PR\ \gamma\text{-}1/\gamma - 1/[N1/\sqrt{\theta_2}/N1/\sqrt{\theta_2})_{des}]^2$
$K\theta$	F100 Circumferential Distortion Factor; See Appendix III
LAMBDA	Normalized Total Temperature Rise Coefficient; See Appendix I
N1	Low Rotor Mechanical Speed ~ rpm
N1C2	Low Rotor Speed Corrected To Station 2 ~ rpm; $N1C2 = N1/\sqrt{\theta_2}$
ODFLCO	Fan Exit OD Flow Coefficient ~ lbm/sec; $ODFLCO = WAD \cdot \theta_{2.5C}/\delta_{2.5C}/[N1/8000]$
PHI/A	Mass Flow Coefficient/Area ~ lbm/sec-ft^2; See Appendix I
PR	Pressure Ratio; $PR = PT_{EXIT}/PT_{INLET}$
PS	Static Pressure ~ psia
PSI	Normalized Static Pressure Rise Coefficient; See Appendix I
PT	Total Pressure ~ psia
$\Delta P_T/P_T$	Circumferential Distortion Factor; $\Delta P_T/P_T = (PT_{max} - PT_{min})/PT_{avg}$
PCN1C2	Percent Design Low Rotor Speed Corrected to Station 2; $PCN1C2 = N1/\sqrt{\theta_2}/9650$
PCWATC2	Percent Design Airflow Corrected to Station 2; $PCWATC2 = WAT\ \sqrt{\theta_2}/\delta_2/217$
%ΔSPR	Percent Surge Margin Loss at Distorted Stalling Airflow; See page 25
$\Delta T_T/T_T$	Circumferential Temperature Distortion Factor; $\Delta T_T/T_T = (TT_{max} - TT_{min})/TT_{avg}$
TT	Total Temperature ~ °R
W	Physical Airflow ~ lbm/sec
WAD	Fan Duct Physical Airflow ~ lbm/sec

LIST OF SYMBOLS

WAT	Fan Inlet Physical Airflow ~ lbm/sec
θ	Total Temperature/518.7°R
δ	Total Pressure/14.696 psia
γ	Specific heat ratio; $\gamma = c_p/c_v$

Subscripts

Avg	Average
Des	Design
Fan	Fan
L	Local
Max	Maximum
Min	Minimum
T	Total
Temp	Temperature
2	Station 2 (Fan Inlet)
2.5C	Station 2.5C (Fan Exit OD)
2.5H	Station 2.5H (Fan Exit ID)